

2008

## Variability in Geologic Framework and Shoreline Change: Assateague and Wallops Islands, Eastern Shore of Virginia

Geoffrey L. Wikel

*College of William and Mary - Virginia Institute of Marine Science*

Follow this and additional works at: <https://scholarworks.wm.edu/etd>



Part of the [Geomorphology Commons](#), and the [Physical and Environmental Geography Commons](#)

---

### Recommended Citation

Wikel, Geoffrey L., "Variability in Geologic Framework and Shoreline Change: Assateague and Wallops Islands, Eastern Shore of Virginia" (2008). *Dissertations, Theses, and Masters Projects*. Paper 1539617877.

<https://dx.doi.org/doi:10.25773/v5-mk4v-4r15>

This Thesis is brought to you for free and open access by the Theses, Dissertations, & Master Projects at W&M ScholarWorks. It has been accepted for inclusion in Dissertations, Theses, and Masters Projects by an authorized administrator of W&M ScholarWorks. For more information, please contact [scholarworks@wm.edu](mailto:scholarworks@wm.edu).

**VARIABILITY IN GEOLOGIC FRAMEWORK AND SHORELINE CHANGE:  
ASSATEAGUE AND WALLOPS ISLANDS, EASTERN SHORE OF VIRGINIA**

---

A Thesis  
Presented to

The Faculty of the School of Marine Science  
The College of William and Mary in Virginia

In Partial Fulfillment  
Of the Requirements for the Degree of  
Master of Science

---

by  
Geoffrey L. Wikel  
2008

APPROVAL SHEET

This thesis is submitted in partial fulfillment of

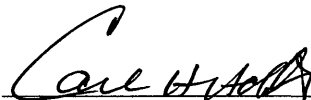
the requirements for the degree of

Master of Arts

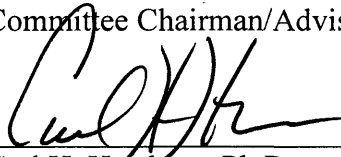


Geoffrey L. Wikel

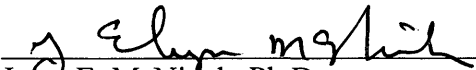
Approved, April 2008



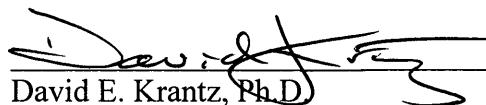
Carl H. Hobbs III., Ph.D.  
Committee Chairman/Advisor



Carl H. Hershner, Ph.D.



Jesse E. McNinch, Ph.D.



David E. Krantz, Ph.D.  
University of Toledo  
Toledo, Ohio

## TABLE OF CONTENTS

	Page
ACKNOWLEDGEMENTS .....	iii
LIST OF TABLES .....	iv
LIST OF FIGURES .....	v
ABSTRACT .....	vii
INTRODUCTION .....	2
LITERATURE REVIEW.....	6
Variability in Shoreline Change .....	6
Framework Geology and Shoreline Behavior.....	8
Nearshore Morphology and Shoreline Behavior.....	12
STUDY AREA.....	17
Geologic Setting.....	17
Physical Setting.....	20
METHODOLOGY .....	22
Shoreline Change Statistics.....	22
Characterization of Nearshore Morphology.....	24
Geophysical Mapping and Seismic Stratigraphic Characterization...	26
Cross-Correlation Analysis.....	28
RESULTS .....	30
Variability in Shoreline Change.....	30
Assateague Island.....	30
Wallops Island.....	32
Nearshore Morphology.....	33
Nearshore of Assateague Island.....	35
Nearshore of Wallops Island.....	37
Historic Morphologic Changes.....	38
Nearshore Seismic Stratigraphy and Geologic Framework.....	40
Pre-Holocene Geology.....	41
Holocene Geology.....	42
Holocene Sand Cover.....	46
Cross-Correlation of Shoreline Change and Geologic Framework...	47
DISCUSSION.....	53
Underlying Geologic Influence on Coastal Evolution.....	53
Correlating Geologic Framework and Shoreline Change.....	61
Shoreline Response Adjacent to Nearshore Morphology.....	66
Challenges to Quantifying the Relationship between	
Geologic Framework and Shoreline Change.....	67
Shoreline Predictions using Nearshore Sand Volume .....	71



CONCLUSIONS.....	76
APPENDIX: REVIEW OF CROSS-CORRELATION ANALYSIS.....	82
Introduction.....	82
Autocorrelation.....	83
Adjusting the Test Procedure: Calculating Effective Sample Size...	85
Pre-Whitening.....	89
Conclusions.....	91
REFERENCES.....	93
TABLES.....	107
FIGURES.....	117
VITA .....	200

## ACKNOWLEDGEMENTS

I sincerely appreciate the support of my committee members: Dr. Carl Hobbs, Dr. Jesse McNinch, Dr. Carl Hershner, and Dr. David Krantz. I am indebted to Dr. David Krantz and Dr. Douglas Levin, who graciously allowed me to participate in their research program sponsored by the North Atlantic Coast Cooperative Ecosystem Studies Unit. Dr. David Krantz deserves special mention for his contribution during our many conversations about the study area.

I acknowledge the following individuals for sharing data: Gregg Williams, engineer with the U.S. Army Corps of Engineers – Norfolk District, provided vibrocore data; Arty Rodriquez, cartographer with the National Park Service, provided DGPS shorelines collected by Park Service personnel; and, Michael Fenster, faculty at Randolph Macon College, provided surface sediment sample data.

I thank Dr. Jennifer Miselis (U.S. Naval Research Laboratory) and Courtney Schupp (National Park Service) for critically reviewing this thesis and offering insightful comments that improved content and direction.

I thank my family for their constant encouragement. I am particularly grateful to my wife, Diane Shearon, for her tireless patience and unwavering support.

## LIST OF TABLES

Table	Page
1. Shoreline position data.....	108
2. Shoreline position uncertainty estimates.....	109
3. Bathymetry digital elevation model data.....	110
4. Bathymetry DEM and isopach uncertainty estimates.....	111
5. Cross-correlation: shoreline mobility and shoreline change.....	112
6. Volume changes between 1933/34 and 1978/1982 by isopach region .....	113
7. Description of Quaternary seismic stratigraphy.....	114
8. Cross-correlation of geologic framework and shoreline change.....	115
9. Comparison of offshore environments and shoreline behavior for Assateague and Wallops Islands.....	116

## LIST OF FIGURES

Figure	Page
1. Map of southern Assateague Island and Wallops Island.....	119
2. Oblique view of nearshore morphology and barrier beach of southern Assateague Island.....	121
3. Conceptual diagram of nearshore zone.....	123
4. Maryland and Virginia inner shelf stratigraphy.....	125
5. Progradation of southern Assateague Island and shoreline mobility near Assateague Point.....	127
6. Map showing geophysical tracklines.....	129
7. Example sections of processed chirp seismic data.....	131
8. Shoreline change and orientation data for southern Assateague Island.....	133
9. Shoreline change data for Wallops Island.....	135
10. Erosion along Toms Cove, Assateague Island.....	137
11. Oblique view of nearshore and inner shelf bathymetry.....	139
12. Photography illustrating engineering practices and overwash processes on Wallops Island.....	141
13. Variability in profile shape along Assateague and Wallops Islands.....	143
14. Variability in eigenfunction weightings along Assateague Island.....	145
15. Bathymetric change map.....	147
16. Cross-section and interpretation of geophysical lines A and B.....	149
17. Cross-section and interpretation of geophysical lines C and D.....	151

18. Side scan sonar images showing different seafloor environments.....	153
19. Cross-section and interpretation of geophysical line E.....	155
20. Cross-section and interpretation of geophysical lines F and G.....	157
21. Cross-section and interpretation of geophysical lines H and I.....	159
22. Map showing relict inlets and offshore distribution of underlying geologic features/facies.....	161
23. Map showing thickness of nearshore sand cover along tracklines.....	163
24. Isopach map showing regional sand prism thickness.....	165
25. Digital photographs of 20-ft vibracores.....	167
26. Plan view of nearshore slope model and sand volume.....	169
27. Shoreline change rates compared to nearshore slope and sand volume.....	171
28. Cross-correlation of nearshore slope and inter-annual shoreline change...	173
29. Cross-correlation of nearshore slope residual and inter-annual shoreline change residual.....	175
30. Cross-correlation of nearshore volume and inter-annual shoreline change.....	177
31. Cross-correlation of nearshore volume residual and inter-annual shoreline change residual.....	179
32. Map showing proposed Chincoteague paleo-valley.....	181
33. Alongshore variability in predominant geomorphologic environments of Assateague Island.....	183
34. Illustration defining cross-shore zones of ‘shoreline’ influence.....	185
35. Nearshore sand volume, volume flux, and years to erode volume.....	187

A-1. Short-term shoreline mobility and shoreline change data for southern Assateague Island.....	189
A-2. Statistical and autocorrelation characterization of short-term shoreline change data for southern Assateague Island.....	191
A-3. Cross-correlation of shoreline mobility and change data following treatment.....	193
A-4. Autocorrelation function and cross-correlation of shoreline mobility and shoreline change using untreated data.....	195
A-5. Autocorrelation function and cross-correlation of shoreline mobility and shoreline change using residuals.....	197
A-6. ARIMA(1,1,0) model and model residuals for shoreline change data....	199

## ABSTRACT

The evaluation of system heterogeneity, including nearshore morphology and underlying geology, not just gross hydrodynamics, is critical to refining scientific understanding and enhancing process-based models of shoreline and morphodynamic behavior given repeated, worldwide documentation of geologic complexity across sediment-starved, storm-dominated coastal settings. One of the first and critical steps in this process is to document the space and time scales over which geology and shoreline change are coupled. The short-term to long-term shoreline behavior and offshore geologic character of Assateague Island and Wallops Island are examined using historical shoreline change data, legacy bathymetry, and newly acquired chirp seismic and side scan sonar to evaluate relationships between shallow coastal stratigraphy, nearshore morphology, and the subaerial beach. The results presented herein reveal a Holocene-dominated sedimentary system that is moderately sand-starved, where the expression of near-surface geology is distinguished by strong alongshore and offshore gradients in morphology, slope, and distribution in sediment facies and texture. The influence of the geologic framework on shoreline behavior, not necessarily independent of hydrodynamic and inlet processes, is observed in differences in profile steepness, density and scale of morphology, and sand prism thickness— characteristics and trends distinguished by multiple alongshore length scales. Spatial and temporal anomalies in shoreline change data are spatially coincident with shoreface-attached ridges, relict spit morphology, and areas of limited sand cover. These qualitative observations are then tested along southern Assateague Island by cross-correlating shoreline change rates with mean nearshore slope and nearshore sand volume, representing the shallow geologic framework. Although complicated by trend and autocorrelation, the geostatistical analysis indicates a strong correlation between the variability in shoreline change and geologic framework over inter-annual and long-term time scales, whereby relative steeper shoreface profiles characterized by relative smaller cross-shore volumes correspond to erosional trends. The dynamic shoreface accounts for a changeable proportion of the geologic and shoreline change variability, the degree of which depends on the alongshore length scale under consideration.

**VARIABILITY IN GEOLOGIC FRAMEWORK AND SHORELINE CHANGE:  
ASSATEAGUE AND WALLOPS ISLANDS, EASTERN SHORE OF VIRGINIA**



## 1 INTRODUCTION

On the Eastern Shore of Virginia along the Delmarva Peninsula, the historic period has witnessed the southern progradation of Assateague Island and concomitant erosion of Wallops Island and the transgressive barrier chain to the south (Figure 1). Published shoreline change data show alternating patterns of erosion and accretion along southern Assateague Island and extensive erosion along the southern half of Wallops Island, compared to gross accretion at the terminal spits of Fishing Point and Gunboat Point near Chincoteague Inlet (*e.g.*, Dolan *et al.*, 1977; Moffat and Nichol, 1986; Kochel and Wampfler, 1989; Galgano, 1998). Distinct alongshore patterns persist in short-term shoreline change data that consider storm response and recovery along Assateague Island in spite of considerable alongshore variability that ranges from no net change to over 150 m of cross-shore change (Stockdon *et al.*, 2002). The observation that alongshore changes in shoreline orientation of Assateague Island were co-located with distinct shoreline undulations and nearshore morphology further piqued interest in these recurring spatial patterns (Figure 2).

Many researchers have noted similar variability and persistence in shoreline change and sought to explain such spatial and temporal phenomena in terms of fundamental forcings (*e.g.*, Fenster and Dolan, 1996; List and Farris, 1999; Zhang *et al.*, 2002; Ruggiero *et al.*, 2005; List *et al.*, 2006). The diverse controls on shoreline behavior are of growing interest to the coastal management community as it seeks to mitigate coastal hazards and safeguard the colossal economic investment in the coastal zone (Kraus and Galgano, 2001). The lion's share of the existing understanding of shoreline and morphodynamic behavior focuses on the complex feedbacks between

hydrodynamics, sediment transport, and morphology on the shoreface, in particular gradients in wave energy and sediment flux, and the accompanying shoreline response (e.g., Wright and Short, 1984; Coco and Murray, 2007). However, the accuracy and skill of conceptual and numerical models used to hindcast or predict shoreline change still fall short of fully reproducing observed trends, and some have attributed this tendency to imperfect assumptions concerning the concepts of equilibrium profile, a quantifiable depth of closure, and a homogenous, replete sediment source in sediment-starved coastal settings (Pilkey *et al.*, 1993; Schwab *et al.*, 2000; Thieler *et al.*, 2000).

Only recently have studies taken a more comprehensive look at coastal behavior in terms of system heterogeneity, recognizing that diverse sediment characteristics, nearshore morphology and underlying geology, not just gross hydrodynamics, must be documented before and ultimately addressed in process-based modeling. Finkelstein (1986), Riggs *et al.* (1995), and List and Farris (1999) were some of the earliest researchers to suggest that shoreface locations with limited sand cover were correlated with erosion over long-term periods and with higher variability in shoreline position over decadal scales. Long-term shoreline change signals have since been linked to variable geologic framework along beaches in New York, Delaware, North Carolina, Virginia, Texas, South Carolina, and Florida (Schwab *et al.*, 2000; Honeycutt and Krantz, 2003; McNinch, 2004; Rodriguez *et al.*, 2004; Harris *et al.*, 2005; Houser *et al.*, in press).

Other studies have quantitatively shown spatial correlation between long-term (decadal to inter-centennial) shoreline change, short-term (seasonal to inter-annual) shoreline variability, and complex nearshore morphology along wave-dominated coastlines (Schupp *et al.*, 2006; Miselis and McNinch, 2006; Houser *et al.*, in press). Still,

others maintain that longshore sediment transport, solely accounting for gradients in breaking wave height, breaking angle relative to shoreline orientation, and the mean grain size of source material, can satisfactorily explain long-term shoreline change (Valvo *et al.*, 2006). However, few could argue that advancing the understanding of shoreline response, improving the skill and predictive capabilities of deterministic models, and enhancing coastal management approaches depend in part on improved parameterization of geologic variables and documentation of affected space and time scales (Honeycutt and Krantz, 2003).

The objectives of this research are three-fold: 1) to characterize and differentiate the shoreline behavior of Assateague and Wallops Islands over a range of spatial and temporal scales using shoreline change rates, 2) to characterize and differentiate the geologic framework occurring off these barrier islands using bathymetric and geophysical data, and 3) to quantify the nearshore morphology and shallow geology in meaningful variables and compare those to shoreline behavior over representative alongshore scales. This research effort also serves a practical purpose, potentially informing future decision-making of National Park Service / U.S. Fish and Wildlife resource managers charged with managing the valuable public beach infrastructure and sensitive habitat for protected species (*e.g.* loggerhead turtles, piping plovers, Chincoteague ponies) on Assateague Island and the southern end of Wallops Island, as well as National Air and Space Administration personnel that face urgent decisions about protecting vulnerable launch infrastructure and adopting wise beach nourishment strategies on a rapidly eroding stretch of Wallops Island.

This thesis is organized as follows. A brief review is first provided characterizing the existing body of work exploring the relationship between geologic framework and shoreline change. Then, the geologic and physical setting of the study area is described, followed by a review of the methods used to document, parameterize, and test the spatial and temporal correlation between shoreline change and geology. The geostatistical methods are explained in further detail in the Appendix. The results of shoreline change, bathymetric, stratigraphic, and statistical analyses and discussions of the subsequent findings are presented thereafter and reveal a sedimentary system offshore Assateague and Wallops Islands that is moderately sediment starved and characterized by strong alongshore and offshore gradients in morphology and patchy sediment distribution. The variability in its near surface expression appears to be related to variability in underlying geology, but the mechanistic linkage remains unclear. The corresponding shoreline behavior of these barrier islands, documented in the shoreline change analyses, show a strong qualitative relationship to documented nearshore morphology and sand volume. This qualitative assessment is explored further using geostatistics to confirm a statistically significant relationship between the variability in shoreline change and that in geologic framework over a range of spatial and temporal scales.

## 2 LITERATURE REVIEW

### 2.1 *Variability in Shoreline Change*

The most common measure of beach change is the net migration of the shoreline over time, which is typically defined in terms of either a proxy-based horizontal reference (*e.g.*, High Water Line from aerial photography) or a datum-based shoreline (*e.g.*, Mean High Water from a lidar topographic model) (Boak and Turner, 2005). Shoreline position data commonly are used for characterizing rates of change (*e.g.*, Dolan *et al.*, 1977; Fenster and Dolan, 1996; Galgano, 1998), sediment budgets (*e.g.*, Leatherman *et al.*, 1984; Headland *et al.* 1987; Kana 1995), and analytical/numerical modeling of morphologic change (*e.g.*, Dean and Work, 1993) to better understand the inter-related processes operating in coastal systems. Since this study explores the relationship between shoreline change and geologic framework over different spatial and temporal scales, it is important to document the range of known controls and their varied scales of influence on shoreline change.

Relative sea level change, incident wave climate, sediment supply, storms, inlet processes, nearshore morphology, geologic framework, anthropogenic engineering, and combinations thereof, may control shore and shoreline variability over daily to millennial time and local to regional space scales (Figure 3) (Kraus and Galgano, 2001; Stive *et al.*, 2002). Within this spectrum, spatial and temporal processes and scales are linked, such that large-scale changes often relate to long-term processes/controls and small-scale changes to short-term processes/controls (List *et al.*, 2006). The different temporal scales of shoreline change considered may magnify short-term processes relative to longer-term trends.

Alongshore gradients in sediment transport are primarily used to explain long-term shoreline change, and these result from gradients in breaking wave height and angle, and/or changes in the shoreline orientation relative to the incoming waves (Hanson and Kraus, 1989; Ashton *et al.*, 1999; Valvo *et al.*, 2006). Dolan *et al.* (1977) reported this correlation between shoreline orientation and long-term change rate and areas prone to storm-overwash along the length of Assateague Island. In microtidal settings, such as Assateague Island, long narrow wave-dominated barriers typically extend for tens of kilometers until cut by ephemeral and migrating inlets. Further south along the Delmarva Coastal Compartment, discontinuous barriers (~1-10 km in length) extend for 80 km to Cape Charles at the Chesapeake Bay mouth; these mixed-energy barrier islands, starting at Wallops Island, are more susceptible to the influence of inlet processes and sediment starvation (Oertel and Kraft, 1994). Recurved spits and complex shoals typically form where inlets interrupt barrier islands, redirecting sediment by a combination of refracting waves, strong flood-tidal currents, and sediment bypassing (Hayes, 1980). This combination of processes often leads to characteristically complex shoreline change signals over both the long and short term (Fenster and Dolan, 1996). Approximately 35 kilometers of shoreline downdrift of and offset from Assateague Island are affected by sediment trapping at Chincoteague Inlet, and the entire embayment has been labeled an erosional hotspot (Kraus and Galgano, 2001).

A variety of seasonal or annual processes (<10 years), such as climatic cycling and human interventions, may lead to shorter-term deviations from the long-term record of shoreline change (Hobbs *et al.*, 1999; Stive *et al.*, 2002). Shoreline change signals may also reflect inter-annual and seasonal changes in wave climate, showing cyclic erosion

and accretion on the order of ten meters (Pajak and Leatherman, 2002). Superimposed on this template is infrequent and unpredictable shoreline change that results from storms (Morton *et al.*, 2003). Individual storms, like the 1962 Ash Wednesday storm, cause the equivalent change of 50 to 60 years of shoreline retreat in a matter of days (Fenster *et al.*, 2001; Honeycutt *et al.*, 2001).

## 2.2 *Framework Geology and Shoreline Behavior*

In transgressive coastal settings, a complete understanding of shoreline behavior necessitates the consideration of the shallow geologic framework: the near-surface stratigraphic units, internal architecture of those units, and geomorphology coupled with the surficial sedimentary cover (Figure 3) (Harris *et al.*, 2005). Numerous studies have shown that the geologic framework can affect shoreline evolution over various spatial and temporal scales given the landward translation over antecedent highs and lows, differential erosion of projected and underlying sediments, and complex morphodynamic coupling on a heterogeneous shoreface, all of which may lead to variations in bathymetry, sediment erodability, and coupled bottom boundary layer processes (Demarest and Leatherman, 1985; Riggs *et al.*, 1995; Schwab *et al.*, 2000; Honeycutt and Krantz, 2003; Locker *et al.*, 2003; Wright and Trembanis, 2003; McNinch, 2004). This study operates in that same vein, first mapping the morphology and shallow stratigraphy of the geological framework, and then attempting to quantitatively relate alongshore variability in geology to shoreline change.

The shoreface along the Mid-Atlantic Bight is typified by a thin veneer of reworked sand superimposed over variable units ranging from mud to sedimentary rock (Riggs *et al.*, 1995). As a result, the antecedent topography often shapes barrier evolution

and morphology as the underlying geology is overridden, intersected, and exhumed by ongoing transgression (Belknap and Kraft, 1985; Foyle and Oertel, 1992). This is especially true along the mixed-energy Eastern Shore barriers where tidal inlets coincide with a paleo-drainage network incised during lower sea levels and adjacent barriers are perched and move landward over intervening Pleistocene topographic highs (Demarest and Leatherman, 1985). On smaller spatial scales, unconsolidated, often poorly sorted inlet fill sequences in wave-dominated settings may erode faster than the adjacent armored sand shoreface and contribute mixed-grained sediment to the littoral system (Pilkey *et al.*, 1993); this may be a relevant phenomena on the shoreface of Assateague Island where numerous inlets have opened and closed over the historic period (McBride, 1999). Or, as in the case of the Delaware headland beaches, shoreface outcropping units of relict shorelines can be a significant sand source for modern barriers (Demarest and Leatherman, 1985). Cohesive muds, which commonly outcrop on the shoreface or occur in the shallow subsurface, may directly retard shoreface erosion compared to adjacent sandy sediment because of reduced erodability (Riggs *et al.*, 1995; Schwab *et al.*, 2000).

Many of these research efforts have qualitatively linked specific geology to observed shoreline change patterns. Riggs *et al.* (1995) reported increased shoreline erosion where relict Holocene sandy channels outcropped on the shoreface, compared to shoreface underlain by relatively more resistant estuarine sediments. Schwab *et al.* (2000) indicated that the most stable part of Fire Island, New York was landward of a field of shoreface-attached ridges. The authors surmised that onshore sediment flux from these sand ridges, linked to the erosion of outcropping, relict headland, provided enough additional coarse sediment to locally maintain island stability. Honeycutt and Krantz



(2003) suggested that the varying erodibility of exposed underlying Holocene and Pleistocene sedimentary units along the Delaware resort beaches contributed to slower rates of erosion and shoreline change patterns on the spatial scale of the controlling geology.

Mapping the nearshore Quaternary stratigraphy of the Delmarva Peninsula, as has been done north and south of study area by Toscano *et al.* (1989) and by Foyle (1994), presumably holds important, but unexplored implications for shoreline behavior. Figure 4 shows the expected stratigraphic sequence of Holocene transgressive sands and backbarrier deposits overlying a range of Pleistocene incised valley fill, transgressive shelf sands, and regressive shelf interbedded muds and sands as mapped on the Maryland and Virginia inner shelves. In these neighboring areas, a ubiquitous erosional surface underlies the actively transported and reworked Holocene sands of the shoreface sand sheet and sand ridges of the inner shelf along the Delmarva Peninsula (Kraft, 1971; Foyle and Oertel, 1992; Toscano and York, 1992). This wave ravinement, resulting from the lowering of the shoreface by storm wave and longshore current erosion, marks the gradual landward progression of the shoreface in response to sea level rise (Swift, 1968). The preserved ravinement is a disconformity representing the hiatus between erosion and the subsequent accumulation that constitutes the prismatic mantle of shoreface sands. On the shallow shoreface, the ravinement surface, which has not reached its final depth, can be more complex given the greater frequency of erosional events in shallower water, and therefore, it should only be considered a proto-ravinement (Swift *et al.*, 2003). Major storm events (*e.g.*, 1991 Halloween Storm) may locally strip the entire mantle of overlying sand and resume deepening of the ravinement; this is particularly true in the

longshore trough and bar region of the profile (Niedoroda *et al.*, 1985; Swift *et al.*, 2003; Schwartz and Birkemeier, 2004). Schwartz and Birkemeier (2004) have reported that ravinement incision on the lower ramp of the shoreface also occurs during fair weather, when cross-shore transport is typically characterized by erosion and onshore flux of lower ramp sands. The preserved ravinement on the lower shoreface generally separates shoreface/nearshore sediment from backbarrier, lagoonal, and inlet-channel fill sediments (Belknap and Kraft, 1985; Demarest and Kraft, 1987; Toscano and York, 1992; Foyle and Oertel, 1997; Schwartz and Birkemeier, 2004). Further offshore is generally the depth where erosional shoreface processes no longer rework underlying lithosomes (Cattaneo and Steel, 2003).

Despite a vast body of regional work, only one study in Delaware has actually evaluated the relationship between framework geology and shoreline change (Honeycutt and Krantz, 2003). This study explores the spatial and temporal scales at which geology may influence shoreline change by linking the two variables with geostatistics. An innovative way of linking geologic framework to shoreline change requires the estimation of sediment available for transport over relevant time scales (Locker *et al.*, 2003; Miselis and McNinch, 2006). This method, which presumes topographic coupling between modern and near-surface underlying geology, requires the delineation of both the lower boundary (*i.e.*, transgressive ravinement / proto-ravinement) and upper boundary (*i.e.*, seafloor) of the nearshore sand prism. The resulting cross-shore volumetric prism is treated as a composite of the transported sediment load for the modern system (Schwartz and Birkemeier, 2004). Miselis and McNinch (2006) defined the prismatic sand thickness as the distance between the seafloor and ravinement in high

resolution seismic data and showed that inter-centennial shoreline change for the northeastern Outer Banks of North Carolina was positively correlated with nearshore sediment volume, calculated between the ~3 m and ~11-12 m isobaths. Simply put, an absent or relatively thin sand cover corresponded to shoreline reaches undergoing erosion. This research adopts and applies a similar methodology to demonstrate the correlation between surface geology and shoreline change.

### 2.3 *Nearshore Morphology and Shoreline Behavior*

Coastal systems exhibit significant three-dimensional morphology indicating alongshore variability in planform, sediment distribution, and underlying geology (Komar, 1998). These variations may include active and relict shore-parallel bars, shore-oblique and transverse bars, shoreface-attached ridges, spit platforms and shoals, ebb tidal deltas, and outcropping semi-lithified sedimentary units. Nearshore morphology has been associated with inlet retreat paths, seafloor exposure of variable lithology of inlet-related facies, interactions between the coarse lithology of underlying paleochannel deposits and hydraulic regime, and hydrodynamic processes (McBride and Moslow, 1991; Snedden *et al.*, 1994; Trowbridge, 1995; Browder and McNinch, 2006). The resultant <0.5-10 km scale perturbations in nearshore bathymetry are often coupled to wave-related phenomena and may influence alongshore susceptibility to shoreline change (Maa and Hobbs, 1998; Nittrouer and Wright, 1999; Maa *et al.*, 2004; Houser *et al.*, in press). The rhythmic nature of nearshore morphology would presumably be echoed in transport pathways and shoreline change patterns, as wave energy is focused along the coast at specific alongshore wavelengths, producing adjacent eroding and accreting sections (Dolan *et al.*, 1977). Bender and Dean (2003) discuss how complex nearshore

morphology can modify the local wave field via refraction, diffraction, reflection, and dissipation, all of which can affect alongshore gradients in wave energy and coupled wave-current sediment transport. This local exchange of sand between the inner shelf, shoreface, and subaerial beach is imprinted on large-scale fluxes induced by regional shoreface gradients, wave exposure, and coastal flows (Swart and Calvete, 2003).

This study differentiates between the nearshore geology and morphology of the geologic framework, which are inherently related by the seafloor surface, but set apart by the subsurface geometry and textural composition. The approach to refocus solely on bathymetry may help to evaluate whether a stronger coupling exists between nearshore morphology and shoreline change over smaller alongshore length and shorter time scales, suggesting wave transformation may play a more prominent role. Along the Mid-Atlantic Bight, Kochel *et al.* (1985) reported that distinctive modes of regional variation in shoreface and inner shelf profile were related to regional differences in wave climate, tidal range, and sediment characteristics. Wave efficiency, in particular, is related to shoreface slope through dissipation (Storms *et al.*, 2002). Larson *et al.* (2000) used canonical correlation analysis on decadal time series of wave and profile data from Duck, North Carolina to show that profile shape and response were in fact strongly correlated with transformed nearshore wave properties and energy dissipation. The authors differentiated between nearshore wave and offshore deep-water wave characteristics, showing a substantially stronger correlation between profile shape and response with transformed waves. Profile shape and morphodynamic state are also sensitive to energetic interaction with cross-shore variations in surface and source grain size, where coarser sediments correspond to steeper, more reflective profiles (Benedet *et al.*, 2004).

Large scale bedforms or nearshore sand ridges represent the most significant morphology and sediment source on the inner shelf of the Delmarva Peninsula (Duane *et al.*, 1972; Swift *et al.*, 1972, Toscano and York, 1992). Shoreface-connected ridges, typically superimposed with smaller-scale sand waves and ripples, start on the shoreface, vary in height from 1 to 6 m in 4 to 30 m water depths, and extend seaward, with alongshore wavelengths of  $\sim 5$  km, forming their characteristic angle of 20-35 degrees with respect to the shoreline (Dyer, 1999; Calvete *et al.*, 2001). The slightly asymmetric ridges, characterized by a steeper seaward flank, migrate alongshore  $\sim 1-10$  m/yr in the direction of longshore transport. The long axis of the ridge is oriented perpendicular to the dominant storm wave approach. Textural partitioning between the trough, crest, and flank is another characteristic feature (Swift and Field, 1981). Inner shelf ridges, detached from the landward-retreating shoreface, exhibit relief up to 10 m and lengths of tens of kilometers. These ridges may be incorporated into shoal-retreat massifs, large scale cape-related features deposited over the Holocene transgression along a common retreat path dictated by longshore convergence and enhanced by wind-driven and tidal-driven circulation (Swift, 1975; Finkelstein, 1983; McNinch and Leuttich, 2000).

The sand ridges are largely considered to be post-transgressive expressions of modern shelf and shoreface processes showing a response related to alongshelf storm currents interacting with a local bathymetric irregularity (Swift and Field, 1981; Swift *et al.*, 1985; McBride and Moslow, 1991; Trowbridge, 1995; Snedden and Dalrymple, 1999). The McBride and Moslow (1991) model supposes that the ridges developed from tidal inlet deltas and owe their oblique orientation to the combined processes of inlet migration and shoreface erosional retreat. Regardless of the initiating mechanism (*i.e.*,

“forced” or “free”), the shelf hydrodynamic regime, offshore deflection of storm-driven alongshore flows at ridge crests and convergence of sediment flux, in less than 20 m is generally considered essential for shaping active sand ridge features (Trowbridge, 1995; Calvete *et al.*, 2001; Lane and Restrepo, 2007; Vis-Star *et al.*, 2007). The recent application of the Mike 21 Boussinesq wave model to investigate the maintenance and evolution of detached sand ridges suggests a more simple interaction between crossing waves refracted by shoaling bottom topography. Waves converging over the sand ridge crest from a dominant wave approach lead to convergence of sediment transport in the direction of wave propagation (Hayes and Nairn, 2004). In this model, the net transport direction is determined by the balance between on-shore transport driven by asymmetric wave orbitals and offshore current flow opposite the direction of wave propagation.

A range of research has focused on shoreface-attached and detached sand ridges along the Mid-Atlantic Bight coast, but only a few of these studies have considered the effect of nearshore sand ridges on shoreline change. Moody (1964) and Goldsmith (1976) reported that alternate zones of wave convergence and divergence developed due to refraction over offshore detached ridge and shoal topography along the Delaware and Virginia coasts on the Delmarva Peninsula, contributing to alongshore variability in wave heights and possible shoreline change patterns. Wave transformation modeling over detached shoals ~5-10 km offshore of Delaware, Maryland, and Virginia show distinct patterns of convergence and enhanced wave heights along the coast, especially for long-period storm waves that may undergo shoaling and break on the shoals (Maa and Hobbs, 1998; Maa *et al.*, 2004). Conversely, areas of extensive wave height attenuation may also occur from depth-induced shoaling and breaking as waves pass over offshore shoals. In

Delaware, zones of convergence have also been documented to occur consistently and immediately north of shoreface-attached sand ridges (Moody, 1964). Dolan *et al.* (1979) contested this notion, showing the lack of correlation between shoreline change and shoal occurrence periodicities. However, their spectral analyses may have failed to show correspondence given that the shoals generally considered were further offshore and not as likely to have a direct morphological effect on the coastline except in extreme sea states dominated by long-period waves. Attached ridges off Fire Island, New York and shore-oblique bars off the Outer Banks, North Carolina have been quantitatively and qualitatively related to shoreline change (Schwab *et al.*, 2000; Schupp *et al.*, 2006). Storm waves shoaling over sand ridges and focusing energy over limited shoreline extent and/or interactions between nearshore bars and sand ridges allowing longshore bars to withstand storm attack more efficiently are possible mechanisms used to explain observed shoreline behavior (Schwab *et al.*, 2000). Smith and Ebersole (1997) used the REF/DIF numerical model to show that erosional hotspots and adjacent cold spots (*i.e.*, zones of accretion) along the nourished beach at Ocean City, Maryland developed in response to wave transformation over irregular nearshore bathymetry, and zones of erosion were co-located with longshore transport divergence near the shoreface-attachment of linear sand ridges. This study supplements the previous efforts testing the scale and strength of alongshore coupling between morphology and distinct shoreline change and how that relationship varies over time.

## 3 STUDY AREA

### 3.1 *Geologic Setting*

The Virginia Coastal Plain and inner shelf of the Mid-Atlantic Bight overlie the Salisbury Embayment, a sedimentary basin located between the South New Jersey Arch and Norfolk Arch (Foyle and Oertel, 1997). These structural highs and the intervening basin directly influenced the Tertiary and Quaternary stratigraphic development along the Mid-Atlantic coast. High-frequency Pleistocene glacioeustatic cycles have contributed to a complex, largely transgressive stratigraphy, first as a reworking of deltaic deposits then as a southern progression of highstand megaspits (Accomack and Nassawadox sequences). These megaspits constitute the core of the Eastern Shore of Virginia (Hobbs, 2004). A Tertiary-age unconformity (see Figure 6) marks the base of the Pleistocene section and deepens north to south, resulting in maximum Pleistocene thicknesses varying from 12 to 40 m from Ocean City, Maryland south to Cape Charles, Virginia (Mixon, 1985; Toscano *et al.*, 1989; Foyle, 1994).

The Quaternary stratigraphy preserved beneath the inner shelf of Maryland and Virginia is highly variable and includes incised valley fill, transgressive shelf sands, and regressive shelf interbedded muds and sands (Figure 4) (Toscano and York, 1992; Foyle, 1994). The Maryland section is generally much thinner since it developed on the oceanic side of Tertiary deltaic systems that formed the core of the Delmarva Peninsula beneath Maryland and forced Pleistocene lowstand fluvial networks south (Figure 4A) (Foyle and Oertel, 1992; Foyle and Oertel, 1997). The modern sand sheet discontinuously overlies late Pleistocene channel fill, early Holocene fluvial-estuarine deposits, and late Holocene tidal inlet-related, backbarrier, and lagoonal facies (Toscano *et al.*, 1989; Foyle, 1994).



The landward barriers are believed to have occupied their present position less than six thousand years ago (Oertel and Kraft, 1994).

This study focuses on the barrier reach of Assateague Island and Wallops Island along the northernmost part of the Eastern Shore of Virginia (Figure 1). Assateague Island, extending 60 km from Ocean City Inlet, Maryland south to Chincoteague Inlet, Virginia, is the last microtidal, wave dominated barrier of the Delmarva Coastal Compartment. Assateague Island varies in width from 300 m at its northern end to over 2 km at its southern end, whereas island elevations range from < 2 m along washover fans up to 10 m high along dunes (Schupp *et al.*, 2007). The U.S. Fish and Wildlife Service and National Park Service co-manage the Virginia segment of the Assateague Island National Seashore. Immediately to the south of Chincoteague Inlet and offset 5 km to the west, the 11 km long, mixed-energy Wallops Island, managed by NASA and maintained as the Wallops Island Flight Facility, marks the boundary between microtidal and near mesotidal conditions (Finkelstein, 1983). Wallops Island varies in width from about 2.1 km at its north end to about 0.2 km at its southern limit (Moffat and Nichol, 1986). The barrier has an average elevation of 2.1 m (Moffat and Nichol, 1986), making the \$800 million of launch facility assets on the island particularly vulnerable to damage from storm inundation. The U.S. Fish and Wildlife Service also manage the southern end of the island as the Wallops Island National Wildlife Refuge.

The southernmost 15 km of Assateague Island developed as a series of prograding spits overlapping pre-existing Holocene barriers, Chincoteague Island, Pitts Island, and Pope Island, and contributing to an extensive offshore shoal complex, Chincoteague Shoals (Figures 1 and 5) (Goettle, 1981). Harris (1992) surmised that this 'regressive',

late Holocene event, also observed in distinct rotational changes in beach ridges on Parramore, Cobb, and Hogg Islands further south, may be related to ephemeral sea level fluctuations and or wave climate. The modern Assateague Island is presently offset approximately ~1-2 km seaward of the late Holocene barriers. The Assateague Channel of Chincoteague Inlet presently separates Assateague and Chincoteague Islands. Assateague/Morris Inlet (a precursor to Assateague Channel) apparently cut through present day Assateague Island at the northern end of Chincoteague Island during the colonial period evidenced by Chincoteague Island's northern truncated dune ridges and preserved flood tidal delta mounds incorporated into Assateague Island (Figure 2) (Kochel and Wampfler, 1989). Over the last three centuries, Chincoteague, Assateague/Morris, Ragged Point, Pope Island, and Green Run Inlets (not shown) also opened to Chincoteague Bay (see Figure 22) (Bartberger, 1976; Halsey, 1978; Kochel and Wampfler, 1989; McBride, 1999). The latest closure of historic inlets, Green Run (MD) Inlet and Pope Island Inlet (VA), in the late nineteenth century, timed with the onset of erosion at Bethany Beach (DE) headland, and subsequent erosion of the abandoned ebb tidal deltas may have contributed to the coalescing of barrier islands, growth of the Fishing Point spit, and offshore Chincoteague Shoals complex (Oertel and Kraft, 1994; McBride, 1999; Honeycutt and Krantz, 2003).

The southern end of Assateague Island is the terminus of a regional longshore sediment transport system (75 km) that moves upward of  $10^6$  m<sup>3</sup> of sediment south along the Delmarva coast (Headland *et al.*, 1987; Oertel and Kraft, 1994). Shoreface and continued erosion of the headland at Bethany Beach in Delaware contribute sand to a system only interrupted by Ocean City Inlet (Demarest and Leatherman, 1985).

Successive years of moderately intense storms and fair-weather conditions result in slow aggrading of the shoreface, until a major storm strips the shoreface and transports large volumes of fine-grained sand offshore in downwelling flows (Swift *et al.*, 1985; Wright *et al.*, 1994). The nearshore shelf is floored by a discontinuous sheet of fine to medium sand molded in linear sand rides and swales, ~1-10 m in height, ~2-4 km apart, and up to tens of kilometers into length (Swift and Field, 1981; McBride and Moslow, 1991). The swales between ridges, upcurrent flanks, and upcurrent shoreface generally erode, whereas ridge crests and downcurrent flanks tend to accrete over centennial scales (Swift and Field, 1981). Offshore of the accreting reach of the Fishing Point spit complex, a series of subparallel and curvilinear sand ridges and subaqueous shoals (Chincoteague Shoals) are located in depths of 2-5 m. The sand ridges disappear abruptly in a featureless basin in the southern lee of Assateague Island. Wave refraction around Fishing Point and the Chincoteague Inlet ebb-tidal delta has contributed to bypassing around the ebb tidal delta and a local reversal in longshore transport and accretion at Gunboat Point, Wallops Island. The shoal and inlet complex serves as an extremely efficient sediment trap, allowing only about 5% of longshore transport to bypass to the south (Moffat and Nichol, 1986).

### 3.2 *Physical Setting*

On the Atlantic side of Chincoteague Inlet, tides are semidiurnal with a mean range of 1.1 m. Predominant winds are from the northwest to northeast leading to easterly and northeasterly waves. The mean deepwater significant wave height in the area is  $1.0 \pm 0.6$  m with a corresponding period of  $6.0 \pm 2.7$  s (WIS Hindcast Waves, 1980-1999, [http://frf.usace.army.mil/cgi-bin/wis/atl/atl\\_main.html](http://frf.usace.army.mil/cgi-bin/wis/atl/atl_main.html)). Maximum significant wave

height and period hindcast over the same period is approximately 6 m and 11 s. A large gradient in the angle of wave approach relative to the local shoreline orientation, coupled with wave sheltering by the recurved spit, leads to reduced wave power along northern Wallops Island and the east-west oriented leg of Fishing Point (Moffat and Nichol, 1986). The wave regime is also subject to strong seasonal variations in energy and approach, punctuated by northeasters and hurricanes (Figure 1). Extratropical storms, most frequent in the fall and winter, are primarily responsible for the most significant coastal erosion (Dolan *et al.*, 1988; Oertel and Kraft, 1994). Tropical storms occur less frequently, usually between June and November, and many years pass without significant activity (Kochel and Wampfler, 1989).

## 4 METHODOLOGY

### 4.1 *Shoreline Change Statistics*

Shoreline Movement Maps, T-sheets, aerial photography, and Global Positioning System (GPS) field surveys were used to determine historical shoreline positions (Table 1). Paper Shoreline Movement Maps, featuring 6 high water line (HWL) shoreline positions between 1850 and 1980, were scanned and rectified using at least six control points per 1:24,000 quadrangle. As detailed by Everts *et al.* (1983) and Anders *et al.* (1990), these shorelines were compiled from historic U.S. Coast and Geodetic Survey (CGS) T-sheets and 1980 National Ocean Service aerial photography, plotted, and digitized at a common scale and projection. A 1915 HWL shoreline for Assateague Island was digitized from a scanned and rectified inked mylar T-sheet (T-3533) provided by the National Oceanic and Atmospheric Administration (NOAA) Coastal Services Center. This historical shoreline dataset was supplemented with shorelines mapped using the visible wet/dry line in orthophotography acquired in 1994, 2002, and 2005 by the U.S. Geological Survey (USGS) National Mapping Program, Virginia Base Mapping Program, and U.S. Department of Agriculture (USDA) National Agriculture Imagery Program. Biannual GPS surveys of the high water line along Assateague Island, collected by National Park Service (NPS) personnel between 1997 and 2005, were incorporated into the shoreline database. The shoreline surveys were collected using a Trimble ProXR® GPS mounted on an ATV, corrected real-time using differential signals from Annapolis, MD or Driver, VA, and post-processed using regional Continuously Operating Reference Stations.

Shoreline vectors were digitized on-screen in a GIS environment, converted to a common horizontal datum and projection, and organized into a single geodatabase to facilitate shoreline change analysis (Figure 5A). The Digital Shoreline Analysis System® (DSAS) was used to calculate rate-of-change statistics at 50-m alongshore intervals cast from a shore-parallel baseline (Thieler *et al.*, 2005). Shoreline position data was fit with a least squares regression for long-term (1850-2005), decadal (1980-2005), and inter-annual (1997-2005; Assateague Island only) time intervals. Shoreline change rate (S) was calculated as:

$$S = \frac{\sigma_{xy}}{\sigma_{xx}}$$

where  $\sigma_{xy}$  is the sample covariance ( $\sigma_{xy} = \frac{1}{N} \sum_{i=1}^N (X_i - \bar{X})(Y_i - \bar{Y})$ ) between dates (X) and corresponding shoreline positions (Y), and  $\sigma_{xx}$  is the sample variance of the shoreline dates ( $\sigma_{xx} = \frac{1}{N} \sum_{i=1}^N (X_i^2 - \bar{X}^2)$ ). Short-term shoreline variability, or shoreline mobility, was calculated as the standard deviation of the mean shoreline position using the 1997-2005 shorelines (Figure 5B).

Total shoreline position uncertainty incorporates all measurement and position bias errors including source error, rectification error, shoreline position error, and digitization error (Table 2). Measurement and positional factors contributing to uncertainty were determined from published records (Anders and Byrnes, 1991; Crowell *et al.*, 1991; Thieler and Danforth, 1994; Galgano *et al.*, 1998; Moore, 2000; Daniels and Huxford, 2001) and the calculation of root mean square (RMS) values (*i.e.*, measures of the misfit between map points and control points). The accuracy of the Shoreline

Movement Maps is documented to meet National Map Accuracy (NMA) Standards, with a worst case error estimate of 10 m (Everts *et al.*, 1983; Anders *et al.*, 1990). The T-sheet survey source error incorporates all errors associated with the mapping process including distance to rodded points, plane table position, and identification of HWL (Shalowitz, 1964), and NMA Standards prescribe an accuracy of  $\pm 10.4$  m for 1:20,000 T-sheets. Total RMS error for the rectification process for Shoreline Movement Maps and T-sheets was maintained below 1 pixel, which is the near equivalent of 5 m. Measurement uncertainty in aerial photography is related to resolution, rectification, and on-screen delineation of the high water line (Table 2). GPS shoreline position is estimated to be accurate to within 1.5 m, but field interpretation of a shoreline indicator may contribute additional positional measurement error (Morton *et al.*, 1993).

The total uncertainty ( $E_{total}$ ) may be represented by summing in quadrature:

$$E_{total} = \pm \sqrt{E_{source} + E_{rectification} + E_{position} + E_{digitization}}$$

Confidence intervals ( $C_i$ ) characterizing measurement and sampling error were determined at the 90% confidence level. The statistical significance of each rate was also determined at the 90% confidence level.

#### 4.2 Characterization of Nearshore Morphology

Two legacy hydrographic surveys (1933/1934, 1978/1982), available from the NOAA National Geophysical Data Center (NGDC), were used to create bathymetric digital elevation models (DEM) (Table 3) and characterize nearshore morphology and morphologic change. Bathymetric data were transformed from Geographic NAD27 datum to Universal Transform Mercator NAD83 datum, and supplemented with contemporaneous shoreline data assigned a fixed elevation height using the average

vertical reference difference ( $0.59 \pm 0.12$  m) between MLW and MHW measured at regional NOS tidal benchmarks and corrected for sea level rise (4 mm/yr). DEMs, with a grid spacing of 25 m, were created using the Surfer® kriging module with an anisotropic linear variogram and smoothed using a gaussian low-pass filter.

Measurement and gridding errors present in each bathymetric DEM can be estimated by comparing elevations at closely spaced, adjacent survey lines (Byrnes *et al.*, 2002). Multiple sets of 10-km line pairs, approximating survey trackline spacing and characterizing the range of surface irregularities, were compared for each modeled bathymetric surface. Variations in elevation between line pairs were linearly interpolated at 5-m intervals, and the absolute values of the differences were averaged to calculate the potential uncertainty for each pair (Table 4). Line pair uncertainty values were then averaged for each surface to estimate potential uncertainty associated with each data set. The RMS of these average values (0.57 m) is the minimum detection level of change when comparing the two surfaces. Volume change calculations were made in Surfer® by differencing bathymetric grids and then integrating those elevation differences over morphologically similar provinces (between the contemporaneous shoreline and 10-m isobath) using the trapezoidal rule.

Empirical Orthogonal Functions (EOF), or eigenfunction analysis, was used to quantify and contrast the cross-shore and alongshore variability in nearshore bathymetry. The eigenfunction analysis reduces the number of variables required to represent the variation in the data, such that the variance explained in each successive mode decreases exponentially (Wijnberg and Terwindt, 1995; Larson *et al.*, 2003). Depth values were extracted from the 1978/1982 bathymetric DEM at 25-m intervals from the 4-m isobath



to a point 2-km seaward (<12 m) along cross-shore transects spaced 50 m. The bar-trough region was not included in the analysis since the source data was sparse in that cross-shore zone. Moreover, data were clipped to an alongshore province that excluded the highly complex bathymetry unique to the Fishing Point spit platform (< N4191800) and Chincoteague Inlet ebb tidal delta (> N4191800). Eigenfunctions were calculated from two data matrices construed of cross-shore depth values, one for Assateague Island and one for Wallops Island. A custom script was developed in Matlab® to perform the mathematical operation, a technique explained in further detail by Wijnberg and Terwindt (1995). The first eigenfunction, unless data are demeaned, is the mean cross-shore profile shape. Eigenfunction weightings, which quantify how each eigenfunction compares to the actual profile shape at each transect, can be used to characterize the alongshore variation in bathymetry. Although alongshore bathymetric variation could be parameterized using eigenfunction weightings, a more intuitive metric was devised to characterize the variability in shallow nearshore morphology for use in subsequent correlation analyses. The elevation gradient (m/m) was calculated at each cell location in the 1978/1982 bathymetric DEM using the directional derivative function in Surfer®. Mean slope and the standard deviation of the slope were determined over normalized cross-shore distances, using the same transects as used in the eigenfunction analysis.

#### *4.3 Geophysical Mapping and Seismic Stratigraphy Characterization*

Over 400 kilometers of geophysical data were collected along the inner-shelf off southern Assateague Island and Wallops Island in June 2004 and May 2005 (Figure 6). An Edgetech® sub-bottom profiler (with a swept-frequency range of 500 Hz – 12 kHz, variable pulse setting providing ~20 cm of theoretical vertical resolution) was towed to

image the shallow stratigraphy. An Edgetech® side-scan sonar (100 kHz, 300-m swath) was towed to collect backscatter data to support seismic interpretation and infer surface sediment texture. Acquisition lines generally covered from approximately 250 m offshore (~4 m depth) to approximately 5 km offshore (~15 m depth) at approximately 1-km alongshore intervals. All data were spatially referenced using GPS corrected real-time using differential signals from Annapolis, MD or Driver, VA. Side scan sonar data collected off Wallops Island were corrupted in a hard drive failure.

SonarWeb Pro® was used to process geophysical data, differentiate seismic units, and export the location of preserved channel cut-fill and inlet-related facies. Seismic units were delimited based on continuous reflection relationships, internal seismic reflection characteristics, side scan sonar backscatter, and legacy sedimentological data. Nearshore thicknesses of the Holocene sand cover were calculated by comparing the elevation difference between the seafloor and interpreted ravinement / proto-ravinement reflection in the seismic data (Figure 7). Estimates of depth to reflectors and thickness of units were computed using a p-wave velocity of 1500 m/s.

The 2004/2005 point elevation differences between the seafloor and ravinement were subtracted from co-spatial point elevations derived from the 1978/1982 bathymetric DEM and used to model the ravinement surface at 250-m alongshore spacing and 25-m cross-shore spacing (within the overlapping boundaries of both datasets) using the Surfer® kriging module with an anisotropic linear variogram. The ravinement surface was interpolated to uniform 25-m spacing and then differenced from the bathymetric DEM to determine nearshore sand thickness. The thickness isopach was clipped to a polygon encompassing the footprint between the 4-m isobath and 8-m isobath (*i.e.*, long-term

depth of closure). Cross-sectional volumes ( $\text{m}^3/\text{m}$ ) were integrated using the trapezoidal rule at the same alongshore intervals. The resultant thickness isopach *may locally underestimate or overestimate* the volume of sand found given the potential inaccuracy in the selected speed of sound, the alongshore migration of sand bodies over the near 25-year interval occurring between the collection of new seismic and legacy bathymetry surveys, and/or the horizontal and vertical data density/resolution differences between the seismic and bathymetry data. Qualitative comparison of seismic and bathymetric data indicated that shoreface-attached shoals generally migrated ~250-500 m to the south over the near 25-year interval. Uncertainty estimates in the thickness isopach were not calculated.

#### 4.4 *Cross-correlation Analysis*

Cross-correlation analysis was used to compare spatial trends in shoreline change, nearshore morphology, and nearshore volume across different time intervals. Cross-correlation tests the linear relationship between two changing series over a range of alongshore lags (*see Appendix* for a more detailed description). In the presence of non-stationarity (*i.e.*, trend) and autocorrelation (*i.e.*, spatial/temporal dependence), untreated cross-correlation coefficients can be misleading as a measure of statistically significant relationships since the measures violate the classical assumption of randomness and serial independence (Chatfield, 2004). The data analyzed were characterized by significant trend and exhibited statistically significant autocorrelation over length scales up to approximately 2 km. Adjusting the sample size ( $N$ ), or computing the effective sample size ( $N^*$ ) for hypothesis testing, helps to address the effect of autocorrelation on statistical significance, but does not account for inherent trend. The effective sample size

(N\*) for hypothesis testing was approximated using the following formula to estimate effective sample size:

$$\frac{1}{N^*} \approx \frac{1}{N} + \frac{2}{N} \sum_{k=1}^{N/5} r_{xx}(k)r_{yy}(k)$$

where  $r_{xx}(k)$  and  $r_{yy}(k)$ , autocorrelations as a function of lag  $k$ , are scaled by  $N/(N-k)$ . Given  $N^*$ , the critical value of  $r_{xy}$  at any significance level ( $\alpha$ ) can be derived using the  $t$  distribution. A conservative  $N^*-2$  degrees of freedom were used to determine the critical value for each test (Pyper and Peterman, 1998). Cross-correlation testing was performed using the `xcov` function in Matlab®. Since this analysis is not uniquely sensitive to correlations at multiple alongshore length scales (*i.e.*, data autocorrelated at multiple length scale), the analysis was run on both untreated and treated (residuals of multi-order polynomial fits to the untreated data) data series in an attempt to address the multiple length scales inherent in the data.

## 5 RESULTS

### 5.1 *Variability in Shoreline Change*

Figures 8 and 9 show shoreline change data, calculated using linear regression, for southern Assateague Island and Wallops Island over discrete time intervals: long-term (>75 yrs), decadal (~25 yrs), and inter-annual (~10 yrs). Long-term and shorter-term shoreline change data along Assateague and Wallops Islands exhibit fairly analogous patterns of erosion and accretion superimposed on a north-south erosional trend. Shorter-term shoreline change data show elevated erosion rates along both barrier islands, larger spatial scales affected by erosion, and increasing shoreline change variability approaching Chincoteague Inlet. Significant reversals across time scales generally occur only in close proximity to Chincoteague Inlet along Fishing Point and Gunboat Point. Short-term shoreline mobility, calculated from inter-annual data for Assateague Island, repeats the strong north-south gradient, where shoreline position variability tends to increase with erosional trends and proximity to the spit complex (Table 5; Appendix).

#### Assateague Island

The long-term rate for the northeast-southwest oriented shoreline of Assateague Island is slightly erosional, averaging -0.8 m/yr. Zones of shoreline retreat and advance alternate south towards Fishing Point where shoreline change signals grow increasingly large and variable (Figure 8). The present-day subaerial character of the island mimics this in morphology, changing from a wider, dune-lined, stable reach (12 km) (Figure 2) to a narrowing, overwash-dominated, unstable reach (5 km) before transitioning again into the south-southwest welding bars and accreting beach ridges of the spit complex (Figure 10) (Kochel and Wampfler, 1989). Progressive straightening has occurred along the

northeast-southwest oriented shoreline (Figure 8). Nonetheless, distinct undulations in orientation persist adjacent to shoreface-attached sand ridges north of a definitive, concave arc that corresponds to the seaward location of the relict, recurved spits (Morris Island south to Assateague Point). The long-term zone of accretion is immediately to the north of this seaward extending arc. About 6 km north of present-day Fishing Point, the shoreline orientation begins a marked transition from  $<30^\circ$  from N to  $>100^\circ$  from N at the southern terminus of the island. Fishing Point spit has extended south nearly 6 km at historical rates upwards of 25 m/yr from the Assateague Point recurved spit that marked the end of the island in the 1850s and continues to grow at comparable rates ( $>25$  m/yr) at the south end by progressive welding of bars (Figure 5A). Severe erosion, with long-term rates exceeding 5 m/yr and inter-annual rates approaching 10 m/yr, has occurred along the low-profile, washover-dominated arm that connects Fishing Point to the relict Assateague Point spit (Figure 10). This segment is presently undergoing rapid narrowing, making it particularly susceptible to breaching and overwash. Only erosion rates along the northern end of Assateague Island, exacerbated by the construction of jetties at Ocean City Inlet, are distinguished by similar magnitudes (Kochel and Wampfler, 1989). Historically, the recurved spit tips diverted Assateague Channel and Chincoteague Inlet to the southwest towards Gunboat Point on Wallops Island. Presently, the alongshore zone of inlet and accreting spit influence is generally limited to the west-east oriented shoreline of the spit. Over the past decade, the westward tip of the spit has been retreating northward at rates exceeding 40 m/yr, and in the early spring of 2005, a short-lived breach of Fishing Point occurred (Gregg Williams, *personal communication*).

In comparison, shoreline position along the northernmost 15 km of the study area appears relatively stable over the entire 150 years considered, showing little evidence of erosion. However, shorter-term data reveal more complex and variable shoreline change. The discrete zones of distinct shoreline change appearing at ~6 km alongshore intervals in the shorter-term data are of particular interest since they are spatially coincident with shoreface-attached ridges (Figure 8, Inter-Annual). These ~2 km zones are distinguished by an ~1 km accretional peak flanked by shorter erosional reaches. These segments are characterized by statistically significant rate determinations compared to insignificant rate determinations for adjacent shoreline (Figure 8). These same discrete zones also tend to exhibit moderately increased cross-shore mobility and larger change rate variability.

#### Wallops Island

Although the historical trend for Wallops Island is erosional, the entire length of Wallops Island has been directly influenced by inlet-related processes and/or human activities. Moreover, the island's curving shoreline orientation common to drumstick barriers critically affects gradients in longshore transport, and the extensive backbarrier marsh system landward of the island may also be a variable factor in barrier translation (Finkelstein, 1983; Moffat and Nichols, 1986; Byrnes, 1988) (Figure 9). The drumstick northern end (~1.5 km) has accreted over the historic period in response to wave sheltering and a local reversal in longshore transport related to refraction over Chincoteague Shoals and the Chincoteague Inlet ebb-tidal delta (Figure 11; Headland *et al.*, 1987). The northern drumstick end of Wallops has grown historically, but the rate of accretion has increased drastically and unpredictably since the shoreface-attachment and sediment bypassing of the ebb-tidal delta. This variability is indicated in the large

standard deviations seen in Figure 9. The immediate downdrift extent of inlet influence is less than 2 km, but the entire, sediment-starved island is arguably affected by the efficient sediment trap of Chincoteague Inlet. Regular shoreline protection has been practiced along the central 4 km of Wallops Island since the 1950s and has included the construction of timber groins, timber seawall, beach nourishment, granite rip-rap seawall, and artificial dunes (Figure 12, A and B) (Morang *et al.*, 2006). Decadal shoreline change data show little statistically significant change along this reach (Figure 9). However, the subaerial beach has been almost completely eroded in areas armored with the seawall (Figure 12B). South of the protected segment, Wallops Island has experienced net shoreline retreat and progressive narrowing. The most severe erosion occurs south of the rock seawall towards Assawoman Island, along a low-profile, washover-dominated segment (Figures 9 and 12C). Long-term and decadal shoreline change data along the southern end of Wallops show the migration and sequential opening-closing of Assawoman Inlet (Figure 9). Some authors have suggested that the southern end of Wallops Island, like the other mixed-energy barriers located along the Eastern Shore's arc of erosion, may be exhibiting threshold behavior, characterized by enhanced migration and overwash (Gutierrez *et al.*, 2007). However, the well-developed backbarrier marsh complex (Figure 12C), which extends approximately 3 km west towards the Peninsula mainland and offers a crucial platform for continued landward migration, may ultimately prevent segmentation like that currently being experienced by southern Metompkin Island and Cedar Island, immediately to the south and not backed by equivalent marshes (Finkelstein, 1986; Wright and Trembanis, 2003).



## 5.2 *Nearshore Morphology*

Inner shelf profiles (< 15 m water depth) off Assateague Island and Wallops Island are distinguished by remarkably different seafloor gradients and bottom topography. The bathymetric DEM in Figure 11 shows four distinct alongshore geomorphic provinces: 1) the equilibrium shoreface (*e.g.*, Dean, 1991) off Assateague Island segmented by attached and detached sand ridges and isolated smaller-scale topographic highs; 2) high relief, undulating shoals abutting the Fishing Point spit platform; 3) the ebb-tidal delta complex off Chincoteague Inlet; and 4) the low gradient, featureless plain off Wallops Island. Alongshore differences in the grain size of surface sediments also coincide with these geomorphic environments, showing a distinct coarsening at the shoal complex superimposed over a moderate north-to-south fining (Fenster *et al.*, 2008).

The empirical orthogonal function analysis shows a significant difference in mean profile shape of the shoreface of the two barrier islands (Figure 13A). While the first eigenfunctions show a characteristic concave profile and account for most of the cross-shore variability, the profile for Assateague Island is considerably more reflective than that of Wallops Island. The shoreface toe off Assateague Island generally occurs within 1 km of the shoreline at the ~8-9 m isobaths (Figure 13B), whereas an equivalent slope break does not occur off Wallops Island except in the vicinity of the Chincoteague Inlet ebb-tidal delta. The mean shoreface gradient off Assateague Island is more than twice that of Wallops Island, whereas the ratio of maximum shoreface slopes is approximately 1:12 if comparing the basin area to shoal flank-crest slopes (Field, 1979). While both shoreface profiles fall under the intermediate morphodynamic state classification of

Wright and Short (1984), Wallops Island exhibits gentler slopes, finer-grained material, smaller, spilling breakers, and lower wave reflectivity, trends that have been corroborated by multiple research efforts (*e.g.*, Gayes, 1983; Finkelstein, 1983; Moffat and Nichol, 1986; Gregg Williams, *personal communication*). Higher order eigenfunctions, addressed in the ensuing sections, reflect enhanced or muted concavity in the equilibrium profile shape and or the local presence of intersecting nearshore morphology.

#### Nearshore of Assateague Island

Three sample profiles in Figure 13B illustrate the degree of variability in cross-shore shape and morphology in the nearshore zone of Assateague Island; two profiles show the shoreface-attachment of linear sand ridges, whereas the third shows a more equilibrium shoreface. The variation in depth and steepness of the profile seaward of the sand ridges is significant, and the difference between profiles appears to be related to the influence of an underlying ebb-tidal delta complex. More than 99.9% of the profile variance is explained in the first four eigenfunctions, which collectively describe the equilibrium profile shape and morphologic perturbations. The first eigenfunction weightings, for the 400 cross-shore profiles considered from the MD/VA state-line south to Toms Cove, describe the alongshore variability in profile shape and regional morphodynamic state (Figure 13C). Figure 13C, where weightings are normalized by subtracting the mean value, shows distinct large-scale wavelengths where the profile state varies between more reflective (+ weighting) and more dissipative (- weighting) states. The profiles shown in panel B are highlighted on panel C for comparison. The ~6 km relatively more dissipative shoreface reach north of Piney Island also corresponds to the long-term accretional reach seen in shoreline change data (Figure 8).

The northernmost part of the study area is characterized by a north-south gradient in shoreface steepness and is notably punctuated by two distinct shoreface-attached sand ridges (Figure 11). The adjacent, lower gradient inner shelf is replete with detached sand ridges and smaller shoals. As seen in Figure 13B, the attached shore-oblique NE/SW trending sand ridges extend seaward from the ~4-m isobath and exhibit increasing variability in scale, relief, and shape with distance offshore. The seaward tails of these shoals, oriented at oblique angles to the shoreline, show increasingly less distinct geometry compared to the place of attachment, which may be co-located with the longshore bar system. Crest-to-trough relief varies from ~1-4 m in less than 8-m water depths (Figure 13A). The northernmost attached ridge is comparatively smaller and less defined (Profile 1 in Figure 13B). The southern sand ridge is distinguished by a bifurcated attachment (Profile 2 in Figure 13B), possibly indicating that a younger sand body is overriding and reworking a precursor ridge (Figure 2). The bifurcated ridge is located along the relatively more dissipative shoreface reach centered at Northing 4203000, the historic Morris Inlet area also characterized by relatively narrow barrier width, historical susceptibility to overwash, and subaerial inlet flood-tidal delta mounds (see Figure 26A) (Morton *et al.*, 2003).

Comparison of the alongshore normalized weightings for the second through fourth eigenfunctions further highlight four comparatively different alongshore areas, such as that offshore of the relict Assateague/Morris Inlet location and offshore of Toms Cove (Figure 14). The weightings of the fourth eigenfunction (normalized by standard deviation) show the alongshore location of shoreface-attached ridges, smaller scale morphology, and associated troughs. Approaching Toms Cove, smaller scale shoals are

evident by their more transverse orientation (Figure 11), marking the northern edge of the Chincoteague Shoal complex and alongshore position of the relict Assateague Light Spit.

As the arm of Fishing Point first extended south from Assateague Spit in the early 1850s, initial extension was south-southwest onto an existing bathymetric high, Ship Shoal (not shown, now underlying Toms Cove/Fishing Point) (NOS HS 298, 1:40K, 1851). By approximately 1880, the leading edge of the spit was encroaching on a deep trough between Ship Shoal and Turners Lump, and the spit turned sharply to the west towards Gunboat Point (NOS Chart 129, 1:80K, 1882). Currently, the inner shelf offshore the narrow barrier arm fronting Toms Cove shallows and grows increasingly dissipative (Figure 13C) towards the south as it is simultaneously molded into a complex of spit-platform attached shoals (Figure 11). The amalgamated upper shoreface shoals built on top of the pre-existing Ship Shoal and are presently being overridden by the modern, southward-accreting spit platform. A deep, 10-12 m trough separates the nearshore shoals from the offshore crests of Chincoteague Shoals, the southern ends of which hook westward and northwestward, mimicking the recurved spit. Recent aerial photography shows that the spit and spit platform have extended ~1.5 km further south since 1982; contemporaneous bathymetry is not available to show the changes in morphology.

#### Nearshore of Wallops Island

Off Wallops Island, the nearshore morphology disappears abruptly into a comparatively featureless, flat basin (termed Chincoteague Bight by Oertel *et al.*, 2007) with the exception of the well-developed, but relatively small ebb delta offshore of Chincoteague Inlet (Figure 11). This trend is illustrated in the alongshore weighting of the first eigenfunction for the 170 cross-shore profiles considered for Wallops Island,

reflecting bathymetric contours that bend south to north under the influence of sediment accumulation near the delta complex (Figure 13D). The actual ebb-tidal delta is excluded from the eigenfunction analysis. The mean shoreface profile slopes to the southeast at less than 2 m/km, whereas the axis of the inner shelf basin slopes north-northwest to south-southeast at about 0.5-1 m/km. The present day north-south trending delta extends approximately 3 km offshore and shows increasingly less east-west asymmetry as sediments are now preferentially accumulated on the southwest side of Chincoteague Inlet. Seaward of the wide flat-bottom area, the seafloor resumes its characteristic ridge and swale topography with Porpoise and Parramore Banks (Figure 1).

#### Historic Morphologic Changes

A bathymetric change isopach for the period between 1933/1934 and 1978/1982 shows coherent alongshore patterns of erosion and accretion consistent with regional shoreline change (Figure 15). Patterns are discussed north to south in the direction of longshore transport. North of Northing 4190000 (Morris Island), bands of erosion and accretion indicate reworking of the shoreface as attached sand ridges migrate south/southwest and smaller-scale, abandoned shoal morphology deflates. While the shoreface-attached ridges migrated a maximum of ~500 m to the south over the time period considered (*i.e.*, ~10 m/yr, but subject to rapid migration during major storm events), the offshore component appears to be more mobile than the upper shoreface component. The central shoreface-attached ridge system (N4201000; relict Morris/Assateague Inlet) is located within the broad depositional, relatively more dissipative zone (Zone I) that showed an annualized volumetric gain of ~69,000 m<sup>3</sup>/yr (Table 6). The south side of each shoreface-attached ridge shows matching >4-km zones

that exhibited nominal elevation change. In contrast, shoreface erosion was pervasive from Assateague Light spit (N4196000) south to the westward deflection of Fishing Point (Zone II). The volumetric change, annualized at  $\sim -330,000 \text{ m}^3/\text{yr}$ , is consistent with the extensive shoreline erosion seen in Figure 8. The abandoned shoals coincident with the relict spit arms show notable erosion and/or deflation. The extensive subaqueous shoals constituting Chincoteague Shoals migrated south/southwest and attached to the bypassing lobe of the Chincoteague Inlet ebb-tidal delta (Figure 15). This 6-km wide and  $\sim 1.5$ -km long pathway is characterized by a maximum elevation change of approximately 8 m; the eastern component is an offshoot of the accreting spit platform. An annualized longshore sediment flux of  $\sim 1.1 \times 10^6 \text{ m}^3/\text{yr}$  (minimum estimate) reaches the sink at the southern terminus of Assateague Island. Since only  $\sim 339,000 \text{ m}^3/\text{yr}$  can be attributed to shoal construction, the remainder appears to be transported along the shoal-delta transport pathway and trapped in the Chincoteague Inlet complex. This volumetric calculation neglects the sediment transported to and trapped in the enormous Chincoteague Inlet flood-tidal delta or subaerial beach ridges and strand plain of Fishing and Gunboat Points, which conservatively represent an additional sink of  $\sim 332,000 \text{ m}^3/\text{yr}$  (calculated from the change in subaerial footprint of the spits in 1933 and 1980, presuming a conservative vertical accretion of 4 m). South of the accreting ebb tidal delta, Wallops Island shows pervasive shoreface erosion ( $\sim -53,000 \text{ m}^3/\text{yr}$ ), consistent with estimates that less than 5% of sediment bypasses Chincoteague Inlet (Moffat and Nichols, 1986). The basin to the east shows little to no change in bed elevation south of Chincoteague Shoals.

### 5.3 *Nearshore Seismic Stratigraphy and Geologic Framework*

Seismic data reveal a series of prominent regional reflectors amid laterally variable seismic units in the upper ~15 m beneath the seafloor (Table 7). Figures 16-21 illustrate the range of stratigraphy in a suite of raw and interpreted geophysical lines. The uppermost seismic unit (A) is mostly transparent, bounded by the seafloor and a shallow, seaward-deepening reflector (R1). The seismic stratigraphy occurring beneath the uppermost seismic unit (A) consists of variable units (B-D), segregated by continuous and discontinuous reflectors (R2-R5) and characterized by complex internal reflections. Internal reflections range from short and chaotic reflections to long parallel and subparallel reflections, and from sigmoid-oblique and parallel clinoforms to complex channel-fill geometries. The four seismic units constituting the shallow geologic framework are interpreted as Tertiary shelf strata (D), Pleistocene shelf deposits (C), Holocene channel-fill and paralic facies (B), and modern surficial sands (A).

Side scan sonar data, available offshore of Assateague Island, support these interpretations, showing that acoustic backscatter is strongly correlated to the complexity of the inner shelf morphology. Uniform high backscatter areas are common to sand ridges and the nearshore sand sheet superimposed with sand waves and ripples, compared to obliquely-oriented, mottled, low backscatter corresponding to inter-ridge lows and outcropping facies of unit B (Figures 16-18). Low, highly mottled backscatter, coupled with seismic data, suggest that lagoonal, backbarrier, and tidal inlet deposits are actively being eroded in inter-ridge swales. The low back scatter is indicative of a seabed composed of finer-grained, poorly sorted sand and mud with a possible patchy lag cover and characterized by diverse microtopography. The third characteristic side scan

signature is a diffuse, moderate backscatter, and it generally occurs where earlier Holocene marine shoal / spit platform sands (A2) outcrop along southern Assateague Island (Figure 18). The same signature also occurs on shoal flanks.

### Pre-Holocene Geology

The base of the Quaternary section and top of the oldest unit (D) is indicated by a faint, discontinuous offshore-sloping reflector (R5) that intermittently appears at -18 m to -24 m across the study area. The depth of this reflector is consistent with the erosional Tertiary unconformity reported by Toscano and York (1992), Mixon (1985), and Foyle (1994), and it probably represents the top of the southeast dipping Yorktown Formation, a poorly sorted deltaic and distributary mouth complex formed during Pliocene marine transgressions (Krantz, 1991). Within Chincoteague Bight, contours marking the top of unit D bend towards Wallops Island (Figure 6) and yield a diminished offshore gradient compared to southern Assateague Island (Mixon, 1985), even though the unit occurs at relatively shallower depths off the barrier that is offset 5 km landward. The immediately overlying undifferentiated Pleistocene unit (C), variable in thickness, generally occurs below ~12-15 m MSL and is distinguished by fairly continuous parallel to subparallel reflectors and internal reflections, with the exception of one wavy reflector (R4) that also shows occasional evidence of minor truncation similar to the M2 reflector reported by Toscano *et al.* (1989). Based on vibracoring results, Halsey (1978) reported that the Pleistocene stratigraphy below Chincoteague Island rises rapidly towards the mainland Peninsula, but is relatively deeper immediately beneath Assateague and Wallops Islands. Because of the seafloor multiple, low amplitude returns, and overlying gas masking, internal stratigraphic differentiation of Pleistocene units is extremely difficult. However, a relatively strong and regionally continuous reflector (R3) defines the



Pleistocene/Holocene unconformity at the top of unit C. This surface is locally incised and overlain by complex fluvial, lagoonal, and/or inlet-channel fill (*e.g.*, Figure 17 (C-C')). R3 shows little gradient off Assateague and Wallops Islands, but the surface is about 2-3 m shallower immediately offshore Wallops Island. In the adjacent regions studied by Toscano *et al.* (1989) and Foyle (1994), Pleistocene units outcrop on the shoreface seaward of the 15-m isobath. In the immediate ~5 km off Assateague Island (VA), no marine isotope stage 2-4 equivalent channels or channel-fill structures could be distinguished in the seismic sections. Offshore of southern Wallops Island and northern Assawoman Island, a north-south oriented, age-equivalent paleochannel occurs below ~ -12 m MSL and parallels the present day barrier island approximately 2.5 km offshore (Figure 21). Intersecting seismic lines show truncation of horizontal reflections, varied channel size and geometry, complex channel fill structure, and multiple thalwegs, suggesting a migrating channel and/or dendritic drainage preserved beneath the seafloor. Figure 22 shows a plan view of the paleo-channel(s) orientation interpreted from seismic data.

### Holocene Geology

Seismic stratigraphic units A and B, interpreted as Holocene, are characterized by striking spatial variability. Regionally available vibracores generally show the seaward-fining unit A to be composed primarily of fine to medium-grained, well-sorted sand (Field, 1979; Berquist and Hobbs, 1988; Conkwright and Gast, 1994; Gregg Williams, *personal communication*). The underlying, high amplitude R1 reflector is slightly concave and similar in shape to the seafloor profile, but it grows increasingly indistinct and topographically complex in shallower water. This is consistent with the findings of

Schwartz and Birkemeier (2004) off Duck, North Carolina that showed a similar contact, interpreted as the wave ravinement, that was sedimentologically distinct on the lower and middle shoreface, but grew indistinct and topographically complex approaching the longshore bar and trough region of the profile. R1 is interpreted to be the Holocene transgressive wave ravinement at the lower shoreface and the proto-ravinement actively being formed in shallower water depths. R1 defines the base of the reworked shoreface sediment veneer (*i.e.*, maximum contemporaneous depth of wave/current reworking) and generally separates overlying homogeneous, seaward-fining marine sands (A1) of the shoreface from underlying poorly sorted, mixed grained paralic deposits (B). R1 locally occurs at the seafloor and/or may be removed at narrow shore-oblique, inter-ridge swales on the upper shoreface (Figures 16-18). While seismic data show that unit A pinches out at multiple cross-shore shoreface depths, it ultimately thins to seismically undetectable thicknesses at depths >10-15 m.

South of Morris and Piney Islands towards the present-day Fishing Point spit platform, delineation of the ravinement surface is complicated by southerly spit and shoal accretion over the last several centuries, which appears to have resulted in localized progradational or regressive sequences. In zones of net accumulation, the ravinement process can be expected to be complex and multiple surfaces may be preserved and separated by intervening strata (Halsey, 1978; Dickson, 1999; Rodriguez *et al.*, 2001). Yet, as seen in Figure 15, the shoreface south of Assateague Light spit has been progressively lowering over the last 75 years, indicative of erosional ravinement. Along this northeast-southwest oriented reach of the Assateague shoreline, R1 marks the base of the A1 facies. On the shoreface, R1 appears to truncate another seismically transparent

facies (A2), presumed to be the regressive shoreface sands, marine shoals, and the overriding spit platform documented by Goettle (1981) beneath Assateague Point, Toms Cove, and Fishing Point as nearshore fining downward, silty sands. Facies A2 in turn overlies another erosional surface (R2) that truncates apparent backbarrier and relict inlet-related deposits (Figures 16-19). South of Assateague Light spit, this R2 surface tilts north-south and dips east-west. The R1/R2 surfaces merge into one composite surface further offshore at >12-15 m. This surface likely formed prior to or during initial spit/shoal extension and may be related to the earlier Holocene transgression that created Chincoteague Island before the older barrier was abutted by Assateague Island's prograding spits. In the present day accretional environment south of Fishing Point, a locally continuous reflector separates two seismic facies that are characterized by short and chaotic seismic reflections; this reflector was used to delineate the locally finer sand or muddy sand cover. In areas where sediment supply exceeds accommodation space, the upper shoreface is ravined by storm waves in the surf zone as it translates seaward (Swift *et al.*, 2003). The reflector identified south of the spit was assumed to be this wave-cut surface (*i.e.*, surf diastem), embedded in what is most likely a downward-fining sequence.

Beneath R1/R2, a range of Holocene depositional environments are encountered including 1) backbarrier facies (B5), 2) tidal inlet and inlet-related facies (B3-B4), 3) lagoonal facies (B2), and 4) paleochannel fill (B1) (Table 7). North of Morris and Piney Islands, inlet-related facies occur directly beneath the ravinement surface along the lower shoreface and inner shelf, whereas possible overwash, tidal flat, or regressive shoreface deposits, characterized by a transparent seismic signature, also are being ravined on the upper shoreface (Figure 16). Seismic data and vibracores collected further north along

Assateague Island in southern Maryland show relict tidal creek and inlet channel sequences preserved beneath the upper shoreface (Field, 1980). To the south, seismic data show thinning inlet-related and lagoonal facies at relatively greater depths, occurring beneath the A2 facies described above. On the low-gradient Wallops Island shelf, a relatively thinner Holocene section is preserved, excluding probable early Holocene channel fill.

Nearly all backbarrier/lagoonal deposits preserved on the inner shelf have been extensively modified by tidal inlet processes evidenced by widespread channeling, channel-fill structures, and inlet-associated facies, including apparent ebb-tidal and flood-tidal delta facies (Figures 16-21). Gas fronts frequently occur in unit B, causing significant loss of resolution in and below B5 and even causing seafloor pock marks in side scan imagery on the inner shelf. The evidence of at least three discrete inlet complexes is preserved off Assateague Island (Figure 22). Part of a ~25 km<sup>2</sup> ebb-tidal delta, characterized by landward and alongshore dipping reflections, is shown in the shallow seismic record in Figure 19. Its offshore location coincides with subaerial flood delta mounds of the historic southward-migrating Morris Inlet (precursor to Assateague Channel), beach ridge truncation on northern Chincoteague Island, the bifurcated shoreface-attached sand ridge, and dissipative profile state. The maze of inlet channel fill and related lithosomes preserved in the subsurface beneath Chincoteague Shoals are of unknown Holocene age, but suggest a complex history of Holocene inlet cycling with multiple retreat paths and markedly different barrier island configurations. Offshore of Wallops Island, inlet channel fill is less developed, but the geometry of channel fill and

possible relict deltas suggest a north-northwest retreat of Chincoteague Inlet and westward and southerly migration of Assawoman Inlet during the Holocene.

### Holocene Sand Cover

Of principal interest to this study and the ensuing statistical analysis is the prism-shaped, discontinuous sand sheet (A1) that thins in the seaward direction. The thickness of the sand lens, calculated between R1 and the seafloor, ranges from 0 to ~7.25 m (Figure 23). This thickness does not account for any sand source (*e.g.*, A2, B5, *etc.*) underlying the R1 surface. Since R1 presumably marks the contemporaneous depth of active shoreface erosion, sand below that surface is assumed to have made no contribution to the sediment budget over the time scales under consideration. Figure 23 presents an isopach showing locally thick sand ridges and shoals intersecting the shoreface and trending obliquely offshore. Conversely, the sand cover is locally absent in adjacent troughs and further offshore, where low backscatter returns in side scan sonar show the ravinement at the seafloor and/or underlying A2/ unit B facies outcropping (Figure 24). The sand cover immediately offshore of the relict recurved spits is thicker than the cover on the adjacent shoreface. The sand prism is also thicker on the upper shoreface compared to the lower shoreface north of the relict Morris Inlet area; that is in direct contrast to the accreting shoreface immediately to the south where there is relatively more sand, but the cross-shore distribution is more equal. These trends are consistent with variations in the profile shape seen in eigenfunction 2 in Figure 14. The thickest deposits and maximum variability occur in the shoal complex constituting Chincoteague Shoals. Twenty-foot (~6.1 m) vibracores collected during the summer 2007 by the U.S. Army Corps of Engineers – Norfolk District in support of a potential beach

nourishment project along Wallops Island show fine to medium sand along the entire core length (Figure 25). Compared to the variable thickness off Assateague Island, much of the area off Wallops Island is a thin veneer or not resolvable by the chirp seismic system. Although side scan sonar data was inopportunately corrupted in a hard disk failure, grab samples collected offshore of Wallops Island in 2006 show a surface sediment texture ranging from 45 to 80% fines seaward of the 6-m isobath indicative of widespread sandy mud or mud (Gregg Williams, *personal communication*). More recent reconnaissance cores collected off southern Wallops Island indicate limited sand cover and instead show a relatively cohesive sandy mud occurring at the seafloor (Figure 24). It is not clear whether this sample shows a dewatered backbarrier mud or fines that have settled out of Chincoteague Inlet's ebb jet plume (Oertel and Kraft, 1994).

#### 5.4 *Cross-Correlation of Shoreline Change and Geologic Framework*

Measurements of nearshore slope and sediment volume were derived to test the strength and significance of the relationship between the shallow geologic framework and shoreline change. Measures chosen to represent geologic variables generally encompass the shoreface footprint between the 4 m isobath and shoreface toe (~8 m), the cross-shore zone from the upper shoreface out on the lower shoreface ramp (Figures 25-26). This cross-shore zone does not encompass the entire profile or A1 prism that seismic data showed thinned at depths below 10 m, but instead defers to the Larson and Kraus (2003) estimate for the cumulative, long-term depth of closure for Assateague Island. Theoretically, the ideal measures would quantify the morphology and sediment volume from the storm-run up limits to the seaward limit of the active shoreface, but this is a dynamic target and inaccessible area making such a wholly representative dataset

unattainable (Schwab *et al.*, 2000). Instead, this analysis relies on quantifying the slope and volumetric envelope of the reworked, finer-grained, more quiescent part of the profile, one significantly less affected by most wave events and more likely to be in equilibrium with long-term average conditions. This means that the longshore bar-trough and beachface segments of the profile and profile envelope that tend to show the most significant morphologic response, greatest changes in sand cover thickness, host the most beach-compatible sand, and exhibit the maximum seafloor gradient are excluded. Even if bathymetric and seismic data were available to evaluate this part of the profile, they may reflect a transient condition, one showing the most recent storm-induced erosional and fair-weather accretional changes over the bar-trough domain. It is possible that such data may not accurately reflect long-term equilibrium shoreface conditions and may contribute to lower correlations with shoreline change.

Shoreline change, nearshore morphology, and shoreface sediment volume datasets (Figures 26-27) were cross-correlated to evaluate multiple alongshore scale trends across multiple time periods along Assateague Island from the Maryland-Virginia state line south to Toms Cove. Data representing the Fishing Point spit complex were excluded from this analysis because of inherently variable shoreline dynamics related to wave refraction and shoaling, as well as inlet sediment bypassing (*e.g.*, Fenster and Dolan, 1996; Galgano, 1998). Moreover, since this part of the study area is considered to be a regressive shoreface dispersal system, volumetric estimates were not determined from identical ravinement surfaces and should not be compared as such. Wallops Island data were not analyzed since 1) the entire shoreline is influenced by historic engineering

and/or tidal-inlet processes and 2) the lower shoreface shows little variability in morphology and sediment volume except near the Chincoteague Inlet ebb-tidal delta

Along Assateague Island, nearshore volume and shoreline change data were characterized by significant north-south trend, whereas untreated slope, volume, and shoreline change data, interpolated at the same 50-m northing intervals, exhibited statistically significant autocorrelation ranging from ~1.0-km to ~1.8-km (not shown). While trend decidedly influences the scale of autocorrelation, the scale of autocorrelation also is affected by the magnitude of variability inherent in the data series. It was observed that if the alongshore sampling range was arbitrarily lengthened or shortened, the corresponding scale of autocorrelation could be affected in increasing and decreasing directions depending on the variability and the length of the data series considered. Since resource management is typically conducted at a regional scale, the cross-correlation analysis was completed for the maximum alongshore length possible before the data were appreciably affected by inter-annual shoreline change reversals (N4191800) associated with spit dynamics. In a complementary effort to accentuate and evaluate smaller spatial scales, the regional trend was removed from each dataset using a polynomial fit. Cross-correlation analyses were performed for both untransformed and transformed data series.

The mean cross-shore slope metric along Assateague Island shows little trend moving south towards Fishing Point compared to shoreline change, but mirrors the alongshore patterns of profile shape and occurrence of upper-shoreface morphology seen in the first and fourth eigenfunctions. Less negative slopes indicate that the shoreface is more dissipative and/or punctuated by morphology. Figure 27 shows higher standard deviation in slope where morphology is intersected compared to adjacent, concave



shoreface profiles. Since the northernmost shoreface-attached sand ridge is relatively small, its place of attachment occurs somewhat lower on the shoreface, and the overall shoreface profile is relatively steep (Figure 26). The mean slope metric does not indicate the presence of this sand body (Figure 27). Regardless, mean nearshore slope was positively correlated to shoreline change over multiple time scales on a regional spatial scale ( $p < 0.1$ ), signifying that 1) more-reflective profiles were paired with eroding beach segments and 2) approximately 40% of variability in shoreline change could be explained by the variability in shoreface slope (Table 8). The spatial lag of the maximum correlation was consistently located 0.5-0.8 km to the south (represented as a negative lag, whereby shifting the shoreline signal northward leads to the maximum correlation). This is the direction and approximate distance sand ridges are expected to migrate in the 25-year interval occurring between the collection of bathymetric and most recent shoreline data. Figures 28 and 29 plot cross-correlation results for untreated and treated slope and inter-annual shoreline change data. The correlogram shows the relatively broad range of lags (30 lags or 1.5 km) over which the two variables show significant correlation. By removing the regional trend via polynomial fits and cross-correlating the residuals, anomalies in shoreline change were compared to anomalies in regional slope. Despite bias introduced by the treatment method (see Appendix), mean slope and shoreline-change residuals were positively correlated ( $p < 0.1$ ) over multiple time scales, but particularly over the inter-annual scale where the slope accounts for almost 35% of block-scale (*e.g.*, ~1 km) shoreline variability (Table 8). The direction of correlation was dependent on the time scale considered, but showed comparable lags to the untreated correlation analysis. The alongshore scale of statistically significant lags is also reduced.

A different metric, such as the standard deviation of slope, captures the presence of smaller-relief morphology, but it also introduces more variability and reduces the strength of correlation by not capturing the mean profile shape. Changing the metric does not reverse any significance finding (not shown).

Figure 26 shows the footprint over which unit A1 thicknesses were transformed into cross-shore sediment volumes ( $\text{m}^3/\text{m}$ ). According to Schwartz and Birkemeier (2004), the envelope of elevation change provides an analogous estimate of the geometry for the shoreface mass over a discrete time period. The nearshore sediment volume calculations are compared to the cross-volume change envelope calculated from the 1933/1982 volumetric isopach at the same cross-shore transects to ensure that the relative trend is reproduced (Figure 27). Both cross-sectional volume measures show a decreasing north-south trend and appear consistent with the large-scale alongshore trends in profile steepness (Figure 27). Like the shoreline-change and nearshore-slope data, the nearshore volume echoes relatively larger local variability at the locations of sand ridge attachment and relict recurved spits (Figure 26). Cross-correlation analysis between nearshore slope and unit A volume indicated a relatively strong positive association that explained between 35-65% of the co-variability depending on the alongshore length scale considered; the correlation strength was reduced by increasing divergence south of the relict Assateague Light spit where the ravinement surface diverges from the seafloor. Figures 30 and 31 show cross-correlation results for untreated and treated nearshore volume and inter-annual shoreline change data series. Table 8 presents the remaining results of regional and local scale testing between nearshore volume and other periods of shoreline change. A near zero lag, strong positive (increasing/decreasing together)

correlation ( $p < 0.1$ ) exists between nearshore volume and shoreline change, suggesting small volumes correspond to shoreline erosion. Removing the regional trend whereby erosion increases to the south, a statistically significant block scale coupling persists between residuals across multiple time scales, but interpretation of correlation direction, lag direction, and strength of spatial coupling is complicated. Both statistically significant positive and negative relationships, lagged in different directions, are possible because of bias introduced during treatment (Figure 31, Table 8). The largest correlation coefficients show an inverse and unintuitive association (larger volumes correlate with erosion at a negative lag). However, comparatively little variability (<15%) in the alongshore shoreline change signal appears related to smaller alongshore deviations in nearshore volume.

It merits repeating that the strength/direction of the correlation and corresponding lag is sensitive to the degree of variability in the alongshore variable, as well as the method of treatment. For example, inclusion of the highly variable data representing the Fishing Point spit complex yields a sudden reversal in all metrics, and this leads to both different correlation coefficients and even correlation directions. For this reason, it is imperative that the length of the tested data series is evaluated using a fitting length scale. Selecting refined alongshore lengths, for example focusing on the shoreline change and independent variables near the centrally-attached sand ridge, can lead to slightly stronger correlation coupling (not shown). Cross-correlation, as a linear statistical measure, is inherently insensitive to the different length scales inherent in a data series. Therefore, correlation coefficients and lags appear to be the practical equivalent of an average of all constituent scales of variation.

## 6 DISCUSSION

### 6.1 *Underlying Geologic Influence on Coastal Evolution*

This study represents the first systematic effort to map the geologic framework offshore of southern Assateague Island and Wallops Island, complementing subaerial investigations in the late seventies and early eighties (*e.g.*, Halsey, 1978; Goettle, 1981; Gayes, 1983). Using a limited number of deep borings, Halsey (1978) concluded that the late Quaternary stratigraphy landward of southern Assateague Island and Wallops Island was quite complicated because of the preservation of inter-fingered transgressive and regressive tracts, deposited in spit, inlet delta, and lagoonal environments during late Pleistocene glacio-marine cycles. The offshore Quaternary geology is also characterized by notable variability in paleo-channel and relict inlet organization and fill, shoreface slope, thickness of shoreface sand deposits, and nearshore morphology. Nonetheless, the stratigraphy encountered within 5 km of the coast appears relatively consistent with the geologic framework reported for the immediately neighboring areas, showing moderately thick successions of Holocene backbarrier deposits beneath a prismatic sandy shoreface that tapers in thickness offshore, except where molded into sand ridges. Below a depth of 12-15 m, the Holocene sand cover is increasingly patchy, and detached sand bodies are presumed to directly overlie Pleistocene strata (Toscano *et al.*, 1989; Conkwright and Gast, 1994; Foyle, 1994). The primary difference is the short-lived regressive sequence related to the late Holocene progradation of Assateague Island, a trend also seen in the seaward growth of dune ridges on the northern drumstick end of Wallops Island.

Results herein have shown obvious differences (Table 9) in profile steepness, modern morphologic and sand prism variability, surficial sediment texture, and shoreline

retreat behavior for the two barrier islands. These differences, similar to the preservation potential of subjacent geology, are predicated on interactions between antecedent topography (*i.e.*, accommodation space), sediment supply, and hydrodynamic processes coupled to rising sea levels (Belknap and Kraft, 1985). Naturally, the geologic framework is increasingly influential when it occurs at or near the surface, limiting profile or plan form evolution and/or introducing similar or dissimilar grained material into the transport system (Jackson *et al.*, 2005). The mid-Holocene and younger deposits are relatively thick and well preserved below the shoreface because accommodation space is relatively large given the deep Pleistocene topography, generally occurring >12-15 m below the Chincoteague Bight basin and Assateague shoreface. The upper Pleistocene units ascend sharply behind both barriers towards the Pleistocene scarp defining the Delmarva mainland (Halsey, 1978; Finkelstein, 1986; Byrnes, 1988). In contrast to northern Maryland and Delaware where Pleistocene headlands intersect the modern shoreface (Wells, 1994; Honeycutt and Krantz, 2003), the effect of Holocene stratigraphy and evolved morphology is more important to shoreline behavior in the study area.

The shoreface sand prism has historically been reworked from a large volume of variably sorted, mixed-grained sediment beneath the modern ravinement surface, but located above the Pleistocene unconformity. While onshore flux from eroding Pleistocene strata further offshore is possible, continued, local reworking of Holocene deposits is unequivocal in seismic and side scan sonar data, which show removal of the ravinement surface and/or enhanced lowering and presumed erosion of backbarrier, lagoonal, tidal inlet, and proximal marine sand facies at inter-swale troughs and on the mid-to-lower shoreface where the sand cover is relatively thin (Figures 16-18). Some

authors suggest that in transgressive settings nearshore sands are so diminutive compared to underlying muddy units that the aggregate millennial scale behavior depends more on the backbarrier sediment supply than the shoreface itself, a dynamic equilibrium unbalanced by transient point sources and sinks, regressive episodes, and gradients in longshore transport (Cowell *et al.*, 2003). A substantial volume of shallow marine/shoal sands is also stored beneath the active shoreface ravinement from the relict Assateague Inlet / Morris Island area south to Chincoteague Shoals (and to a lesser extent north towards Pope Island). These sands are being ravined locally and transported south to be stored transiently in the accreting Chincoteague Shoals. South of the influence of the Chincoteague Inlet ebb delta, the shoreface sand prism off Wallops is comparatively thinner and generally limited to within the 4-5 m isobaths. Increasingly muddy, finer-grained sands occur at or near the surface with increased distance seaward of Wallops Island (Figure 11). Although not investigated, it is suspected that, because of the thick marsh sequence behind Wallops Island and occurrence of similar deposits on the beach following storms (Morang *et al.*, 2006), such outcrops occur in the upper shoreface, surf, and foreshore zones (Finkelstein, 1986).

Given the range of stratigraphy across the study area, substrate erosion and sediment supply are presumed to have varied substantially, but have been a fundamental process over the course of barrier island growth and retreat, exerting a strong influence on ravinement lowering and coupled sediment transport processes. Continued intersection between the active shoreface and Holocene geologic perturbations will promote shoreface bathymetric variability and differential rates of retreat along the coast (Storms *et al.*, 2002; Cowell *et al.*, 2003; Harris *et al.*, 2005; Stopler *et al.*, 2005). Although the

Pleistocene topography is believed to play a less significant role on the modern barrier behavior in profile, evidence suggests that the planform evolution of Wallops Island may be related to inlets reoccupying paleo-drainage systems and the relative position of Chincoteague Island to underlying, topographically higher shoals constructed during the last transgressive-regressive cycle (Halsey, 1978; Oertel *et al.*, 2007). The following discussion elucidates what are believed to be principal geological factors, enhanced by near- and far-field, long-term hydrodynamic processes, contributing to the large-scale physical organization and morphology of this complex coastal system: (1) paleo-drainage systems, (2) former inlet systems, and (3) progradational spit complexes.

(1) Oertel *et al.* (2007) hypothesized that the existence of the Chincoteague Bight basin and dissipative profile shape of the Wallops-area shoreface may be partially explained by the oblique intersection of the coastline with a late Pleistocene / early Holocene paleo-valley. The current 5-km offset between Fishing Point and Gunboat Point did not exist as recently as ~2-3 ka when Chincoteague Island is believed to have entirely abutted the coastal ocean (Goettle, 1981). The precursor coastline was more concave in shape, embayed from Assawoman Island to Chincoteague Island north to the historic Pope Island (Figure 32). This curvature presumably evolved through the long-term influence of transgressive processes acting on the accommodation space created by antecedent drainage (Oertel *et al.*, 2007). The authors supported their hypothesis with seismic data collected offshore Parramore Island showing paleo-tributaries flowing to the north/northeast towards a proposed confluence with a Chincoteague paleo-valley. Interestingly, the name “Chincoteague,” of Native American origin, translates to “a large stream” (Halsey, 1978). The fact that the southern extension of the late Pleistocene scarp

of Sinepuxent Neck has been entirely eroded in the Virginia portion off Chincoteague Bay may further support this idea (Figure 32). Seismic data collected in this study showed a similarly oriented paleo-channel aligned with the southwest bearing of Chincoteague Bay and another apparently draining Assawoman Creek to the west of Wallops Island; seismic line G in Figure 21 shows this channel towards the north. The relatively low width-to-depth ratios, complex fill structures, and multiple, nested thalwegs suggest repeated incision over the late Pleistocene. Proximity to the relatively small catchments associated with Assawoman Creek, Little Mosquito Creek, and Swan's Gut Creek would support a northward extending paleo-tributary.

Assuming that part of the modern Chincoteague Bay represents a flooded paleo-valley, its orientation markedly diverges from the southeast flowing tributaries associated with the St. Martin River watershed to the north (Toscano *et al.*, 1989). The modern drainage divide on the coastal plain adjacent to Assateague Island extends northeast-southwest from the preserved Sinepuxent Neck headland area near Ocean City, Maryland to Wallops Island (Oertel and Kraft, 1994). The absence of paleo-tributaries off southern Assateague may support the capture of the seaward-most watershed prior to the last glacial maximum. However, the absence could also result from tidal incision removing any evidence of lowstand tributaries. Geophysical surveying did not document any paleo-channels along the northern half of Wallops Island extending towards the Chincoteague Inlet throat (Chincoteague Channel located west of Chincoteague Island), which would presumably be co-located with the northern extension of the paleo-valley thalweg. Approaching this area, seismic penetration was particularly limited because of the increasingly strong returns from the sandy outer halo of the ebb-tidal delta. The



interpreted Pleistocene unconformity in the Chincoteague Bight exhibits a relatively subtle offshore gradient, generally less than the nominal seafloor gradient. As the proposed paleo-valley and adjacent basin were transgressed, flooding would have occurred from both the landward side of the basin because of its low gradient and from the southern limit of the incised paleo-valley, a topographic low presently located off Metompkin Island (Figure 32). This may have facilitated rapid retreat of primordial barrier islands across a low-gradient, wide lagoonal system that trapped sediment debouched from small mainland catchments. The likelihood for such an evolution is affirmed by the basin's dearth of morphology compared to the banks lining the basin's seaward rim, relatively absent sand cover, and relative thick sequences of lagoonal and backbarrier Holocene deposits. During landward retreat, the planform evolution of the Wallops barrier would have been influenced by the location of paleo-valleys and inlets subsequently reoccupying topographic lows. The transition to a mixed-energy regime would reinforce this geologic template, dictating relative barrier position, island dimension, and drumstick curvature (Hayes, 1979; Harris *et al.*, 2005).

(2) The ubiquitous preservation of inlet and tidal creek channeling (Figure 22), delta formation, and subsequent infilling suggest that the area of southern Assateague Island / Chincoteague Island has been a significant sediment sink over the late Holocene, preventing longshore transport to the south and progressively contributing to the arc of erosion. Although Assateague Island is presently uninterrupted by tidal inlets for over 60 km, the present condition is not representative of past conditions as historical records alone indicate former tidal inlets at eight locations, at least four in the study area: Assateague Inlet, Morris/Assateague Inlet, Ragged Point Inlet, and Pope Island Inlet

(Figure 22) (Bartberger, 1976; Halsey, 1978; Kochel and Wampfler, 1989; McBride, 1999). Seismic interpretations confirm a network of former inlet systems and delta complexes buried off Assateague Island and Wallops Island, suggesting multiple generations of inlet opening, migration, and closing. This multiplicity suggests the mixed-energy conditions characteristic of the southern Virginia barriers in the Delmarva Coastal Compartment extended further north (Halsey, 1979). Although the southern, washover-dominated end of Wallops may be described as transgressive, both islands exhibit characteristics of channel-dominated, inlet-fill shorefaces (Riggs *et al.*, 1995).

The northwest retreat path of inlet-related facies offshore of Wallops Island suggests that Chincoteague Inlet has migrated between Wallops and the oceanfront barrier to the north over the Holocene transgression. The marsh complex constituting part of the modern flood delta is believed to overlie co-located Pleistocene tidal delta and shoal systems (Halsey, 1978). The southern migration of Assawoman Inlet seen in historic shoreline-change data is captured in the seismic data. Chincoteague Inlet may not have been the dominant inlet over the entire time period, despite the enormity of its present day flood-tide delta that extends 12 km north from Bogues Bay into Chincoteague Bay. The extent of the ebb-delta facies preserved off the historic Assateague/Morris Inlet is indicative of a rather large tide-dominated inlet. The prograding shoreline, dissipative shoreface, and bifurcated shoreface-attached sand ridge are spatially coincident with this large ebb-tidal delta complex. This observation seemingly contradicts findings in North Carolina that showed that higher rates of shoreline retreat were associated with old inlet and channel-fill structures (Riggs *et al.*, 1995); but, in this setting, the relatively sand-rich ebb-tidal delta represents a

topographic high and local sediment supply. Rodriguez *et al.* (2001) explain that shoreface profiles can deviate from the regional gradient and locally prograde given a point-source sediment supply.

Multiple authors have noted that inlet fill, delta, and backbarrier facies are characterized by spatial variability in texture, compaction, and erodability, and because of these varying properties may lead to differential erosion, profile shapes, and translation of the shoreface (Kumar and Sanders, 1974; Moslow and Tye, 1985; Snedden *et al.*, 1994; Riggs *et al.*, 1995; Honeycutt and Krantz, 2003; Rieu *et al.*, 2005; Stopler *et al.*, 2005). At a regional scale, the most significant accumulations of sediment, including Chincoteague Shoals, occur in proximity to relict inlet systems and offshore preserved remnants, but spatial correlation as suggested by the Moslow and McBride (1991) model or Browder and McNinch (2006) model is impossible given the data resolution and the complexity of spatial distribution and lateral/vertical variability in preserved inlet-related facies. A significant challenge remains to mechanistically relate the underlying geology to the surface sand deposit through coupled oceanographic and bottom boundary-layer processes.

(3) Holocene spit-related deposits, ranging from beach ridges and dunes to inter-spit marsh/lagoon swales, occur along Assateague Island for the 15 kilometers south of the abandoned Ragged Point relict spit (Morton *et al.*, 2007) (Figure 33). The subaerial morphology correlates strongly with shoreface morphology and sediment thicknesses; provided continued landward translation, the coupled shoreface expression will become increasingly influential on morphodynamic behavior (Figure 33). These sequential regressive deposits and their spit platforms likely developed on top of existing

bathymetric highs (*e.g.*, Ship Shoal) comprised of abandoned tidal deltas deposited in the accommodation space created by shoreface erosion associated with Chincoteague Island. However, the late Holocene progradation of Assateague Island evident in the sequential recurved spits is not idiosyncratically reflected in the offshore seismic geometries. The seismic stratigraphy shows a surprising homogeneity that may reflect the relatively rapid growth of the island over a relatively short period (*i.e.*, ~600 years assuming a constant 25 m/yr long-term alongshore rate). Regardless, the sequential spit growth reflects a substantial influx of sediment into the littoral system over the colonial period.

The shoreline and shoreface east of the narrow arm of Toms Cove, Assateague Point, and Assateague Light Point are presently eroding compared to the rapid progradation still occurring at Fishing Point. Older proximal shoreface and spit-platform deposits preserved beneath the modern ravinement are being supplied to the transport system, especially seaward of Toms Cove. Provided the continued landward translation of the barrier island, sediment eroding in the shoreface may represent a localized sediment source or a topographic barrier to retreat, thereby leading to shoreface steepening and perhaps lower erosion rates. However, the notable curvature in the shoreline reach along Toms Cove enhances longshore transport divergence because of the angle between the shoreline and incident waves, so this supplementary material may instead continue south and contribute to enhanced spit and offshore shoal growth (Kochel *et al.*, 1985).

## 6.2 *Correlating Geological Framework and Shoreline Change*

This study shows that the alongshore variation in shoreline change along Assateague Island is related at a regional scale to shoreface bathymetry and nearshore

sand-prism volume. Over relatively small spatial lags, relatively steeper shoreface profiles characterized by relatively smaller shoreface volume tend to correspond to shoreline reaches undergoing retreat. The correlations persist over inter-annual to long-term time scales and generally explain a consistent fraction of the alongshore shoreline change variability. The persistence and relative strength of the relationship can be largely attributed to the large scale, north-south trend, with smaller fluctuating length scales superimposed on that trend that locally enhance correlation. True determination of statistical significance and the proportion of variability at the regional scale is ultimately imperfect because of persistent non-normality and autocorrelation in the data series. However, this is valuable information in itself reflecting the spatial continuity of the processes that influence both the predicting and response variables, including incident wave climate and shoreline orientation (Dolan *et al.*, 1977; Larson and Kraus, 2003). The inability to distinguish between modern and relict influences is common to geomorphic systems illustrating the problem of equifinality, the principle that in open systems a given state can be reached by many, interacting mechanisms (Kochel *et al.*, 1985).

The greatest affinity between geology and shoreline change generally occurred over the inter-annual time scale, where the hypothesized controls and corresponding responses were documented within an alongshore distance less than 500 m. Schupp *et al.* (2006) have suggested that longshore lags can be attributed to incident storm waves interacting with bar morphology, as well as the alongshore migration of shoal morphology. On the other hand, these lags may be attributed to uncertainty present in the source data. Shorter-term shoreline data captures the local scale (< 2-3 km) variations superimposed over the long-term or regional trend, especially in the vicinity of shoreface-

attached sand ridges, locations also accentuated in metrics used to describe the geological framework. The greater affinity may partially result from the recency of the data used to parameterize shoreline change and geology. The 150-year long-term shoreline-change data exhibit comparatively strong alongshore smoothing, partly reflecting the alongshore migration of morphologic features, where reversing erosion-accretion signals cancel each other as the shoreface-attached ridge migrates in the direction of longshore transport. Correlations collapse when the data series is extended south to include the full shoal complex and accreting tip of Fishing Point. Adjacent reversing accretion/erosion zones and rates ranging over an order of magnitude characterize this coastline segment. Such shoreline behavior is expected and commonly observed near inlets and associated spit complexes where the uniformity and continuity of waves, currents, and sediment transport are interrupted over complex spatial and temporal domains (Fenster and Dolan, 1996; Fitzgerald *et al.*, 2000). This observation illustrates the sensitivity of cross-correlation to sudden trend reversal and large variance (*see Appendix*).

Removing the regional alongshore trend contributed to substantial reductions in the length scales of statistically significant autocorrelation, thereby highlighting the persistence of smaller alongshore length scales. The maintenance of statistically significant correlations indicates that the variability introduced at smaller spatial scales is central to hindcasting shoreline change over inter-annual, decadal, and long-term time scales. While data transformation helps address trend and severe autocorrelation, it also introduces bias into the residuals, meaning results are more susceptible to Type II errors (Dolan *et al.*, 1992). The bias introduced into residuals, diagnosed by negative autocorrelation values, presumably relates to the statistical outcomes that are difficult to

interpret given opposing statistically significant correlation directions (Figure 31). In spite of this limitation, statistically significant relationships indicate that smaller-scale deviations in morphology and volume are related to the anomalies in shoreline change.

This finding corroborates the work of Miselis and McNinch (2006) and Schupp *et al.* (2006) that reported that a notable fraction (<40%) of shoreline change variability from Duck to Oregon Inlet in the Outer Banks (NC) could be explained by alongshore differences in nearshore sediment volume and nearshore morphology. Using eigenfunction and co-spectral methods, Houser *et al.* (in press) qualitatively related the location of large-scale transverse ridge crests to storm response and historic shoreline change along the Florida Panhandle, although correlation lags and phases varied. While direct comparison between studies is not particularly useful since all use different cross-shore measures and scales, the growing body of literature confirms the link between geology, geomorphology, and shoreline change. Defining nearshore sediment volume as the mass overlying the active ravinement / proto-ravinement on the shoreface at a discrete instance appears to adequately represent the alongshore, relative long-term sediment load, even without delineating the internal textural properties, determining the fraction of material size compatible with the beach, or calculating the entire activated cross-shore volume.

Using a shoreface vibrocoring campaign coupled to systematic shoreface profiling, Schwartz and Birkemeier (2004) determined that the entire shoreface mass off Duck, North Carolina was likely mobilized, transported, and redeposited over a 12-year period. Based on this observation, the authors argued that the shoreface prism could be thought of as a homogeneous mass. In comparison, the alternative, describing

morphology on the shoreface using a derivative model of legacy bathymetry data, can be adopted and used with relative ease in all coastal settings. Eigenfunction and cross-correlation analyses convincingly show that regional trends and local irregularities in bathymetry are coupled to regional and local shoreline change. The principal mode of bathymetric influence is presumed to be its impact on incident wave conditions; however, since shoreface volume and bathymetry are not independent (*i.e.*, a common surface is shared), locally variable geologic framework and hydrodynamic climate are morphodynamically coupled. As such, the dynamic shoreface also accounts for a changeable proportion of the variability in geology.

Larson and Kraus (2003) have recently applied a regional, long-term sediment-transport model (Cascade) to the Delmarva Coastal compartment. The model performed reasonably well in predicting >75 years of shoreline evolution where the principal driving parameter was wave energy. Multiple authors have noted that gradients in wave approach relative to the shoreline orientation drive longshore transport divergence, contributing to acceleration of shoreline erosion along reaches where alongshore flux is maximized (Murray, 2007). No author has deterministically considered how these two phenomena — waves and geology — relate to or influence profile shape over *longer* periods of time. However, this tendency for steeper equilibrium profiles to support smaller sand volumes may relate to enhanced wave dissipation over more gentle profiles and/or onshore flux from a relatively sediment-rich source that ultimately promotes shoreline stability (Larson *et al.*, 2000; Schwab *et al.*, 2000; Cooper and Navas, 2004). The most prominent example is the relatively sand rich zone co-located with the centrally shoreface-attached sand ridge. The shoreline stability documented here, despite evidence of repeated historic



overwash, may indicate the contribution of sand from historic inlets now closed in that location, as well as enhanced dissipation over the more moderately sloped profile.

### 6.3 *Shoreline Response Adjacent to Nearshore Morphology*

Local (<1 to 10 km) cycling between erosion and accretion over inter-annual to decadal time scales (Figure 8) is of particular interest to coastal planners and managers. This study confirms a distinct shoreline response in the vicinity of complex bathymetry that occurs within 2-3 kilometers of shoreface attachment; however, the exact magnitude and location of the response varies in space and time, likely reflecting the variability in dynamic wave and current interaction with the changing size and location of shoreface-attached shoals. In general, accretion occurs to the south of the sand ridge, whereas erosion occurs to the north. These bathymetric irregularities may offset or magnify any regional trends in wave convergence and divergence already induced by transformation of longer-period waves over offshore topographic features (Maa and Hobbs, 1998; Maa *et al.*, 2004). Offshore of Assateague Island, Winter Quarter Shoal and Blackfish Bank shoal to a depth of ~5 m, shadowing the shoreline in the presence of northeast, long period waves for east and southeast quadrants. As discussed by Cooper and Navas (2004), natural bathymetric evolution, such as the migration of a shoal, also induces temporal gradients in wave transformation. Off Delaware's Bethany Beach, Moody (1964) observed northeast storm waves being refracted by shoreface-attached ridges and traveling perpendicular to contours. He hypothesized this led to wave energy concentration along zones of convergence, a process validated in a recent Bousinesq model application on offshore detached ridges (Hayes and Nairn, 2004). In Moody's analysis, zones of convergence tended to be located north of the shoreface-attached sand

ridge, symptomatic of zones of erosion related to increased longshore sediment transport divergence—a shoreline pattern described at these locations in the shoreline-change analyses of Galgano (1989). Everts *et al.* (1983) examined the shoreface-attached ridges that intersect Bodie and Hatteras Islands between False Cape, VA and Cape Hatteras in North Carolina. At these four locations, the shoreline also retreated north of and prograded south of the attached ridge. Smith and Ebersole (1997) is the only published modeling study to numerically investigate transport divergences owing to wave transformation over shoreface-attached shoals. Model results showed companion erosional and accretional zones at complex alongshore length scales that only partially coincided with observations from shoreline position and beach-profile data (Stauble, 1994). More advanced hydrodynamic modeling, addressing wave-current interaction, is necessary to more fully understand the gradients forced by bathymetric irregularities and coupled morphodynamic feedbacks (List *et al.*, submitted).

#### 6.4 *Challenges to Quantifying the Relationship between Geology and Shoreline Change*

Objective evaluation of the techniques used in this study reveal that quantifying the relationship between geology and shoreline change is not uncomplicated. Parameterization and statistical analysis are convoluted for four primary reasons: (1) geologic variables (*e.g.*, slope, grain size, profile shape, sand prism thickness) are coupled to hydrodynamics; (2) shoreline behavior and morphologic evolution are non-linear and discontinuous (Southgate *et al.*, 2003); (3) measurements of shoreline change and shoreface character may not be independent at the interval sampled (Dolan *et al.*, 1992); and (4) correlation between variables may be spatially or temporally variable.

(1) Kochel *et al.* (1985) and Honeycutt (2003) acknowledge that the difficulty in parameterizing coastal morphology and geology is in differentiating it from oceanographic processes. The same large scale hydrodynamic climate operates on both the shoreface and beach, potentially affecting geology and shoreline change variables in the same direction and/or magnitude. A fundamental premise underlying the analysis herein is that the errors superimposed over signal are random and uncorrelated across variables (*i.e.*, errors do not introduce directional bias). In unconsolidated sandy settings, that scenario is unlikely since sand is regularly transferred between the shoreface and subaerial beach in response to the same forcing, simultaneously affecting the shoreline, shoreface profile, and shoreface cross-sectional volume (Larson *et al.*, 2000). The same relationship can be seen in the relatively strong correlations between slope and nearshore volume. Geologic variables may be more independent in sediment poor coastal environments where the seafloor is characterized by indurated or semi-indurated sedimentary units and consequently less responsive to waves and currents. Valvo *et al.* (2006) argue that waves are the foremost control on coastal behavior and can even overprint the distinct influence of geology over the long term. In their deterministic model runs, long-term shoreline change patterns were not statistically different at locations that were initiated with comparatively different mean grain sizes.

(2) Another key challenge in relating shoreline behavior to geologic variability lies in selecting a representative data model to describe and using appropriate statistical methods to compare shoreline change and geology. For example, traditional shoreline-change rate methods, such as end-point rate and least squares regression, assume shoreline migration can be explained as linear and spatially independent

phenomena. More advanced, parsimonious methods recognize the non-linearity of shoreline change over time by fitting polynomials to shoreline change positions to increase the accuracy and capture temporal variations in shoreline trend (Frazer *et al.*, submitted). Recognizing the potential for storm, seasonal, and climatic fluctuations to mask the long-term signal is critical, since cross-shore profile and associated volumes are also affected over similar event and time scales (Larson and Kraus, 1994; Nicholls *et al.*, 1998; Larson *et al.*, 2000). Bathymetry and seismic surveys, where access is ultimately limited by depth and wave conditions, can *only* capture geologic conditions at discrete times and over part of the shoreface; consequently, there is considerable uncertainty in what a single profile or supported shoreface volume represents (Figure 34). Even avoiding storm response and immediate recovery periods, there is no assurance that a random fair-weather survey adequately represents average cross-shore alongshore conditions. This analysis presumes, based on observations that the surf zone and upper shoreface are more dynamic and subject to change (Kraus and Larson, 1994), that lower parts of the profile, significantly less affected by most wave events, are more likely to be in equilibrium with long-term average conditions. Nicholls *et al.* (1998), based on 12 years of repeated profiles at the Field Research Facility in Duck, North Carolina, suggests a minimum of 4 m separates the active surf zone from the less active offshore zone. However, the same authors also note that the gross change in the zone that extended down to 8 m was 15 times the net change. Ironically, sand exchange on the lower shoreface is typically ignored for sub-decadal prediction because of its relatively smaller fluxes (Hanson *et al.*, 2003)– it is presumed that the flux of finer grained sediment is not relevant to the upper shoreface and surf zone budget (Cowell *et al.*, 2003).

This analysis assumes a long-term average closure (~8 m isobath), but the best research on closure shows it is event dependent, a viable concept for the 100-year event, but not necessarily so for a 100-year period (Nicholls *et al.*, 1998). Figure 34 shows a conceptual illustration showing possible length scales that could be used to define a cross-shore zone of influence. The thickness isopach determined from seismic data shows a seaward thinning prism out beyond 4 km at this one location. The elevation change between 1978/1982 and 1933/1934 at this sample location suggests a different long-term depth of closure (~ -10 m). Defining the equivalent cross-shore zone is even more challenging in the presence of attached and detached morphology.

(3) Results of autocorrelation analyses show both shoreline change and geologic framework exhibit multiple and persistent scales of spatial dependence. Numerous researchers have recognized similar spatial phenomena, indicating correlation scales between 300 m and 8 km (Dolan *et al.*, 1992; Honeycutt and Krantz, 2003; Walton, 2000; Schupp *et al.*, 2006; Houser *et al.*, in press). These authors have attributed these phenomena to a range of properties, including kilometer-scale transitions in sediment types, longshore bar morphologies, and regional variations in wave climate. Classical statistical inference demands that data be independent and stationary. Such criteria are extremely difficult to attain in natural systems, where controlling processes are spatially contiguous (Dolan *et al.*, 1992). Removing trend and treating autocorrelation allows the statistician to evaluate the smaller scale relationships, but because of potential bias in the residuals related to the treatment method, complex relationships emerge and subsequent spatial and causal inferences are more difficult.

(4) In this study, cross-correlation analysis was used to determine the strength and lag of spatial co-dependence. This technique assumes a linear relationship between variables when the relationship may be non-linear; moreover, it assumes a linear alongshore response when it may be non-linear. When using cross-correlation, it is also unclear whether the correlation addresses a single scale or all alongshore scales of variation occurring in the data. For practical purposes, it is assumed that the correlation coefficient averages the correlation at all length scales (Houser *et al.*, in press).

#### 6.5 *Shoreline Change Predictions using Nearshore Sand Volume*

It is imperative to recognize that this hindcast relationship may not be a perfect predictor for future change, without accounting for the possible (re)introduction of (new) sediment. In the absence of modern fluvial input, transgressive barrier islands adjust to rising sea levels by shoreface erosion or bypassing of former back-barrier and inlet facies and Pre-Holocene facies, thereby introducing significant volumes of new sand into the sediment budget (Swift, 1968; Kraft, 1971; Belknap and Kraft, 1985; Finkelstein, 1986; McNinch *et al.*, 1999; Gayes *et al.*, 2003; Kelley *et al.*, 2005). This reintroduction of material to barrier islands is necessary to explain the maintenance of barriers over the Holocene transgression (Riggs *et al.*, 1995; McNinch *et al.*, 1999; Cowell *et al.*, 2003). Even if sand is exhumed on the lower shoreface, it can be transported shoreward as bed load under fair-weather conditions (Schwartz and Birkemeier, 2004).

This is a process accepted over transgressive time and space scales (*e.g.*, millennia, ~100 km, see Stopler *et al.*, 2005), but it is not well understood or documented over resource management time and space scales, despite estimates that the mid-Atlantic shoreface is retreating at rates of 1-3 m/yr (Niedoroda *et al.*, 1985). The process of

ravinement is particularly important in the northern Delmarva Coastal Compartment, where beach-compatible sand reserves in headlands have recently become available to the littoral system as the eroding shoreline intersected it and notably increased the potential sediment budget for the lower Peninsula (Honeycutt and Krantz, 2003). A few authors have surmised that the variable, but generally coarse lag of the ravinement surface may inhibit wave stirring and suspension of material below the ravinement over relevant time scales (Goff *et al.*, 2005; Miselis and McNinch, 2006). Offshore of Martha's Vineyard, Goff *et al.* (2005), using a mass-balance comparison of grain sizes above and below the ravinement, determined that underlying glacio-fluvial sediments were not a likely source for shoreface sands. While it is possible that the coarse lithology of the ravinement surface may serve to armor underlying sediments during energy events of a certain scale, it could also promote enhanced wave-orbital turbulence, scour below the ravinement lag, and sequential suspension of finer grained material through interstitial pore space, and advection of sediment by combined flow (Dickson, 1999). In order to clarify this process, the temporal and lateral/vertical scales relevant to ravinement must be studied.

The sand budget may increase or decrease locally depending on the volume and grain size of available material that is being reworked, which itself varies spatially on the landward-translating shoreface (Finkelstein, 1986; Honeycutt and Krantz, 2003). The results herein incorporate any past erosion and release of underlying or outcropping lithosomes into the discrete measurement of shoreface volume. The corresponding volume estimate does not address the quantity, erodability, and compatibility of material below the ravinement depth, or how that material is introduced and moved through the

transport system. If the nearshore sand volume measure had included that underlying A2 unit in the study area, local thicknesses may have increased upwards of 5 m and likely reversed the correlation findings. Miselis and McNinch (2006) developed a measure to predict future change, premised on the assumption that underlying sources represent an insignificant contribution to the sediment budget, compared to longshore transport, over decadal and centennial scales. Supporting this notion, Finkelstein (1986) reported that the annualized sand volume introduced by backbarrier lithosomes was only a fraction of predicted longshore transport along the rapidly eroding barriers of the Eastern Shore of the Virginia.

The net sediment flux (*i.e.*,  $\sim 10^6$  m<sup>3</sup>/yr) to the southern end of Assateague Island dwarfs that calculated at Ocean City Inlet, Maryland (*i.e.*,  $\sim 10^5$  m<sup>3</sup>/yr in Dean and Perlin, 1977, Rosati and Ebersole, 1996), 60 km north along Assateague Island. The longshore transport rates account for the sediment trapping capacity at Ocean City Inlet that has existed since the inlet was stabilized in 1935, shortly after it was opened by the *Storm of the Century*. The volumetric change analysis shows that a critical volume of sediment needs to be introduced into the system to account for the volume stored at the inlet/spit sink. Volumetric change estimates (*i.e.*,  $<70,000$  m<sup>3</sup>/yr) indicate little inner shelf contribution in the study area, despite widespread evidence that offshore sediment sources are important elsewhere (Larson and Kraus, 1994; Gayes *et al.*, 2003). Within the study area, the shoreface fronting Toms Cove is shedding  $\sim 300,000$  m<sup>3</sup>/yr. Side scan imagery in this area suggests the resource in unit A2 may be increasingly important to the local sediment budget. Further north, the shoreface has accreted over the historic period.



It is also possible that sediment from shoreface erosion further upstream makes up the  $10^6$   $m^3$  deficit.

A rudimentary exercise was undertaken to evaluate the rate at which the seafloor lowers compared to the thickness of the sand prism (Figure 35). In this simplified, steady-state model, it was assumed that the ravinement did not change relative to the lowering seafloor, despite the fact that side scan sonar and seismic data suggest otherwise. Bathymetric change rates were derived and transformed to sediment fluxes ( $m^3/yr$ ) by multiplying each value by cell area. Areas experiencing accretion were masked. The sand-thickness isopach was converted to volume by multiplying thickness by cell area. A time scale is derived by dividing the sand-thickness isopach by the sediment flux. The resulting scale provides an approximate time frame over which the ravinement is exposed at the seafloor, or the ravinement must lower and be buried by some overlying *equilibrium* shoreface deposit. Timescales of less than 20 years are derived for large regions seaward of Toms Cove and in the landward trough of the largest shoreface-attached sand ridge; this suggests the ravinement process is relevant to predicting future supported volumes and shoreline change. Shoreface bypassing is most likely to occur during extreme events when the shoreface is disturbed at locations where the overlying sand prism is absent or relatively thin. Settings characterized by a relatively thick sand prism, such as detached and attached sand ridges, are consequently less prone to bypassing over shorter time scales. Seismic data show the ravinement is topographically higher beneath the core of sand bodies, partly an artifact related to sound travel, but it also reflects that the ravinement is not lowering at a rate as fast as in adjacent troughs where the sand cover is limited. While the shoreface is shown to be lowering in place at

an average rate of  $<5$  cm/yr, the ravinement may be lowering at a different rates at different locations over the same time frame.

## 7 CONCLUSIONS

The utility of shoreline-change data increases when the data are examined in context of the myriad factors that collectively contribute to observed behavior; spatial and temporal complexities need to be evaluated in terms of both self-organized processes and the influence of forcing templates. This practice is best achieved through both deterministic modeling and observational verification, culminating in an improved understanding of how the hydrodynamic regime interacts with the geologic setting and vice versa. As an intermediate step to the more deterministic evaluation, the geologic framework, including stratigraphic and morphologic elements, can be defined, quantified, and tested against affected space and time scales of shoreline change. This study applies this approach along southern Assateague Island and Wallops Island on the Eastern Shore of Virginia, elucidating the complex spatial and temporal scales over which coastal scientists and managers alike need to be concerned about the influence of geology on shoreline behavior. The key findings are summarized as follows:

(1) Shoreline change data for Assateague Island and Wallops Island reveal patterns consistent with respective wave and mixed-energy morphologies. Long-term and shorter-term shoreline change data show analogous patterns of erosion and accretion superimposed on a north-south erosional trend. Shorter-term data show elevated erosion rates along both barriers, larger spatial scales affected by erosion, and increasing mobility near Chincoteague Inlet. Along Assateague Island, discrete zones of shoreline change are magnified and spatially coincident with shoreface-attached ridges. Over the historic period, the stretch of shoreline from Assateague Island along Toms Cove Hook has switched from rapid spit progradation to progressive erosion. In comparison, the entire 11

km coastline of Wallops Island has been influenced by inlet related processes and historical engineering. Nominal rates of sediment bypassing at Chincoteague Inlet, a sediment transport reversal longshore transport south of Gunboat Point, and longshore divergence related to shoreline curvature are consistent with overall erosional trends. In contrast to Assateague Island, Wallops Island is backed by extensive marsh that may influence barrier migration as it is encountered in the shoreface and surf zone.

(2) Assateague Island and Wallops Island exhibit comparatively different seafloor gradients and bottom topography, presumably related to different energy regimes, as well as variability in underlying geology. Prograding, relatively more dissipative zones offshore Assateague Island are spatially coincident with stable and accreting shoreline reaches. Shoreface-attached sand ridges represent significant alongshore irregularities in context of regional bathymetric gradients, and consequently, may be important to shallow water wave transformation processes.

(3) A longshore sediment load of approximately  $1.5 \times 10^6 \text{ m}^3$  is transported to the sink at the southern terminus of Assateague Island each year. A sediment budget deficit on the order of  $10^6 \text{ m}^3$  exists in the study area; this suggests that there must be a significant contribution from shoreface erosion and/or onshore flux from the nearshore along the 60 km Assateague Island. In comparison, only 5% of the sediment load bypasses Fishing Point, Chincoteague Inlet, and the coupled nodal point along northern Wallops Island.

(4) The surface-expressed geologic framework encountered within 5 km of the coast includes two spatially variable stratigraphic units: 1) modern marine sands, organized into the shoreface sand sheet, attached and detached sand ridges, and underlying spit

platform/shoal deposits, and 2) underlying mid- to late-Holocene age paralic deposits. The active, modern sand cover is locally thick at sand ridges and shoals, absent in adjacent troughs, and thins to near seismic resolution at depths greater than 10 m. The southern 15 km of the Assateague Island sand sheet is underlain by shallow marine sands constituted during spit progradation over the colonial period. Relatively thick and variable Holocene depositional environments, including backbarrier, tidal inlet, lagoon, and paleo-channel fill facies, occur beneath the overlying fine to medium sand deposits offshore both islands. The shoreface off of Assateague Island is characterized by widespread evidence of historic inlet systems, indicating the south Assateague Island / Chincoteague Island area has been a long-term sediment sink starving the mixed-energy barriers to the south. Seismic reflection and side scan sonar data show evidence of heterogeneous micro-topography and textural distribution at the seafloor on the lower shoreface and near inter-ridge swales, indicative of active substrate erosion and shoreface lowering. Given these observations, part of the overlying sand cover is presumed to be reworked from these underlying units, suggesting the preserved mid-Holocene stratigraphy is important to the future evolution of the barrier islands. The underlying Pleistocene units are comparatively deep, and as such, appear to have had limited influence on profile development. However, the planform evolution of the islands, that is the relative barrier position, dimension, and curvature, may be influenced by the location and orientation of the Chincoteague paleo-drainage system.

(5) The influence of the geologic framework on the two barrier islands, not necessarily independent of hydrodynamic and inlet processes, is observed in the differences in profile steepness, modern morphologic and sand prism thickness

variability, sediment texture, and island retreat behavior. Shoreface translation, as well as the stability and erosion of the barrier islands, may be related to the sediment contribution and topographic effect imparted by underlying marine/shoal sands and mixed-grained backbarrier, lagoonal, and relict inlet deposits. The southern 15 km of Assateague Island exhibits a range of subaerial morphology consistent with southern progradation by right-handed spit formation; in the future, these subaerial components and related shoreface platform and shoal deposits will represent a local sediment supply and potentially slow shoreline erosion on <2-3 km length scales. However, more prominent, concurrent factors, such as coastal strike relative to incident storm waves, may promote transport divergence and overshadow geologic influences.

(6) Offshore Assateague Island, framework geology is quantified using two measures: mean shoreface slope and sediment volume above the wave ravinement/proto-ravinement. Consistent with shoreline change measurements, local fluctuations are generally superimposed over a north-south regional trend. Volume and slope are higher in the presence of nearshore morphology. Cross-correlation statistics demonstrate relatively strong spatial coupling of nearshore morphology and shoreface sand prism to inter-annual, decadal, and long-term shoreline change. Over relatively small spatial lags, relative steeper shoreface profiles characterized by relative smaller shoreface volume correspond to erosional trends. The correlations are strongest for inter-annual time scales since short-term shoreline-change data capture more pronounced shoreline response at the local scale, especially in the vicinity of shoreface-attached sand ridges. Approximately half of the variability in nearshore volume measurements can be attributed to differences in bathymetric profile, but it depends on the alongshore length

scale considered. The dynamic shoreface accounts for a changeable proportion of the variability in geology and shoreline behavior in space and time.

(7) Using cross-correlation, determination of statistical significance and proportion of variability at regional and sub-regional scales is complicated by non-normality, autocorrelation, and bias introduced in treatment methods. Correlations are extremely sensitive to large variances and sudden trend reversals, so great care needs to be taken in selecting naturally fitting alongshore length scales. The effectiveness of parameterization and statistical analysis is further complicated by coupling between geology and hydrodynamics, non-linear and discontinuous shoreline behavior and morphologic evolution, and spatially and temporally variable correlation between indicators in an evolving natural system. Despite these limitations, correlation persists across shoreline change and geologic variables.

(8) Additional study is needed to improve parameterization of geologic variables and test for independence from hydrodynamic forcing. The logical progression of scientific inquiry would involve the comparison of wave-current model output to regional shoreface gradients, nearshore morphology, and nearshore sand volume. Breaking wave heights or wave boundary layer orbital velocities at the zone of breaking/shoaling could be tested against shoreline change, profile slope, and volume measurements. Future applications should refine the cross-shore scale over which volume and profile measurements are measured; this study used the zone between 4-m and 8-m isobaths under the assumption that this region of the shoreface is less affected by waves, and accordingly more likely to be in equilibrium with long-term average conditions. A better definition and measurement scheme of relevant cross-shore scales may be needed to more

fully account for the influence of geologic variability. If these measures are to be used for prediction, it may be important to document the variability in quantity and character of geologic units underlying the ravinement, as well as the time and space scales over which sand volume changes on the mid and lower shoreface occur, a process dictated by both seafloor and ravinement evolution. Although widely accepted over transgressive time scales, the process of shoreface ravinement may be relevant in areas characterized by limited sand cover over time frames germane to coastal management.



A.1 *Introduction*

Cross-correlation analysis has been used to test lagged linear correlation between a variety of data series characterizing a range of coastal geologic and hydrodynamic settings (Garrett and Petrie, 1981; Garret and Toulany, 1981; Walton, 1999; Plant *et al.*, 1999; List *et al.*, 2003; Duffy and Hughes-Clarke, 2005; Schupp *et al.*, 2006; Browder and McNinch, 2006; Miselis and McNinch, 2006; Thornton *et al.*, 2007; Houser *et al.*, in press). Yet, a review of the literature reveals little consensus on how to address (*if at all*) the major statistical challenges common to spatial data and time series: the inertia or persistence common to physical systems or processes, especially long-wavelength or low-frequency variability (Dolan *et al.*, 1992).

In the presence of non-stationarity (*i.e.*, trend) and autocorrelation (*i.e.*, spatial/temporal dependence), untreated cross-correlation coefficients are often misleading as a measure of statistically significant relationships since the measures violate the assumption of randomness and serial independence required for classical inference tests (Thiebaut and Zwiers, 1984; Emery and Thomson, 2001; Haining, 2003; Chatfield, 2004). The classical assumption states that the processes operating on tested variables are identical, but operate independently at a scale equal to less than the sampling interval (Dolan *et al.*, 1992). A correlation between trended, autocorrelated data series has fewer degrees of freedom (*i.e.*, a larger variance) than assumed under classical testing, and consequently, the Type I error rate (*i.e.*, concluding the correlation is statistically significant when it is not) is not accurately represented by the test level (*e.g.*,  $\alpha=.01$ ,  $\alpha=.05$ , etc.).

## A.2 Autocorrelation

Two measures of shoreline change, based on 18 GPS shorelines collected along Assateague Island, Virginia between 1997 and 2005 and interpolated at 50 m alongshore intervals, are shown in Figure A-1. The shoreline mobility (deviation in cross-shore position) and shoreline change rate data exhibit north-south trends (Figure A-2A) contributing to a non-normal distribution of alongshore values (*i.e.*, the mean and variance depend on the alongshore position) (Figure A-2B). The data are positively autocorrelated, meaning positive departures from the mean tend to be followed by positive departures from the mean, whereas negative departures tend to be followed by negative departures (Figure A-2C). Since both spatial data series are characterized by trend and statistically significant autocorrelation, special treatment is generally considered necessary to use conventional statistical testing (Haining, 2003; Chatfield, 2004). Unfortunately, removing trend may remove important information about a common process or phenomena influencing a region, although maintaining trend may mask co-variation at shorter wavelength or higher frequencies. Pyper and Peterman (1998) caution researchers about removing trend when data series distinctly co-vary, even though not following methods as described below for adjusting the test procedure may not adequately control type I error rates.

Figure A-2B shows histograms for data residuals following transformation using least squares, polynomial fitting, and first differencing (Panel A-3A shows the least squares and polynomial fit). The correlograms in Panels C-E show autocorrelation as a function of lag, where  $r_k$  is the autocorrelation at lag  $k$ . The correlation between observations separated by  $k$  steps is given by

$$r_k = \frac{\sum_{n=1}^{N-k} (x_n - \bar{x})(x_{n+k} - \bar{x})}{\sum_{n=1}^N (x_n - \bar{x})^2} \quad (1)$$

where  $r_0$  (zero lag) is unity. If a data series is characterized by trend,  $r_k$  only approaches zero at very large lags (Figure A-2C). This is because an observation on one side of the mean tends to be followed by related observations on the same side of the mean. Little can be inferred from non-stationary correlograms as the trend dominates all other length scales. Panels C-E of Figure A-2 show decreasing persistence in the autocorrelation function for the transformed, or treated, shoreline change data. In panels D and E, the data residuals are characterized by statistically significant autocorrelation through 5-7 lags, the equivalent of a 250 to 350 m independence length scale ( $L_i$ ). In comparison, a random data series is typically characterized by a near-zero correlation coefficient for all non-zero lags. Transforming the data may introduce bias into the residuals, indicated by sudden negative autocorrelation values (Figure A-2E).

If spatial data are autocorrelated, the number of independent observations is fewer than the sample size since the information represented by each sample is not independent from other adjacent observations (Emery and Thomson, 2001). As a result, the sampling variance, a function of actual observations, is underestimated using conventional formulas that treat data observations as if they were independent (Haining, 2003). To address this problem, two qualitatively different approaches are typically used: one involves an effective sample size and the other, called pre-whitening, removes the autocorrelation by modeling the time series and uses residuals for testing correlations.

### A.3 *Adjusting the Test Procedure: Calculating Effective Sample Size*

Adjusting the sample size (N), or computing the effective sample size for hypothesis testing, is the most common way to address the impact of autocorrelation on statistical significance. This step is not necessary if the sampling interval is greater than the length scale of statistically significant autocorrelation. All adjustments to N assume that corresponding data are weakly stationary, characterized by a relatively constant mean and variance (Haining, 2003). Chatfield (2004) indicates that the variances of sample cross-correlations depend on the autocorrelation functions of both data series. Therefore, the effective sample size (N\*) for hypothesis testing using autocorrelated data can be theoretically approximated using

$$\frac{1}{N^*} \approx \frac{1}{N} + \frac{2}{N} \sum_{k=1}^{\infty} \frac{(N-k)}{N} r_{xx}(k)r_{yy}(k) \quad (2)$$

where N is the sample size and  $r_{xx}(k)$  and  $r_{yy}(k)$  are autocorrelations of X and Y as a function of lag k (Pyper and Peterman, 1998; Garrett and Petrie, 1981). Given N\*, the critical value of  $r_{xy}$  at any significance level ( $\alpha$ ) can be derived using the t distribution. When both data series contain positive autocorrelation, values of N\* will be less than N, resulting in larger, more conservative critical values and leading to fewer rejections of the null hypothesis. In practice, autocorrelations are typically estimated over the first N/3 to N/5 lags using some variant of the estimator provided in Equation 1. Based on simulations of error rate performance using different adjustment procedures, Pyper and Peterman (1998) recommend using the following formula to estimate effective sample size:

$$\frac{1}{N^*} \approx \frac{1}{N} + \frac{2}{N} \sum_{k=1}^{N/5} r_{xx}(k)r_{yy}(k) \quad (3)$$

where  $r_{xx}(k)$  and  $r_{yy}(k)$  are scaled by  $N/(N-k)$ . The authors further recommend using  $N^*-2$  degrees of freedom to conservatively determine the critical value.

Emery and Thomson (2001) and Plant *et al.* (1999) offer arguably more complicated alternatives to determine effective sample size. Emery and Thomson (2001) show that  $N^*$  can be calculated as  $N^*=N\Delta s/S$  where  $\Delta s$  is the distance between two consecutive observations and  $S$  is the integral space scale for the data series. In the discrete case,  $S$  is proportional to the autocovariance function  $c(s)$  as a function of lag  $s$ :

$$S = \frac{1}{c(0)} \sum_{k=0}^{N-1} \frac{\Delta s}{2} [c(s_k + \Delta s) + c(s_k)] \quad (4)$$

where  $m$  is the number of lag values incorporated in the integral and  $\frac{1}{2}[c(s_k + \Delta s) + c(s_k)]$  is the mean value of  $c$  for the midpoint of the lag interval  $(s_k, s_k + \Delta s)$ . The autocovariance function at lag  $k$  is simply  $r_k \times c_0$ . In comparison, Plant *et al.* (1999) estimate  $N^*$  by deriving a proportionality factor ( $v$ ) and a different critical value derived from a chi square distribution assuming one degree of freedom. The proportionality factor ( $v$ ) is defined as  $v = 1 / E\{r^2N\}$  where  $E\{\}$  is the expected value of the product of the square of the sample correlation coefficient and the sample size. Albeit many sample correlation estimates are possible at different positive and negative lags, a simplification uses the average  $r^2N$  over a subset of positive and negative lags in order to estimate  $v$ .

Pyper and Peterman (1998) caution that all of these methods may ultimately perform poorly in practice because (1) the expressions for  $N^*$  are based on asymptotic formulas that may not be accurate for short or sub-population data series, (2) estimates of autocorrelation functions are known to be both imprecise and biased, (3) distributions assumed by the critical value may be inappropriate, (4) it is unknown how many lags should be used when estimating  $N^*$ , and (5) treatment may introduce bias. Some authors

have noted the complicated nature of the aforementioned approaches and opted for a more simplistic, but potentially less conservative approach. Schupp *et al.* (2006), citing List *et al.* (2003), rely on the autocorrelation function to determine the alongshore distance over which data is spatially dependent and derive a corresponding factor of proportion (P) for scaling the sample size. For example, Figure A-2 shows 389 observations at 50 m intervals representing less than 20 km of shoreline. The untreated data are characterized by statistically significant autocorrelation through approximately 30 lags, or 1.5 km. Following the methodology of Schupp *et al.* (2006), the effective sample size  $N^*_{Li}$  is 13; in comparison, the method prescribed by Pyper and Peterman (1998), calculated in spite of obvious trend, results in  $N^*_{ACF}$  equals 8. Following least squares detrending, the effective sample sizes for the transformed data series are  $N^*_{Li}=56$  and  $N^*_{ACF}=23$ . It is important to note that multiple independent length scales occur in data series, which are clearly delineated by the different correlograms in Figure 2. Detrending accentuates these other length scales at the expense of the regional, dominant scale. The simplest procedure follows the work of Miselis and McNinch (2006) and requires the use an alongshore sampling interval that is larger than statistically significant autocorrelation. However, this method cannot be used to address phenomena that occur over smaller space scales and is therefore somewhat limiting.

Figure A-3 shows the normalized (*i.e.*, demeaned) cross-correlation of shoreline mobility and shoreline change rate (using Equation 3) for the untreated data series, as well as residuals from least squares and polynomial detrending. The critical values reported in Figure A-3A and A-4 are more sensitive to Type I errors since the effective sample size estimation used therein is only valid for stationary data. Results show that the shoreline

change rate is inversely related to shoreline mobility and the maximum correlation occurs at a positive lag, or in the direction of time-averaged longshore transport. Detrending reduces regional-scale autocorrelation thus tending to magnify smaller scale co-variation (Figure A-2C-2E). As alongshore variability is magnified in the autocorrelation function, the cross-correlation coefficients decrease and lag patterns increasingly vary (Figure A-3). Polynomial detrending produces a maximum correlation near zero lag (Figure A-3C), whereas least squares detrending has little to no effect on the lag (Figure A-3B). In general, the alongshore length scale of statistically significant correlation is reduced by detrending. But, detrending may lead to statistically significant correlations at multiple lags and in opposite directions that are difficult to interpret using a causal logic. Regardless, the autocorrelation function and effective sample size calculation are sensitive to the transformation method used and scale of variability represented in the data series. Figures A-4 and A-5 show cross-correlation results for the same shoreline mobility and change data, but the data series is shortened from the south by approximately 50 observations or 2.5 km. This effectively removes the distinct signal corresponding to the spit complex at the southern terminus of Assateague Island (south of Northing 4192000). The magnitude of the maximum correlation coefficient changes little relative to the significant change in the lag location. Treatment of the data produces rather different results. Figure A-5 shows that statistically significant co-variation at multiple shorter-wavelength scales in the shoreline mobility and change data is maintained, but the direction is reversed. This tendency is an artifact related to the introduction of bias by the treatment method.

#### A.4 *Pre-whitening*

The other common approach to deal with spatial dependence is to pre-whiten the spatial data series. The premise underlying this method is that transformed spatial data are free of autocorrelation and can be evaluated using classical statistical inference tests. Pre-whitening involves modeling data to both detrend and remove higher-order autocorrelation properties. Autoregressive Integrated Moving Average models are typically employed to remove autocorrelation. An ARIMA, or autoregressive (AR), differencing or integration (I), and moving-average (MA), model is used to describe the random disturbances that affect the difference between two observations in a series. Each of the three components of an ARIMA model (not all components are necessarily included) has its own characteristic way of responding to a random disturbance. In its simplest form, an ARIMA model is typically expressed as ARIMA(p,d,q) where p is the order of autoregression, d is the order of differencing, and q is the order of moving-average involved.

ARIMA modeling begins with first-differencing to adjust non-stationary series to a stationary series accounting for both non-seasonal and seasonal trends. Such a model is called integrated because the stationary model that is fitted to the differenced data has to be summed to provide a model for the original non-stationary data (Chatfield, 2004). Data could also be de-trended using a different transformation such as a log-transformation; in such a case, the differencing order in the ARIMA model would be set to zero. The autoregressive (AR) model expresses spatial data as a linear function of its adjacent values, where the order (p) of the AR model indicates how many lagged values are included. AR(p) models generally exhibit exponentially declining values of the autocorrelation function (possibly with alternating positive and negative values) and have precisely p



spikes in the first  $p$  values of the partial autocorrelation function. The partial autocorrelation function at lag  $k$  is the autocorrelation that remains after removing autocorrelation with an  $AR(k-1)$  model. The residuals generated from the model are assumed to be random in space and normally distributed. In comparison, the moving average (MA) model expresses spatial data as an geographically-weighted moving average of a random error, or residual (Chatfield, 2004). The order ( $q$ ) of the MA model indicates the number of lags used.  $MA(q)$  models generally have  $q$  spikes in the first  $q$  values of the autocorrelation function and exponentially declining values of the partial autocorrelation function.

Parsimony dictates that statisticians find a model with as few parameters as possible—so not all components are necessarily used. Identification of the model, model structure, and component order occurs by using an iterative procedure to fit model coefficients, determine goodness-of-fit statistics, and subsequently compare the autocorrelation and partial autocorrelation functions. Diagnostic checking of the model ensures that the residuals are random and estimated parameters are statistically significant (Chatfield, 2004). The autocorrelation function and partial autocorrelation function of the residual series should not be significantly different from zero. One or two high-order correlations may exceed the 95% confidence level by chance; however, if the first- or second-order correlation is large, the model is likely to be incorrectly specified.

In preparing for cross-correlation, one of the series should be ARIMA modeled and converted to residual values (*i.e.*, the process of pre-whitening). The same filter should be applied to the second series before computing the cross-correlation function (Chatfield, 2004). Some authors recommend pre-whitening both series with unique ARIMA models.

However, with one treated data series, two uncorrelated series can be tested to see if the cross-correlation is significantly different from zero. The conventional confidence interval estimation used to evaluate significance of a correlation coefficient can be applied.

Pre-whitening typically removes long wavelength or low frequency variability that is common to spatial data series and may underestimate subsequent covariance determinations (Pyper and Peterman, 1998). As a result, the probability that a statistically significant relationship between two data sets characterized by long-wavelength system processes will be excluded increases (Type II error). Figure A-6A shows an ARIMA (1,1,0) model fit to the shoreline change rate data and its corresponding residuals. The autocorrelation and partial autocorrelation functions show that most of the variability at scales of interest has been removed (Panels B and C in Figure A-6). Since longer wavelength variability is the dominant source of covariation between the two spatial data series, removing autocorrelation, rather than adjusting the sample size, proves ineffective (Pyper and Peterman, 1998).

#### A.5 *Conclusions*

There is no single, perfect method to use when dealing with non-stationary, autocorrelated data in cross-correlation analysis, even if noise is first filtered out using a decompositional transformation (Walton, 2000). Likewise, it is important to realize that the cross-correlation function tests for linear relationships when the relationships may be non-linear and the nature of the variables or strength of the relationship between variables may actually change over time. The researcher must choose a method that adequately addresses trend, variance, and scales of co-variation that are of interest. Since pre-whitening effectively removes all variability of interest, transforming the data series and adjusting the

test procedure is the default treatment method. Since scales of coastal change can range from basin to block scales (Harris *et al.*, 2005), it is recommended that the adjustment procedure described above be performed on both untreated and treated data and only on data series characterized by a length scale fitting for the hypothesis being tested. Dolan *et al.* (1992) have suggested natural geomorphologic boundaries, such as headlands, inlets, bathymetric discontinuities, and changes in shoreline orientation be used to define the appropriate length scale. The authors further recommended that the alongshore length be at least 5 km to capture alongshore information greater than the maximum autocorrelation length scale.

Cross-correlation, as a linear statistical measure, is inherently insensitive to the different length scales that contribute to alongshore variability in the spatial data series. Therefore, all correlation coefficients and lags are best interpreted as the practical equivalent of an average of all constituent scales of variation. A critical limitation to this method is that reversing, statistically significant correlation relationships may be difficult to interpret following treatment for trend and autocorrelation. There are other methods for testing the spatial relationship between two variables that may be substituted, such as spectral cross-coherence (Houser *et al.*, in press) and wavelet cross covariance (Whitcher *et al.*, 2000; Tebbens *et al.*, 2002), which treat data in the frequency domain and do not necessarily assume, like cross-correlation, a linear relationship between lagged variables. The treatment of observed data for these alternative procedures is even more mathematically complex than that described herein; in keeping with the practical origin of this study, further exploration of these alternatives is beyond the point of diminishing return.

## 9 REFERENCES

- Anders, F.J. and Byrnes, M.R., 1991. Accuracy of shoreline change rates as determined from maps and aerial photographs. *Shore and Beach*, 59(1): 17-26.
- Anders, F.J., Reed, D.W. and Meisburger, E.P., 1990. Shoreline Movements: Report 2 -- Tybee Island, Georgina to Cape Fear, North Carolina, 1851-1983. CERC-83-1, U.S. Army Corps of Engineers - Waterways Experiment Station.
- Ashton, A.A., Murray, A.B. and Arnault, O., 2001. Formation of coastline features by large-scale instabilities induced by high-angle waves. *Nature*, 414: 296-300.
- Bartberger, C.E., 1976. Sediment sources and sedimentation rates, Chincoteague Bay, Maryland and Virginia. *Journal of Sedimentary Petrology*, 46(2): 326-336.
- Belknap, D.F. and Kraft, J.C., 1985. Influence of antecedent geology on stratigraphic preservation potential and evolution of Delaware's barrier systems. *Marine Geology*, 63: 235-262.
- Bender, C.J. and Dean, R.G., 2003. Wave field modification by bathymetric anomalies and resulting shoreline changes: a review with recent results. *Coastal Engineering*, 49: 125-153.
- Benedet, L., Finkl, C.W., Campbell, T. and Klein, A., 2004. Predicting the effect of beach nourishment and cross-shore sediment variation on beach morphodynamic assessment. *Coastal Engineering*, 51: 839-861.
- Berquist, C. R. Jr., and C. H. Hobbs, 1988. Study of economic heavy minerals of the Virginia inner continental shelf. Virginia Division of Mineral Resources Open File Report 88-4, 149 pp.
- Boak, E.H. and Turner, I.L., 2004. Shoreline definition and detection: a review. *Journal of Coastal Research*, 21(4): 688-703.
- Browder, A.G. and McNinch, J.E., 2006. Linking framework geology and nearshore morphology: correlation of paleo-channels with shore-oblique sandbars and gravel outcrops. *Marine Geology*, 231, 141-162.
- Byrnes, M.R., 1988. Holocene geology and migration of a low-profile barrier island system, Metompkin Island, Virginia. Ph.D. Dissertation, Old Dominion University, Norfolk, VA, 423 pp.
- Byrnes, M.R., Baker, J.L. and Feng, L., 2002. Quantifying potential measurement errors and uncertainties associated with bathymetric change analysis. ERDC/CHL CHETN-IV-50, U.S. Army Engineer Research and Development Center, Vicksburg, MS.

- Calvete, D., Falques, A., De Swart, H.E. and Walgreen, M., 2001. Modelling the formation of shoreface-connected sand ridges on storm-dominated inner shelves. *Journal of Fluid Mechanics*, 441: 169-193.
- Cattaneo, A. and Steel, R.J., 2003. Transgressive deposits: a review of their variability. *Earth-Science Reviews*, 62: 887-228.
- Chatfield, C., 2004. The analysis of time series: an introduction. 6<sup>th</sup> edition. Chapman and Hall, London, U.K.
- Coco, G. and Murray, A.B., 2007. Patterns in the sand: form forcing templates to self-organization. *Geomorphology*, 91: 271-290.
- Conkwright, R.D. and Gast, R.A., 1995. Potential offshore sand resources in southern Maryland shoal fields. Maryland Geological Survey, File Report No. 95-4, 42 pp.
- Cooper, J.A.G. and Navas, F., 2004. Natural bathymetric change as a control on century-scale shoreline behavior. *Journal of Geology*, 32(6): 513-516.
- Cowell, P.J., Stive, M.J., Niedoroda, A.W., Swift, D.P., de Vriend, H.J., Buijsman, M.C., Nicholls, R.J., Roy, P.S., Kaminsky, G.M., Cleveringa, J., Reed, C.W., and de Boer, P.L., 2003. The coastal-tract (part 2): applications of aggregated modeling of low-order coastal change. *Journal of Coastal Research*, 19(4): 828-848.
- Crowell, M., Leatherman, S.P. and Buckley, M.K., 1991. Historical shoreline change: error analysis and mapping accuracy. *Journal of Coastal Research*, 7(3): 839-852.
- Daniels, R.C. and Huxford, R.H., 2001. An error assessment of vector data derived from scanned national ocean service topographic sheets. *Journal of Coastal Research*, 17(3): 611-619.
- Dean, R.G., 1991. Equilibrium beach profiles: characteristics and applications. *Journal of Coastal Research*, 7(1): 53-84.
- Dean, R.G. and Perlin, M., 1977. Coastal engineering study of Ocean City Inlet, Maryland. Proceedings, Coastal Sediments '77, American Society of Civil Engineers, 520-542.
- Dean, R.G. and Work, P.A., 1993. Interaction of navigational entrances with adjacent shorelines. *Journal of Coastal Research*, SI 18: 91-110.
- Demarest, J.M. and Leatherman, S.P., 1985. Mainland influence on coastal transgression: Delmarva Peninsula. *Marine Geology*, 63: 19-33.

- Dickson, S.M., 1999. The role of storm-generated combined flows in shoreface and inner continental shelf sediment erosion, transport, and deposition. Ph.D Dissertation, University of Maine, Orono, ME, 321 pp.
- Dolan, R., Hayden, B., and Felder, W., 1979. Shoreline periodicities and linear offshore shoals. *Journal of Geology*, 87: 393-402.
- Dolan, R., Hayden, B., and Heywood, J., 1977. Shoreline forms and shoreline dynamics. *Science*, 197: 79-51.
- Dolan, R., Lins, H. and Hayden, B., 1988. Mid-Atlantic coastal storms. *Journal of Coastal Research*, 4(3): 417-733.
- Dolan, R., Fenster, M.S. and Holme, S.J., 1992. Spatial analysis of shoreline recession and accretion. *Journal of Coastal Research*, 8(2): 263-285.
- Duane, D.B., Field, M.E., Meisburger, E.P., Swift, D.J.P. and Williams, S.J., 1972. Linear shoals on the Atlantic inner continental shelf, Florida to Long Island. In: D.J.P. Swift, D.P. Duane and O.H. Pilkey (Editors), *Shelf Sediment Transport: Process and Pattern*. Dowden, Hutchinson & Ross, Stroudsburg, Pennsylvania, pp. 447-498.
- Duffy, G.P. and Hughes-Clarke, J.E., 2005. Application of spatial cross correlation to detection of migration of submarine sand dunes. *Journal of Geophysical Research*, 110, F04S12, doi: 10.1029/2004JF000192.
- Dyer, K.R. and Huntley, D.A., 1999. The origin, classification and modeling of sand banks and ridges. *Continental Shelf Research*, 19: 1285-1330.
- Emery, W.J. and Thomson, R.E., 1999. *Data analysis methods in physical oceanography*. 2<sup>nd</sup> edition. Elsevier, Burlington, MA.
- Everts, C.H., Battley, J.P. and Gibson, P.N., 1983. *Shoreline Movements: Report 1 -- Cape Henry, Virginia to Cape Hatteras, North Carolina, 1849-1989*. CERC-83-1, U.S. Army Corps of Engineers -Waterways Experiment Station.
- Fenster, M.S. and Dolan, R., 1996. Assessing the impact of tidal inlets on adjacent barrier island shorelines. *Journal of Coastal Research*, 12(1): 294-310.
- Fenster, M.S., Dolan, R. and Morton, R.A., 2001. Coastal storms and shoreline change: signal or noise? *Journal of Coastal Research*, 17(3): 714-720.
- Fenster, M.S., Dolan, R., and Jones-Smith, J., 2008. What grain size distributions reveal about sediment sources and sinks for the Virginia barrier islands. Geological Society of America, Southeastern Section – 57<sup>th</sup> Annual Meeting.
- Field, M.E., 1979. Sediments, shallow subbottom structure, and sand resources of he

- inner continental shelf, central Delmarva Peninsula. Technical Paper No. 79-2, U.S Army Corps of Engineers, Coastal Engineering Research Center, Ft. Belvoir, VA, 122 pp.
- Field, M.E., 1980. Sand bodies on coastal plain shelves: Holocene record of the U.S. Atlantic inner shelf off Maryland. *Journal of Sedimentary Petrology*, 50(2): 505-528.
- Finkelstein, K., 1983. Cape formation as a cause of erosion on adjacent shorelines. In: O.T. Magoon and H. Converse (Editors), Third symposium on coastal and ocean management; Coastal Zone '83. American Society of Civil Engineers, San Diego, CA, pp. 620-640.
- Finkelstein, K., 1986. Backbarrier contributions to a littoral sand budget, Virginia Eastern Shore, USA. *Journal of Coastal Research*, 2(1): 33-42.
- Fitzgerald, D.M., 1996. Geomorphic variability and morphologic and sedimentologic controls on tidal inlets. *Journal of Coastal Research*, SI 23: 47-71.
- Fitzgerald, D.M., Kraus, N.C. and Hands, E.B., 2001. Natural mechanisms of sediment bypassing at tidal inlets. ERDC/CHL CHETN-IV-30, U.S. Army Engineer Research and Development Center, Vicksburg, MS.
- Foyle, A.M., 1994. Quaternary seismic stratigraphy of the inner shelf and coastal zone, southern Delmarva Peninsula, Virginia. Ph.D Dissertation, Old Dominion University, Norfolk, VA, 604 pp.
- Foyle, A.M. and Oertel, G.F., 1992. Seismic stratigraphy and coastal drainage patterns in the Quaternary section of the southern Delmarva Peninsula, Virginia, USA. *Journal of Sedimentary Geology*, 80(3-4): 261-277.
- Foyle, A.M., and Oertel, G.F., 1997. Transgressive systems tract development and incised-valley fills within a Quaternary Estuary-Shelf System: Virginia Inner Shelf, U.S.A. *Marine Geology*, 137: 227-249.
- Frazer, N.F., Genz, A.S and Fletcher, C.H., in press. Toward parsimony in shoreline change prediction (I): new methods. *Journal of Coastal Research*.
- Galgano, F.A., 1989. Shoreline recession and nearshore response: the Atlantic Coast of Delaware. M.S. Thesis, University of Maryland, College Park, Maryland, 161 pp.
- Galgano, F.A., 1998. Geomorphic analysis of modes of shoreline behavior and the influence of tidal inlets on coastal configuration, U.S. East Coast. Ph.D. Dissertation, University of Maryland, College Park, Maryland, 332 pp.
- Galgano, F.A., Douglas, B.C. and Leatherman, S.P., 1998. Trends and variability of shoreline position. *Journal of Coastal Research*, SI 26: 282-291.

- Garrett, C., and Petrie, B., 1981. Dynamical aspects of the flow through the Strait of Belle Isle. *Journal of Physical Oceanography*, 11: 376-388.
- Garret, C., and Toulany, B., 1981. Variability of the flow through the Strait of Belle Isle. *Journal of Marine Research*, 39:163-189.
- Gayes, P.T., 1983. Primary consolidation and subsidence in transgressive barrier island systems. M.S. Thesis, Penn State University, State College, Pennsylvania, pp.
- Gayes, P.T., Schwab, W.C., Driscoll, N.W., Morton, R.A., Baldwin, W.E., Denny, J.J., Wright, E.E., Harris, M.S., Katuna, M.P., Putney, T.R., and Johnstone, E., 2003. Sediment dispersal pathways and conceptual sediment budget for a sediment starved embayment: Long Bay, South Carolina. Coastal Sediments '03. World Scientific Publishing, Clearwater Beach, FL.
- Goettle, M.S., 1978. Geological development of the southern portion of Assateague Island, Virginia. M.S. Thesis, University of Delaware, Newark, DE, 143 pp.
- Goettle, M.S., 1981. Geological development of the southern portion of Assateague Island, Virginia. *Northeastern Geology*, 3(3/4): 278-282.
- Goff, J.A., Mayer, L.A., Traykovski, P., Buynevich, I., Wilkens, R., Raymond, R., Glang, G., Evans, R.L., Olson, H., and Jenkins, C., 2005. Detailed investigation of sorted bedforms, or "rippled scour depressions," within the Martha's Vineyard Coastal Observatory, Massachusetts. *Continental Shelf Research*, 25: 461-484.
- Goldsmith, V., 1976, Continental shelf wave climate models: A critical link between shelf hydraulics and shoreline processes, in Davis, R. A. (editor), Beach and nearshore sedimentation: Nearshore processes - Physical and biological: SEPM Special Publication 23, American Association of Petroleum Geologists, Tulsa, OK, pp. 39-60.
- Gutierrez, B.T., Williams, S.J., and Thieler, E.R., 2007. Potential for shoreline changes due to sea-level rise along the U.S. Mid-Atlantic Region. U.S. Geological Survey, Open-File Report 2007-1278 (on-line).
- Haining, R., 2003. Spatial data analysis: theory and practice. Cambridge University Press, Cambridge, U.K.
- Halsey, S.D., 1978. Late quaternary geologic history and morphologic development of the barrier island system of the Delmarva Peninsula of the Mid-Atlantic Bight. Ph.D. Dissertation, University of Delaware, Newark, DE, 592 pp.
- Halsey, S.D., 1979. Nexus: new model of barrier island development. In Leatherman, S.P. (ed.), Barrier Islands from the Gulf of St. Lawrence to the Gulf of Mexico. Academic press, New York, pp.185-210.



- Hanson, H. and Kraus, N.C., 1989. GENESIS: Generalized Model for Simulating Shoreline Change. Report 1: Technical Reference. Vicksburg, Mississippi: U.S. Army Corps of Engineers Waterways Experimental Station, Technical Report, CERC-89-19.
- Hanson, H., Aarninkhof, S., Capobianco, M., Jimenez, J.A., Larson, M., Nicholls, R.J., Plant, N.G., Southgate, H.N., Steetzel, H.J., Stive, M.J.F., and de Vriend, H.J., 2003. Modelling of coastal evolution on yearly to decadal time scales. *Journal of Coastal Research*, 19(4): 790-811.
- Harris, M.S., 1992. The Geomorphology of Hog Island, Virginia: A Mid-Atlantic Coast Barrier. M.S. Thesis, University of Virginia, Charlottesville, VA, 76 pp.
- Harris, M.S., Gayes, P.T., Kindinger, J.L., Flocks, J.G., Krantz, D.E., and Donovan, P., 2005. Quaternary geomorphology and modern coastal development in response to an inherent geologic framework: an example from Charleston, South Carolina. *Journal of Coastal Research*, 21(1): 49-64.
- Hayes, M.O., 1979. Barrier island morphology as a function of tidal and wave regime. In: S.P. Leatherman (Editor), *Barrier Islands: from the Gulf of St. Lawrence to the Gulf of Mexico*. Academic Press, Inc., New York, NY, pp. 1-28.
- Hayes, M.O., 1980. General morphology and sediment patterns in tidal inlets. *Sedimentary Geology*, 26: 139-156.
- Hayes, M.O. and Nairn, R.B., 2004. Natural Maintenance of sand ridges and linear shoals on the U.S. Gulf and Atlantic continental shelves and the potential impacts of dredging. *Journal of Coastal Research*, 20(1): 138-148.
- Headland, J.R., Vallianos, L. and Sheldon, J.G., 1987. Coastal processes at Wallops Island, VA. In: N.C. Kraus (Editor), *Coastal Sediments '87*. American Society of Civil Engineers, New Orleans, LA, pp. 1305-1320.
- Hobbs, C.H., 2004. Geological history of Chesapeake Bay, USA. *Quaternary Science Reviews*, 23: 641-661.
- Hobbs, C.H., Milligan, D.A. and Hardaway, C.S., 1999. Long-term trends and short-term variability in shoreline change rates: southeastern Virginia. In: N.C. Kraus and W.C. McDougal (Editors), *Coastal Sediments '99*. American Society of Civil Engineers, Long Island, NY, pp. 1268-1283.
- Honeycutt, M.G., 2003. Spatial variability in shoreline change along the Atlantic Coast of Delaware: influence of geologic framework. Ph.D Dissertation, University of Delaware, Lewes, DE, 197 pp.

- Honeycutt, M.G. and Krantz, D.E., 2003. Influence of the geologic framework on spatial variability in long-term shoreline change, Cape Henlopen to Rehoboth Beach, Delaware. *Journal of Coastal Research*, SI 38: 147-167.
- Honeycutt, M.G., Crowell, M. and Douglas, B.C., 2001. Shoreline position forecasting: impact of storms, rate-calculation methodologies, and temporal scales. *Journal of Coastal Research*, 17(3): 721-730.
- Houser, C., Hapke, C., and Hamilton, S, in press. Controls on coastal dune morphology, shoreline erosion, and barrier island response to extreme storms. *Geomorphology*.
- Jackson, D.W.T., Cooper, J.A.G., and del Rio, L., 2005. Geological control of beach morphodynamic state. *Marine Geology*, 216: 297-314.
- Kana, T.W., 1995. A mesoscale sediment budget for Long Island, New York. *Marine Geology*, 126: 87-110.
- Kelley, J.T., Barber, D.C., Belknap, D.F., Fitzgerald, D.M., van Heteren, S., and Dickson, S.M., 2005. Sand budgets at geological, historical, and contemporary time scales for a developed beach system, Saco Bay, Maine, USA. *Marine Geology*, 214: 117-142.
- Kochel, R.C. and Wampfler, L.A., 1989. Relative role of overwash and aeolian processes on washover fans, Assateague Island, Virginia-Maryland. *Journal of Coastal Research*, 5(3): 453-475.
- Kochel, R.C., Kahn, J.H., Dolan, R., Hayden, B.P., and May, P.F., 1985. U.S. Mid-Atlantic barrier island geomorphology. *Journal of Coastal Research*, 1(1): 1-9.
- Komar, P.D., 1998. *Beach Processes and Sedimentation*. Prentice Hall, Upper Saddle River, NJ, 544 pp.
- Kraft, J.C., 1971. Sedimentary facies patterns and geologic history of a Holocene marine transgression. *Geological Society of America Bulletin*, 82: 2131-2158.
- Krantz, D.E., 1991. A chronology of Pliocene sea-level fluctuations: the U.S. Middle Atlantic Coastal Plain record. *Quaternary Science Reviews*, 10: 163-174.
- Kraus, N.C. and Galgano, F.A., 2001. Beach erosional hot spots: types, causes, and solutions. ERDC/CHL CHETN-II-44, U.S. Army Engineer Research and Development Center, Vicksburg, MS.
- Kumar, N. and Sanders, J.E., 1974. Inlet sequence: a vertical succession of sedimentary structures and textures created by the lateral migration of tidal inlets. *Sedimentology*, 21: 491-532.

- Lane, E.M. and Restrepo, J.M., 2007. Shoreface-connected ridges under the action of waves and currents. *Journal of Fluid Mechanics*, 582: 23-52.
- Larson, M. and Kraus, N.C., 1994. Temporal and spatial scales of beach profile change, Duck, North Carolina. *Marine Geology*, 117: 75-94.
- Larson, M. and Kraus, N.C., 2003. Modeling regional sediment transport and coastal evolution along the Delmarva Peninsula, USA. Coastal Sediments '03. World Scientific Publishing, Clearwater Beach, FL.
- Larson, M., Capobianco, M. and Hanson, H., 2000. Relationship between beach profiles and waves at Duck, North Carolina, determined by canonical correlation analysis. *Marine Geology*, 163: 275-288.
- Larson, M., Capobianco, M., Jansen, H., Rozyński, G., Southgate, H.N., Stive, M.J.F., Wijnberg, K.M., and Hulscher, S., 2003. Analysis and modeling of field data on coastal morphological evolution over yearly and decadal time scales. Part 1: background and linear techniques. *Journal of Coastal Research*, 19(4): 760-775.
- Leatherman, S.P., Dean, R.G., Everts, C.E. and Fulfor, E., 1984. Shoreline and sediment budget analysis of north Assateague Island, Maryland. In: N.C. Kraus (Editor), Coastal Sediments '87. American Society of Civil Engineers, New Orleans, LA, pp. 1460-1471.
- List, J.H. and Farris, A.S., 1999. Large-Scale Shoreline Response to Storms and Fair Weather. In: N.C. Kraus and W.C. McDougal (Editors), Coastal Sediments '99. American Society of Civil Engineers, Long Island, NY, pp. 1324-1338.
- List, J.H., Farris, A.S., and Sullivan, C., 2003. Large-scale response of foreshore slope to storm events. Coastal Sediments '03. World Scientific Publishing, Clearwater Beach, FL.
- List, J.H., Farris, A.S. and Sullivan, C., 2006. Reversing storm hotspots on sandy beaches: spatial and temporal characteristics. *Marine Geology*, 226: 261-279.
- List, J.H., McNinch, J.E., Haines, D.M., and Lescinski, J., *in review*, Shoreface control of shoreline change hotspots, *Marine Geology*.
- Locker, S.D., Hine, A.C. and Brooks, G.R., 2003. Regional stratigraphic framework linking continental shelf and coastal sedimentary deposits of west-central Florida. *Marine Geology*, 200: 351-378.
- Maa, J.P.-Y. and Hobbs, C.H., 1998. Physical impact of waves on adjacent coasts resulting from dredging at Sandbridge Shoal, Virginia. *Journal of Coastal Research*, 14(2): 525-536.

Maa, J.P.-Y., Hobbs, C.H., Kim, S.C., and Wei, E., 2004. Potential impact of sand mining offshore of Maryland and Delaware: part I—impacts on physical oceanographic processes. *Journal of Coastal Research*, 20(1): 44-60.

McBride, R.A., 1999. Spatial and temporal distribution of historical and active tidal inlets: Delmarva Peninsula and New Jersey, USA. In: N.C. Kraus and W.C. McDougal (Editors), *Coastal Sediments '99*. American Society of Civil Engineers, Long Island, NY, pp. 1505-1521.

McBride, R.A. and Moslow, T.F., 1991. Origin, evolution, and distribution of shoreface sand ridges, Atlantic inner shelf, U.S.A. *Marine Geology*, 97: 57-85.

McNinch, J.E., 2004. Geologic control in the nearshore: shore-oblique sandbars and shoreline erosional hotspots, Mid-Atlantic Bight, USA. *Marine Geology*, 211: 121-141.

McNinch, J.E. and Luettich, R.A., 2000. Physical processes around a cusped foreland: implication to the evolution and long-term maintenance of a cape-associated shoal. *Continental Shelf Research*, 2000: 2367-2389.

McNinch, J.E., Wells, J.T. and Snyder, S.W., 1999. The long-term contribution of pre-Holocene sands to transgressing barrier islands. In: N.C. Kraus and W.C. McDougal (Editors), *Coastal Sediments '99*. American Society of Civil Engineers, Long Island, NY, pp. 786-801.

Miselis, J.M. and McNinch, J.E., 2006. Calculating shoreline erosion potential using nearshore stratigraphy and sediment volume, Outer Banks, North Carolina. *Journal of Geophysical Research*, 111, F02019, doi:10.1029/2005JF000389.

Mixon, R.B., 1985. Stratigraphic and geomorphic framework of uppermost Cenozoic deposits in the southern Delmarva Peninsula, Virginia and Maryland. U.S. Geological Survey Prof. Paper 1067-G, 53 pp.

Moffatt & Nichol, 1986. Wallops Island Shore Protection Study. NASA/Goddard Space Flight Facility, Wallops Island, Virginia. 72 pp.

Moody, D.W., 1964. Coastal morphology and processes in relation to the development and submarine sand ridges off Bethany Beach, Delaware. Ph.D. Dissertation, Johns Hopkins University, Baltimore, MD, 167 pp.

Moore, L.J., 2000. Shoreline mapping techniques. *Journal of Coastal Research*, 16(1): 111-124.

Morang, A.; Williams, G.G., and Swann, J.W., 2006. Beach Erosion Mitigation and Sediment Management Alternatives at Wallops Island, VA. Vicksburg, Mississippi: U.S. Army Corps of Engineers, ERDC/CHL TR-06-21, p. 97.

- Morton, R.A., Leach, M.P., Paine, J.G., and Cardoza, M.A., 1993. Monitoring beach changes using GPS surveying techniques. *Journal of Coastal Research*, 9(3): 702-720.
- Morton, R.A., Guy, K.K., Hill, H.W., and Pascoe, T., 2003. Regional morphological responses to the March 1962 Ash Wednesday storm. Coastal Sediments '03. World Scientific Publishing, Clearwater Beach, FL, pp.11.
- Morton, R.A., Bracone, J.E., and Cooke, B., 2007. Geomorphology and deposition sub-environments of Assateague Island MD/VA. U.S. Geological Survey Open File Report 2007-1388 (on DVD).
- Moslow, T.F. and Tye, R.S., 1985. Recognition and characterization of Holocene tidal inlet sequences. *Marine Geology*, 63: 129-151.
- Murray, A.B., 2007. Reducing model complexity for explanation and prediction. *Geomorphology*, 90: 178-191.
- Nicholls, R.J., Birkemeier, W.A., and Lee, G-H., 1998. Evaluation of depth of closure using data from Duck, NC, USA. *Marine Geology*, 148: 179-201.
- Niedoroda, A., Swift, D.P., Figueiredo, A.G., and Freeland, G.L., 1985. Barrier island evolution, middle Atlantic shelf, USA, part II: evidence from the shelf floor. *Marine Geology*, 63: 363-396.
- Nittrouer, C.A. and Wright, L.D., 1994. Transport of particles across continental shelves. *Reviews of Geophysics*, 32(1): 85-113.
- Oertel, G.F. and Kraft, J.C., 1994. New Jersey and Delmarva barrier islands. In: R.A. Davis, Jr. (Editor), *Geology of Holocene barrier island systems*. Springer-Verlag, Berlin, Federal Republic of Germany, pp. 207-232.
- Oertel, G.F., Allen, T.R., Foyle, A.M., and McLoed, G, 2007. The Chincoteague Paleovalley and Chincoteague Bight. Geological Society of America Abstracts with Programs, Vol. 39, No. 2, p. 73
- Pajak, M.J., and Leatherman, S., 2002. The high water line as shoreline indicator. *Journal of Coastal Research*, 18(2): 329-337.
- Pilkey, O.H., Young, R.S., Riggs, S.R., Smith, A.W.S. and Wu, H., 1993. Concept of shoreface profile of equilibrium: a critical review. *Journal of Coastal Research*, 9(1): 255-278.
- Plant, N.G., Holman, R.A., and Freilich, M.H., 1999. A simple model for interannual sandbar behavior. *Journal of Geophysical Research*, 104 (C7): 15,755-15,776.

- Pyper, B.J., and Peterman, R.M., 1998. Comparison of methods to account for autocorrelation in correlation analyses of fish data. *Canadian Journal of Fisheries and Aquatic Sciences*, 55: 2127-2140.
- Rieu, R., van Heteren, S., van der Spek, J.F., and de Boer, P.L., 2005. Development and preservation of a mid-Holocene tidal-channel network offshore the western Netherlands. *Journal of Sedimentary Research*, 75(3): 409-419.
- Riggs, S.R., Cleary, W.J. and Snyder, S.W., 1995. Influence of inherited geologic framework on barrier shoreface morphology and dynamics. *Marine Geology*, 126: 213-234.
- Rodriguez, A.B., Fassell, M.L., and Anderson, J.B., 2001. Variations in shoreface progradation and ravinement along the Texas coast, Gulf of Mexico. *Sedimentology*, 48: 837-853.
- Rodriguez, A.B., Anderson, J.B., Siringan, F.P. and Taviani, M., 2004. Holocene evolution of the east Texas coast and inner continental shelf: along-strike variability in coastal retreat rates. *Journal of Sedimentary Research*, 74(3): 405-421.
- Rosati, J.D. and Ebersole, B.A., 1996. Littoral impact of Ocean City Inlet, Maryland, USA. Edge, Billy L. [ed.]. *Coastal Engineering 1996: Proceedings of the 25th International Conference*, American Society of Civil Engineers, 3: 2779-2792.
- Ruggiero, P., Kaminsky, G.M., Gelfenbaum, G. and Voigt, B., 2005. Seasonal to interannual morphodynamics along a high-energy dissipative littoral cell. *Journal of Coastal Research*, 21(3): 553-578.
- Schupp, C., Bass, G.P., and Grosskopf, W.G., 2007. Sand bypassing restores natural processes to Assateague Island, Maryland. *Coastal Sediments '07*. World Scientific Publishing, Clearwater Beach, FL, pp.14.
- Schupp, C., McNinch, J.E., and List, J.H., 2006. Nearshore shore-oblique bars, gravel outcrops, and their correlation to shoreline change. *Marine Geology*, 233: 63-79.
- Schwab, W.C., Thieler, E.R., Allen, J.R., Foster, D.S., Swift, B.A., and Denny, J.F., 2000. Influence of inner-continental shelf geologic framework on the evolution and behavior of the barrier-island system between Fire Island Inlet and Shinnecock Inlet, Long Island, New York. *Journal of Coastal Research*, 16(2): 408-422.
- Schwartz, R.K., and Birkemeier, W.A., 2004. Sedimentology and morphodynamics of a barrier island shoreface related to engineering concerns, Outer Banks, North Carolina, USA. *Marine Geology*, 211: 215-255.
- Shalowitz, A.L., 1964. *Shoreline and sea boundaries*, V1, Pub. 10-1. U.S. Government Printing Office, Washington D.C., 420 pp.

Smith, S.J. and Ebersole, B.A., 1997. Numerical modeling evaluation of hot spots at Ocean City, MD. Proceedings 16th National Conference on Beach Preservation Technology, FSBPA, 230-245.

Snedden, J.W. and Dalrymple, R.W., 1999. Modern shelf sand ridges: from historical perspective to a unified hydrodynamic and evolutionary model. In: K.M. Bergman and J.W. Snedden (Editors), *Isolated Shallow Marine Sand Bodies: Sequence Stratigraphic Analysis and Sedimentologic Interpretation*. Society for Sedimentary Geology, Tulsa, OK, pp. 13-28.

Snedden, J.W., Tillman, R.W., Kreisa, R.D., Schweller, W.J., Culver, S.J., and Winn, R.D., 1994. Stratigraphy and genesis of a modern shoreface-attached sand ridge, Peahala Ridge, New Jersey. *Journal of Sedimentary Research*, B64(4): 560-581.

Southgate, H.N., Wijnberg, K.M., Larson, M., Capobianco, M. and Jansen, H., 2003. Analysis of field data of coastal morphological evolution over yearly and decadal timescales. Part 2: non-linear techniques. *Journal of Coastal Research*, 19(4): 776-789.

Stive, M. J. F.; Aarninkhof, S.; Hamm, L.; Hanson, H.; Larson, M.; Wijnberg, K.M.; Nicholls, R.J.; and Capobianco, M., 2002. Variability of shore and shoreline evolution. *Coastal Engineering*, 47: 211-235.

Stockdon, H.F., Sallenger, A.H., List, J.H. and Holman, R.A., 2002. Estimation of shoreline position and change using airborne topographic lidar data. *Journal of Coastal Research*, 18(3): 502-513.

Stopler, D., List, J.H., and Thieler, E.R., 2005. Simulating the evolution of coastal morphology and stratigraphy with a new morphological-behaviour model (GEOMBEST). *Marine Geology*, 218:17-36.

Storms, J.E.A., Weltje, G.J., van Dijke, J.J., Géel, C.R., and Kroonenberg, S.B., 2002. Process-response modeling of wave dominated coastal systems: simulating evolution and stratigraphy on geological timescales. *Journal of Sedimentary Research*, 72(2): 226-239.

Stable, D.K., 1994. Evaluation of hotspots for beach fill project performance. In: L.S. Tait (ed.), *Alternative technologies in beach preservation*, Proceedings of the 7<sup>th</sup> national conference on beach preservation technology, Florida Shore and Beach Preservation Association, Tallahassee, FL, pp.198-215.

Swart, H.E. and Calvete, D., 2003. Non-linear response of shoreface-connected sand ridges to interventions. *Ocean Dynamics*, 53: 270-277.

Swift, D.J.P., 1968. Coastal erosion and transgressive stratigraphy. *Journal of Geology*, 76: 444-456.

Swift, D.J.P., 1975. Tidal sand ridges and shoal-retreat massifs. *Marine Geology*, 18: 105-134.

Swift, D.J.P. and Field, M.E., 1981. Evolution of a classic sand ridge field: Maryland sector, North American inner shelf. *Sedimentology*, 28: 461-482.

Swift, D.J.P., Kofoed, J.W., Saulsbury, F.P. and Sears, P., 1972. Holocene evolution of the shelf surface, central and southern Atlantic Shelf of North America. In: D.J.P. Swift, D.B. Duane and O.H. Pilkey (Editors), *Shelf Sediment Transport: Process and Pattern*. Dowden, Hutchinson & Ross, Stroudsburg, Pennsylvania, pp. 499-574.

Swift, D.J.P., Niedoroda, A.W., Vincent, C.E. and Hopkins, T.S., 1985. Barrier island evolution, middle Atlantic shelf, U.S.A. Part I: Shoreface dynamics. *Marine Geology*, 63: 331-361.

Swift, D.J.P., Parsons, B.S., Foyle, A. and Oertel, G.F., 2003. Between beds and sequences: stratigraphic organization at intermediate scales and the Quaternary of the Virginia coast, USA. *Sedimentology*, 50: 81-111.

Tebbens, S.F., Burroughs, S.M., and Nelson, E.E., 2002. Wavelet analysis of shoreline change on the Outer Banks of North Carolina: an example of complexity in the marine sciences. *Proceedings of the National Academy of Sciences*, 99(1), 2554-2560.

Thiebaux, H.J. and Zweirs, F.W., 1984. The interpretation and estimation of effective sample size. *Journal of Climate Applied Meteorology*, 23: 800-811.

Thieler, E.R. and Danforth, W.W., 1994. Historical shoreline mapping (I): improving techniques and reducing position errors. *Journal of Coastal Research*, 10(3): 549-563.

Thieler, E.R.; Pilkey, O.H.; Young, R.S.; Bush, D.M., and Fei, C., 2000. The use of mathematical models to predict beach behavior for U.S. coastal engineering: a critical review. *Journal of Coastal Research*, 16(1): 48-70.

Thieler, E.R., Himmelstoss, E.A., Zichichi, J.L. and Miller, T.L., 2005. Digital shoreline analysis system (DSAS) version 3.0; an ArcGIS extension for calculating shoreline change. U.S. Geological Survey, Open Report 2005-1304, pp.

Thornton, E.B., MacMahan, J., and Sallenger, A.H., 2007. Rip currents, mega-cusps, and eroding dunes. *Marine Geology*, 240: 151-167.

Toscano, M.A. and York, L.L., 1992. Quaternary stratigraphy and sea-level history of the U.S. middle Atlantic coastal plain. *Quaternary Science Reviews*, 11: 301-328.

Toscano, M.A., Kerhin, R.T., York, L.L., Cronin, T.M., and Williams, S.J., 1989. Quaternary stratigraphy of the inner continental shelf of Maryland. Report of Investigations No. 50, Maryland Geological Survey, 117 pp.



- Trowbridge, J.H., 1995. A mechanism for the formation and maintenance of shore-oblique sand ridges on storm-dominated shelves. *Journal of Geophysical Research*, 100(C8): 16,071-16,086.
- Valvo, L.M., Murray, A.B. and Ashton, A., 2006. How does underlying geology affect coastline change? An initial modeling investigation. *Journal of Geophysical Research*, 111: F02025, doi:10.1029/2005JF000340.
- Vis-Star, N.C, de Swart, H.E. and Calvete, D., 2007. Effect of wave-topography interactions on the formation of sand ridges on the shelf. *Journal of Geophysical Research*, 112: C06012, doi:10.1029/2006JC003844.
- Walton, Jr., T.A., 1999. Shoreline rhythmic pattern analysis. *Journal of Coastal Research*, 15(2): 379-387.
- Walton, Jr., T.A., 2000. Separation of shoreline change signal from random noise. *Ocean Engineering*, 27: 77-86.
- Wells, D.V., 1994. Non-energy resources and shallow geological framework of the inner continental margin off Ocean City, Maryland. Open File Report No. 16, Maryland Geological Survey.
- Whitcher, B., Guttorp, P., and Percival, D.B., 2000. Wavelet analysis of covariance with application to atmospheric time series. *Journal of Geophysical Research*, 105 (D11): 14941-14962.
- Wijnberg, K.M. and Terwindt, J.H.J., 1995. Extracting decadal morphological behaviour from high-resolution, long-term bathymetric surveys along the Holland coast using eigenfunction analysis. *Marine Geology*, 126: 301-330.
- Wright, L.D. and Short, A., 1984. Morphodynamic variability of surf zones and beaches: a synthesis. *Marine Geology*, 56: 93-118.
- Wright, L.D. and Trembanis, A., 2003. Complex shoreface morphology of a rapidly transgressing barrier island: Cedar Island Virginia. Coastal Sediments '03. World Scientific Publishing, Clearwater Beach, FL.
- Wright, L.D., Xu, J.P. and Madsen, O.S., 1994. Across-shelf benthic transports on the inner shelf of the Middle Atlantic Bight during the "Halloween storm" of 1991. *Marine Geology*, 118: 61-77.
- Zhang, K., Huang, W., Douglas, B.C. and Leatherman, S., 2002. Shoreline position variability and long-term trend analysis. *Shore & Beach*, 70: 31-35.



TABLE 1:  
SHORELINE POSITION DATA

Data	Source	Year
Historic	Shoreline Movement Maps	1849-51, 1887, 1908, 1915, 1933, 1959/62, 1980
	T-Sheet	1915 <sup>1</sup>
Recent	Aerial Photography	1994, 2002 <sup>2</sup> , 2005 <sup>2</sup>
	DGPS	Spring and Fall 1997-2005 <sup>1</sup>

<sup>1</sup> Assateague Island only, <sup>2</sup> Wallops Island only

TABLE 2:  
SHORELINE POSITION UNCERTAINTY ESTIMATES

Data	Source	Measurement Errors (m)				Total Error
		Source	Rectification	Position	Digitizing	
Historic	Shoreline Movement Maps	10	5	0	1	11.2
	T-Sheet	10	5	0	1	11.2
Recent	Aerial Photography					
	1994	0	7	5	1	8.7
	2002	0	3	5	1	5.9
	2005	0	10	5	1	11.2
	DGPS	1.5	0	5	0	5.2

TABLE 3:  
BATHYMETRY DIGITAL ELEVATION MODEL DATA

Data	Source	Smooth H-Sheet (Scale)
Bathymetry	US Coast and Geodetic Survey (Geographic NAD 1927) (MLW ft)	<i>1933</i>
		H05347 (1:20000)
		H05353 (1:40000)
		H05356 (1:40000)
		H05357 (1:20000)
		H05358 (1:20000)
		<i>1934</i>
		H05673 (1:40000)
		H05675 (1:10000)
		H05702 (1:40000)
		H05703 (1:20000)
		H05714 (1:20000)
		H05715 (1:40000)
		H05716 (1:10000)
	H05769 (1:10000)	
	H05771 (1:40000)	
	National Ocean Service (Geographic NAD 1927) (MLW ft)	<i>1978</i>
		H09796 (1:20000)
		<i>1982</i>
		H010044 (1:20000)
H010045 (1:20000)		
H010046 (1:20000)		

TABLE 4:  
BATHYMETRY DEM AND ISOPACH UNCERTAINTY ESTIMATES

Bathymetric DEM	Uncertainty Estimate (m)
1933/34 DEM	<i>Line Pair Elevation Difference</i> 1. 0.16 2. 0.21 3. 0.67 4. 0.40 5. 0.46 <u>Average: 0.41</u>
1978/82 DEM	<i>Line Pair Elevation Difference</i> 1. 0.20 2. 0.22 3. 0.71 4. 0.51 5. 0.49 <u>Average: 0.40</u>
Isopach	<u>0.57</u>

TABLE 5:  
CROSS-CORRELATION: SHORELINE MOBILITY AND SHORELINE CHANGE

Shoreline Mobility (m)	Shoreline Change (m/yr)		
<i>Spatial scale</i>	Long-Term	Decadal	Inter-Annual
<i>Local</i>			
Samples (N)	341	341	341
Effective sample size (N*)	6	7	7
Critical correlation coefficient ( $r_{90\%}$ )	0.61	0.55	0.55
Max cross-correlation ( $CC_m$ )	-0.78	-0.66	-0.67
Lag (m) for $CC_m$	0	0	0
$r^2$	0.61	0.44	0.45
<i>Block</i>			
Samples (N)	341	341	341
Effective sample size (N*)	63	53	60
Critical correlation coefficient ( $r_{90\%}$ )	0.16	0.18	0.17
Max cross-correlation ( $CC_m$ )	0.30	0.28	0.30
Lag (m) for $CC_m$	1250	1250	400
$r^2$	0.09	0.08	0.09

TABLE 6:  
 VOLUME CHANGES BY ISOPACH REGION BETWEEN 1933/34 AND 1978/1982

Isopach Zone	Volume Change (m <sup>3</sup> )	Planar Area (m <sup>2</sup> )	Annualized Volume Change (m <sup>3</sup> /yr)	Annualized Elevation Change (m/yr)
I (0-10 m)	3.4 x 10 <sup>6</sup>	33.9x10 <sup>6</sup>	~ 69,000	0.002
II (0-10 m)	-16.1 x 10 <sup>6</sup>	15.5x10 <sup>6</sup>	~ -330,000	- .02
III (0-10 m)	16.6 x 10 <sup>6</sup>	25.2x10 <sup>6</sup>	~ 339,000	0.01
IV (0-10 m)	14.1 x 10 <sup>6</sup>	16.0x10 <sup>6</sup>	~ 288,000	0.02
V (0-10 m)	21.3 x 10 <sup>6</sup>	11.6x10 <sup>6</sup>	~ 434,000	0.04
VI (0-10 m)	-2.6 x 10 <sup>6</sup>	25.8x10 <sup>6</sup>	~ -53,000	- 0.002



TABLE 7:  
DESCRIPTION OF THE SEISMIC UNITS COMPRISING THE QUATERNARY STRATIGRAPHY

Unit	Subunit or facies	Reflector	Internal reflection configuration	Sidescan sonar signature	Depositional environment	Toscano <i>et al.</i> (1989) units	Foyle (1994) units	
A	A1		transparent, discontinuous parallel and subparallel	uniform, high backscatter	marine sand sheet and shoals	Q5	A	
	<i>Transgressive wave ravinement / proto-ravinement*</i>							
	A2	----R1----	transparent, discontinuous parallel and subparallel	mottled, medium backscatter	marine shoals and spit platform			
	<i>Local ravinement (*R1/R2 join offshore)</i>							
	B5	----R2----	variable, mostly transparent, short discontinuous parallel and subparallel		backbarrier (e.g., overwash, tidal flat)			
B	B4		sigmoid, oblique, parallel clinofolds	mottled, hummocky low	inlet delta and spit	Q4	B	
	B3		transparent to chaotic, variable channel fill geometry	to medium backscatter	inlet channel and tidal creek fill			
	B2		variable, continuous to discontinuous, parallel and subparallel, wavy, gas masking		lagoonal/estuarine			
	B1		transparent to chaotic, variable channel fill geometry	no surface expression	paleochannel fill	Q3		
<i>Holocene/Pleistocene Unconformity</i>								
C		----R3----		no surface expression		Q2		
	undifferentiated	----R4----	long, continuous and discontinuous, parallel to wavy	no surface expression		Q1	C-G	
	<i>Pleistocene/Tertiary Unconformity</i>							
D	undifferentiated	N/A		no surface expression		T1	T	

TABLE 8:  
CROSS-CORRELATION OF GEOLOGIC FRAMEWORK AND SHORELINE  
CHANGE

Variable	Shoreline Change (m/yr)		
	Long-Term	Decadal	Inter-Annual
<i>Spatial scale</i>			
<b>Nearshore Morphology (m/m)</b>			
<i>Local</i>			
Samples (N)	341	341	341
Effective sample size (N*)	8	8	9
Critical correlation coefficient ( $r_{90\%}$ )	0.51	0.51	0.47
Max cross-correlation ( $CC_m$ )	0.59	0.60	0.64
Lag (m) for $CC_m$	-800	-650	-500
$r^2$	0.35	0.36	0.41
<i>Block</i>			
Samples (N)	341	341	341
Effective sample size (N*)	29	24	27
Critical correlation coefficient ( $r_{90\%}$ )	0.25	0.27	0.25
Max cross-correlation ( $CC_m$ )	0.25	0.28	0.58
Lag (m) for $CC_m$	150	-1000	-200
$r^2$	0.06	0.08	0.34
<b>Nearshore Volume (m<sup>3</sup>/m)</b>			
<i>Local</i>			
Samples (N)	341	341	341
Effective sample size (N*)	7	8	8
Critical correlation coefficient ( $r_{90\%}$ )	0.55	0.51	0.51
Max cross-correlation ( $CC_m$ )	0.73	0.68	0.72
Lag (m) for $CC_m$	50	50	250
$r^2$	0.53	0.46	0.52
<i>Block</i>			
Samples (N)	341	341	341
Effective sample size (N*)	29	24	27
Critical correlation coefficient ( $r_{90\%}$ )	0.25	0.27	0.25
Max cross-correlation ( $CC_m$ )	-0.033 / 0.26	-0.34 / 0.24	-0.39 / 0.36
Lag (m) for $CC_m$	-1150 / 600	-900 / 1050	-1100 / 550
$r^2$	0.11 / 0.07	0.12 / 0.06	0.15 / 0.13

TABLE 9:  
COMPARISON OF OFFSHORE ENVIRONMENTS AND SHORELINE BEHAVIOR  
FOR ASSATEAGUE AND WALLOPS ISLANDS

Variable	Assateague Island	Wallops Island
Energy	wave dominated	mixed energy
Planform	elongated right-handed spit	short drumstick
Shoreline behavior	parallel retreat	parallel retreat and rotational instability
Shoreline orientation	straight to convex	concave
Shoreface gradient	intermediate	dissipative to intermediate
Morphology	high relief	planar
Grain size	fine to medium sand	mud to fine sand
Sand prism thickness	<7.25 m	<3 m
Inlet history	pervasive	local
Modern inlet influence	west of Fishing Point	pervasive

11 FIGURES

FIGURE 1

(a) Map of Assateague Island and Wallops Island, located on the Eastern Shore of Virginia along the Delmarva Peninsula. Bathymetric contours (m) show the ridge and swale topography of the inner shelf of the Mid-Atlantic Bight. (b) Wave rose diagrams show seasonal, hindcast wave height ( $H_{sig}$ ) and direction from 1980 to 1999 for WIS station 176 located in 19 m water depth off Assateague Island.

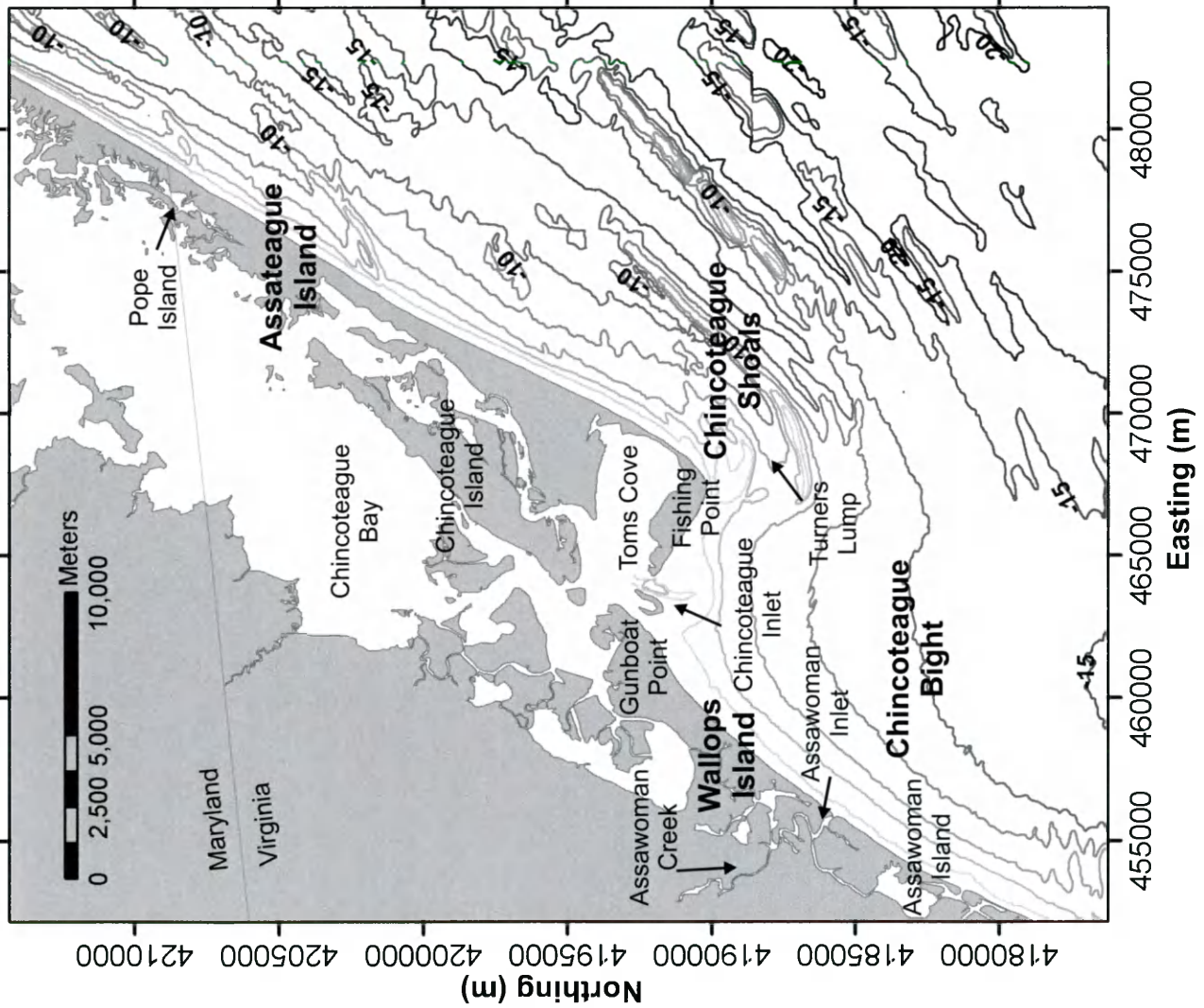
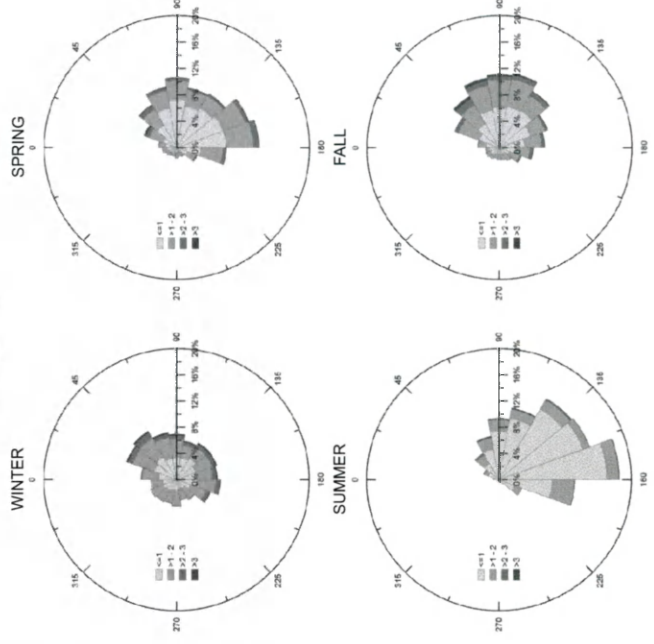
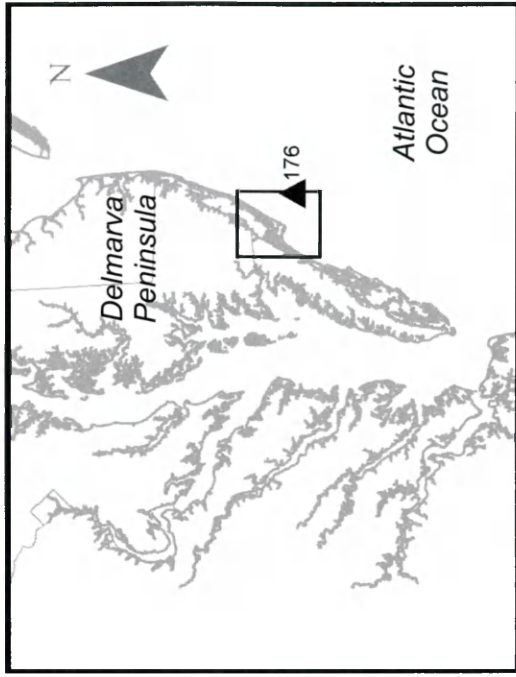
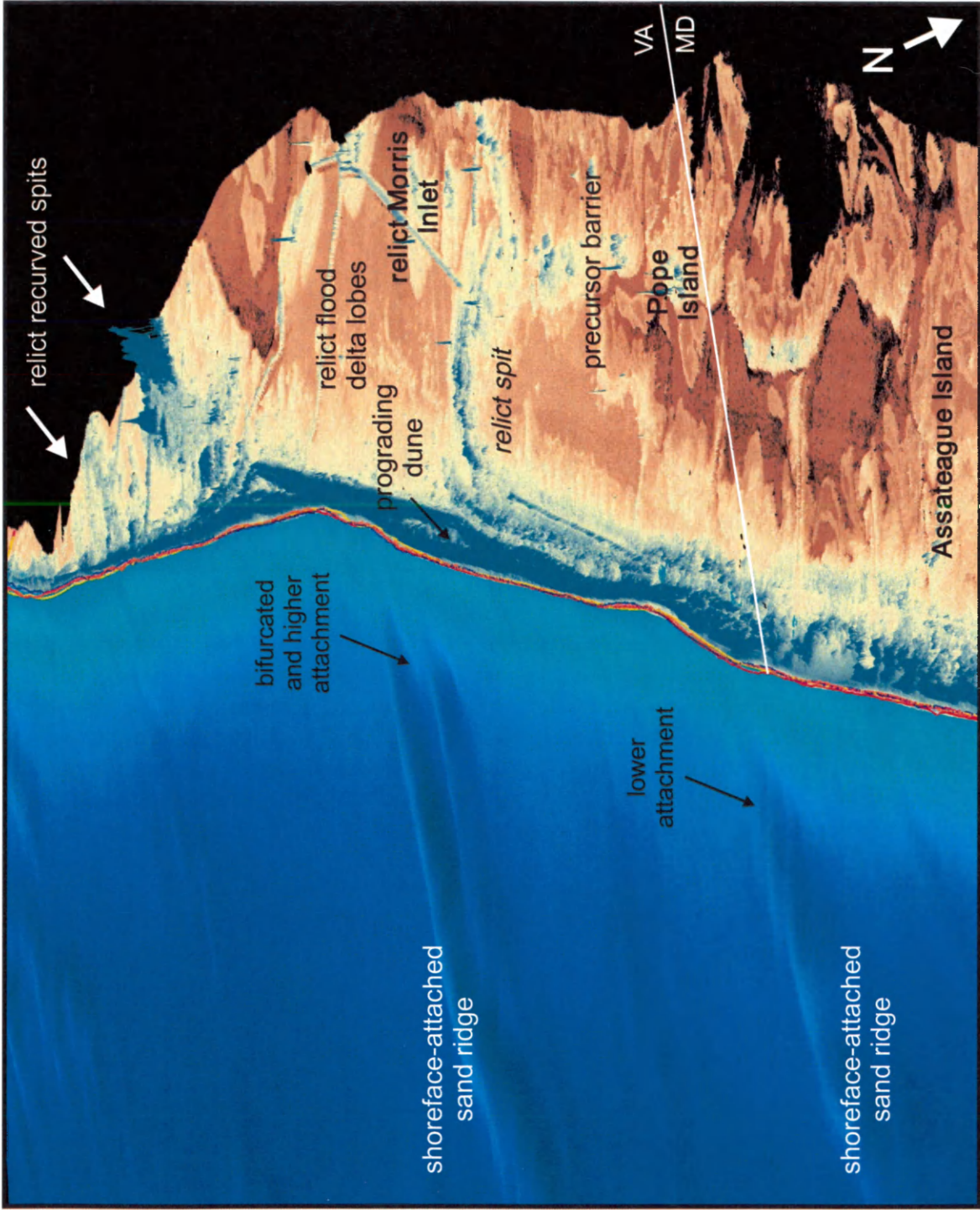


FIGURE 2

Oblique view (view from northeast) of nearshore morphology and adjacent barrier beach of southern Assateague Island. Bathymetric DEM was created from legacy hydrographic survey data available from NOAA. The topographic DEM was created from LiDAR data collected by NASA/USGS and provided by the National Park Service. Pronounced indentations and changes in shoreline orientation are co-located with the shoreface-attachment of linear sand ridges. Subaerial ridges of relict spits and relict flood tidal delta lobes (see also Figure 26A) mark the location of a historic migrating inlet (Assateague/Morris Inlet) that is spatially coincident with the larger, bifurcated shoreface-attached sand ridge.







### FIGURE 3

Conceptual diagram of the nearshore (after Ruggiero *et al.*, 2005) illustrating the potential for system heterogeneity and response scales reflecting a wide range of coastal processes and morphodynamic feedbacks. The schematic of a hypothetical cross-shore profile shows a sand cover of variable thickness overlying back-barrier sediments. A proto-ravinement, actively being formed by the boundary layer action of waves coupled with longshore currents, separates the facies characterized by different lithologies. The variability in nearshore morphology and volume, part of the geologic framework, shape energy impacts (*e.g.*, wave focusing or storm downwelling currents) and sediment flux that may affect shoreline and subaerial beach change. The plan view inset indicates irregular shoreline change, indicative of gradients in longshore sediment transport along an undulating shoreline.

Shoreline Change

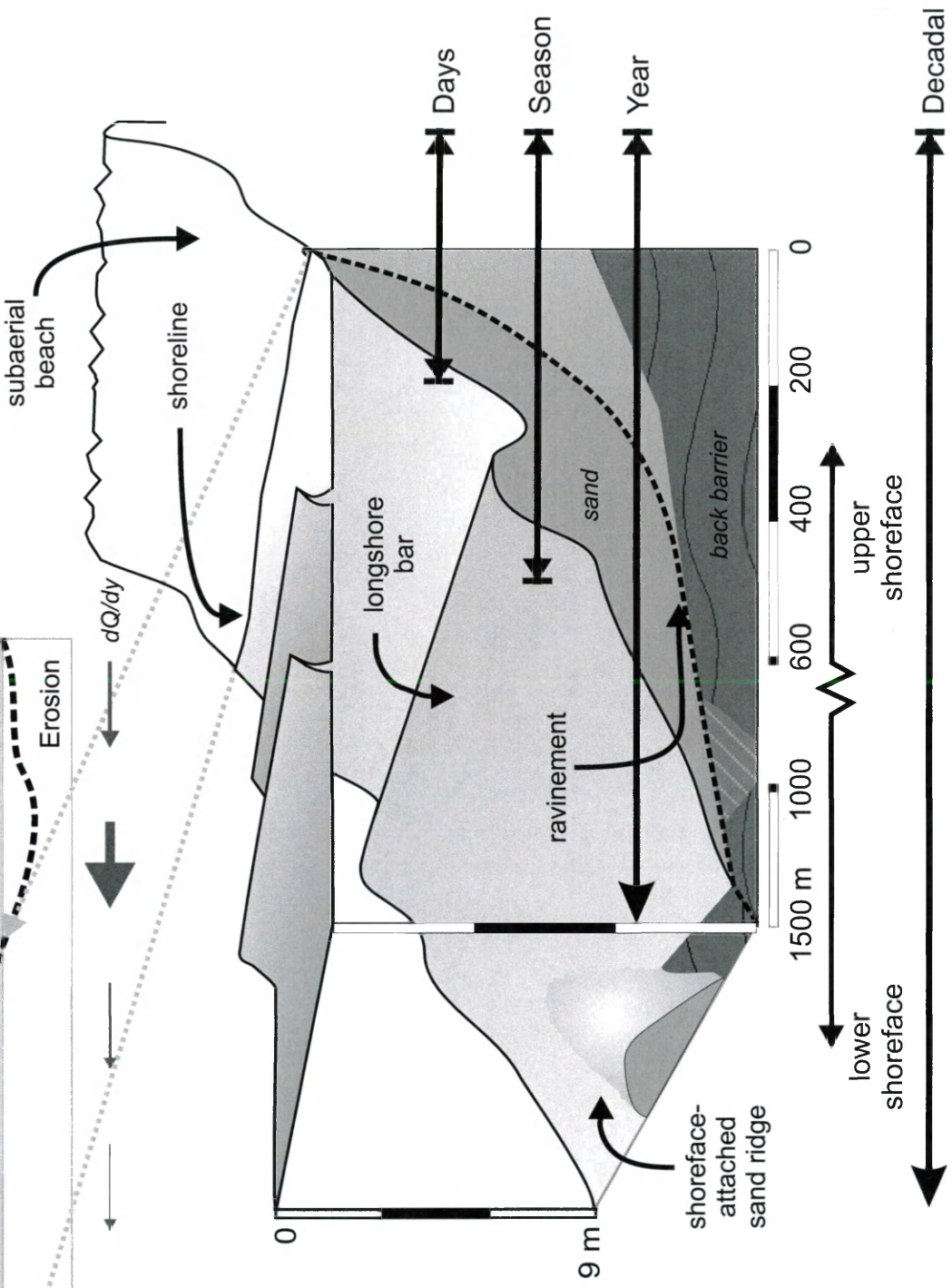
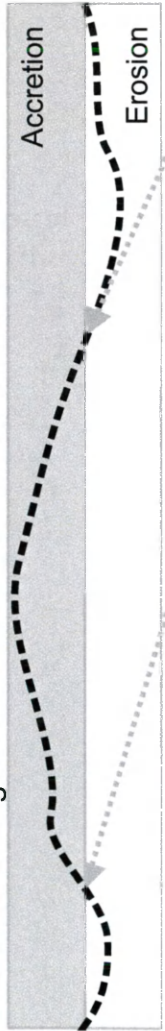


FIGURE 4

(a) Stratigraphic cross-section for southern Maryland (modified from Toscano *et al.*, 1989) and (b) comparison of Maryland and Virginia inner shelf stratigraphy (modified from Foyle, 1994).

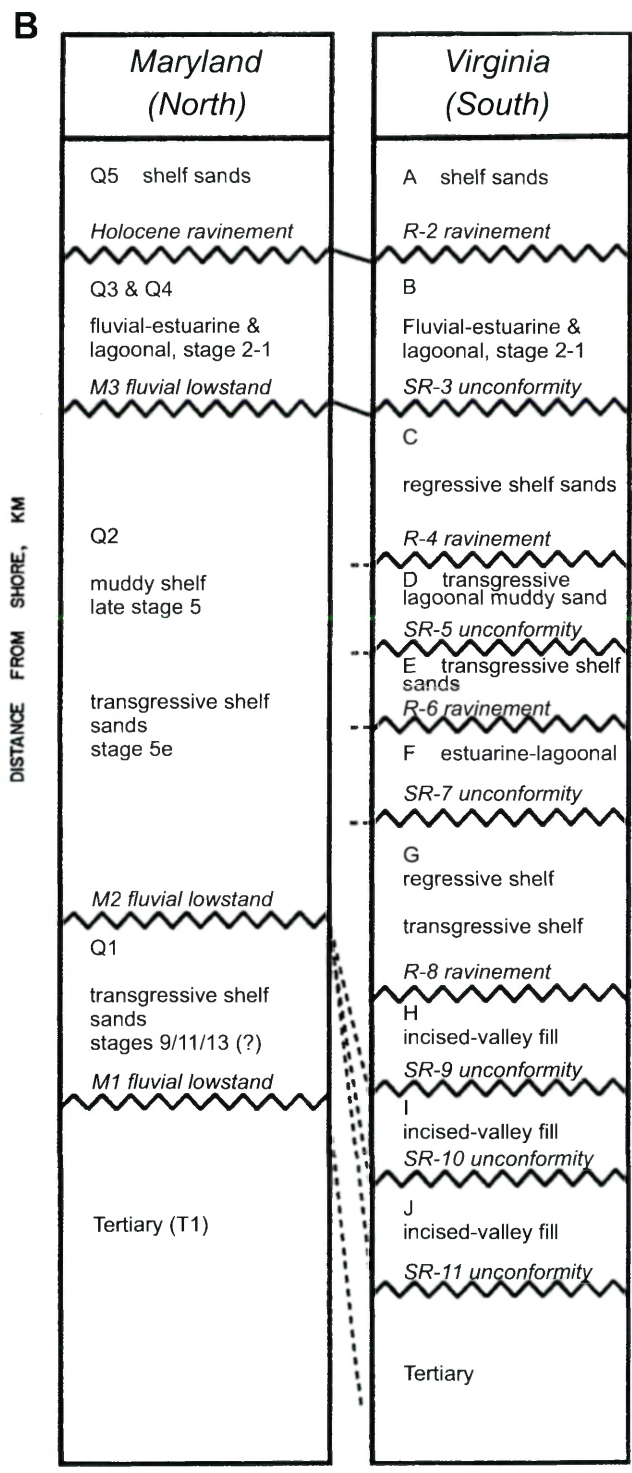
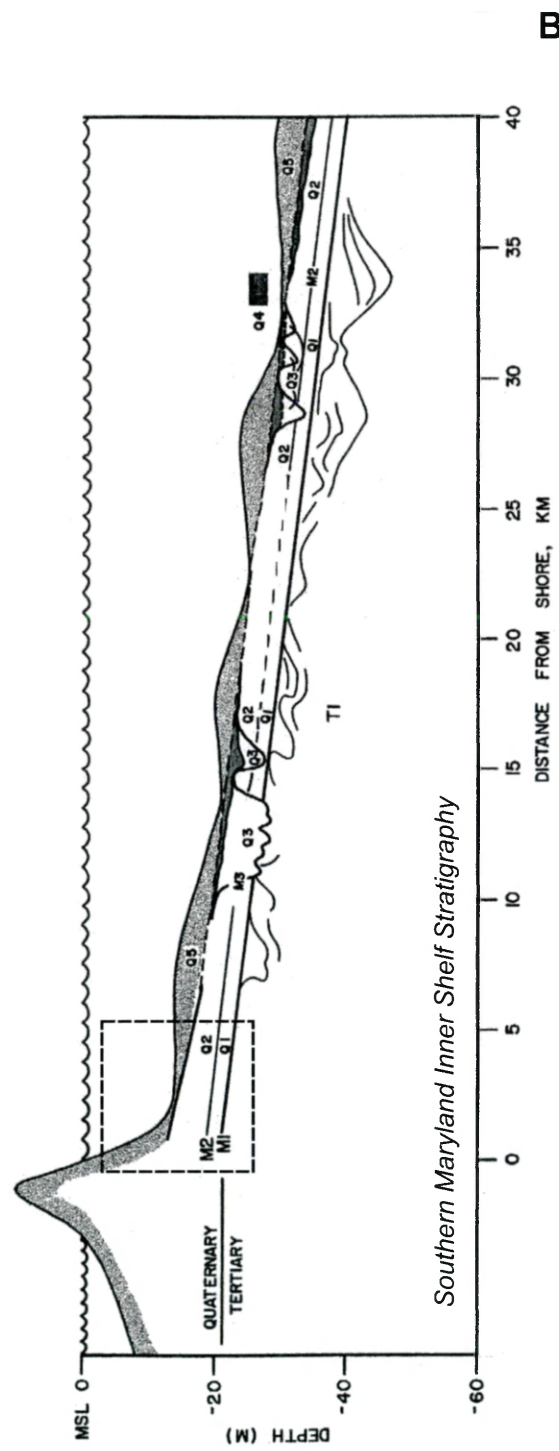


FIGURE 5

(a) Historic progradation of southern Assateague Island as a series of right-handed spits overlapping Chincoteague Island and precursor Holocene barriers, Pitts Island and Pope Island (not shown). Toms Cove Hook and Fishing Point elongated south as a thin, frequently overwashed arm from Assateague Point beginning in the 1850s. (b) The inset compares historic and modern shoreline position data (overlaid on 2005 aerial photography) at the westward extension of the 1850 Assateague Point shoreline, showing significant cross-shore and alongshore mobility.

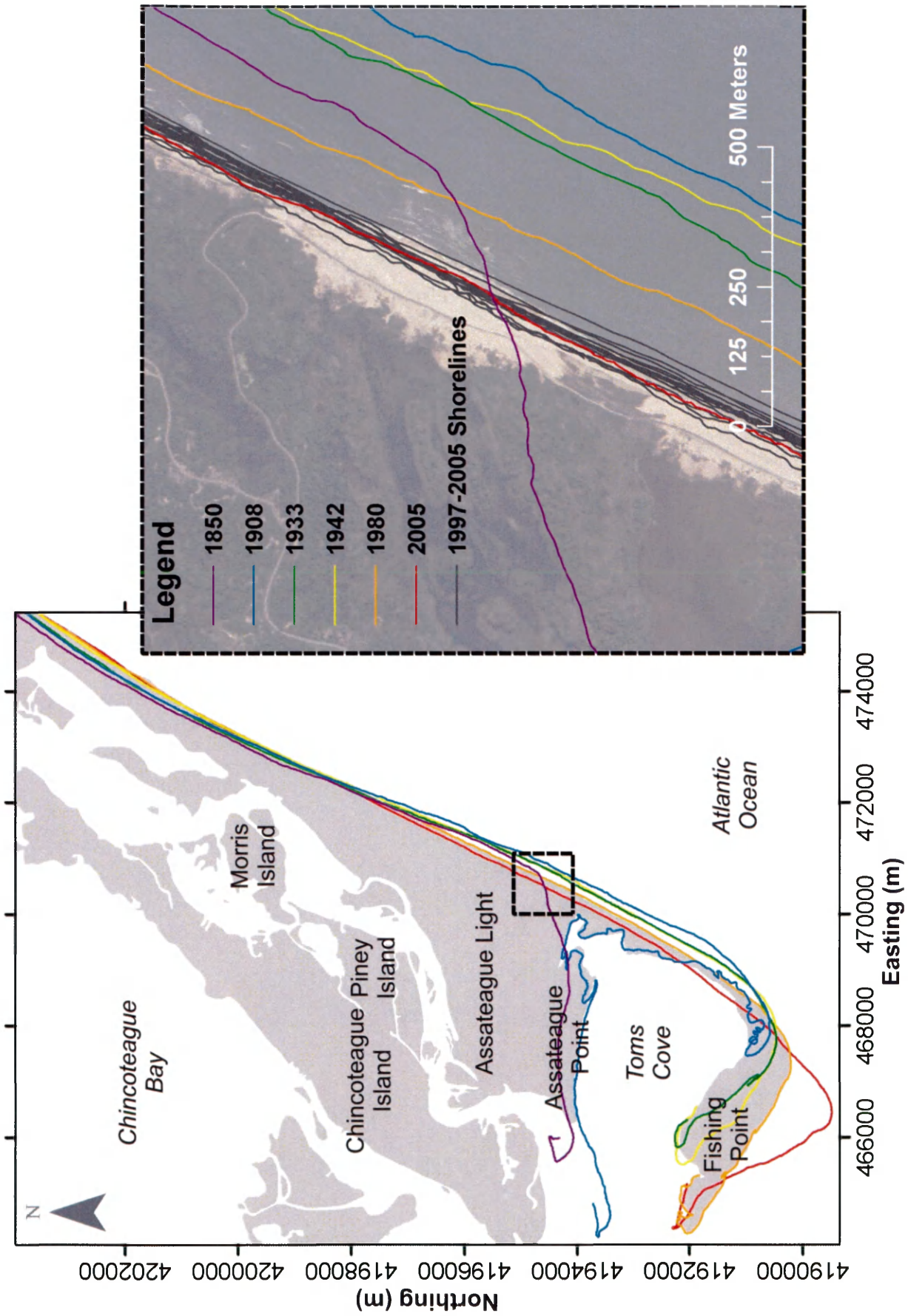
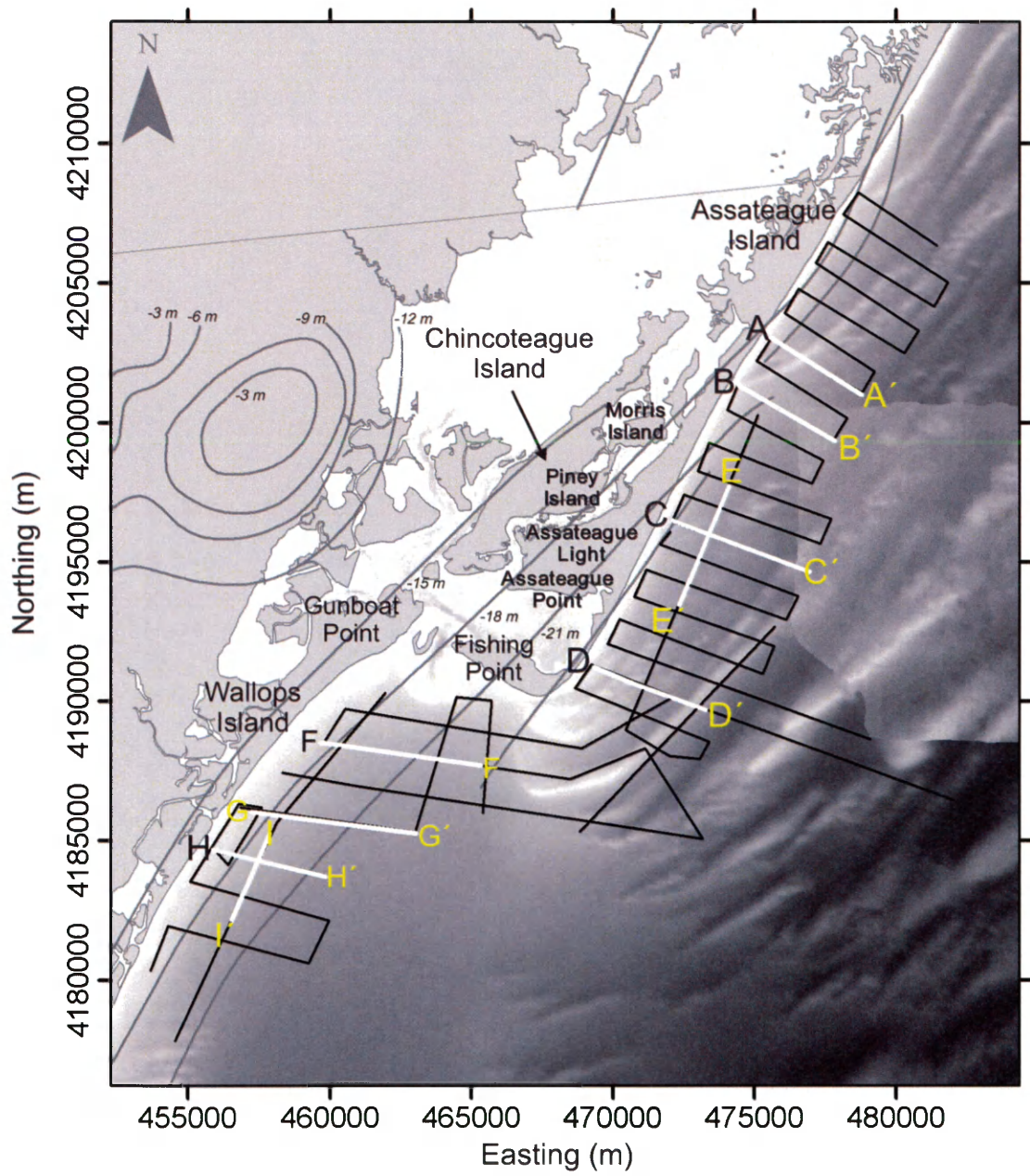


FIGURE 6

Map showing tracklines for geophysical data. Bold lines mark the location of seismic sections and side scan sonar imagery described in subsequent figures. Contours (m) show the top of the Tertiary unconformity presented in Mixon (1985).

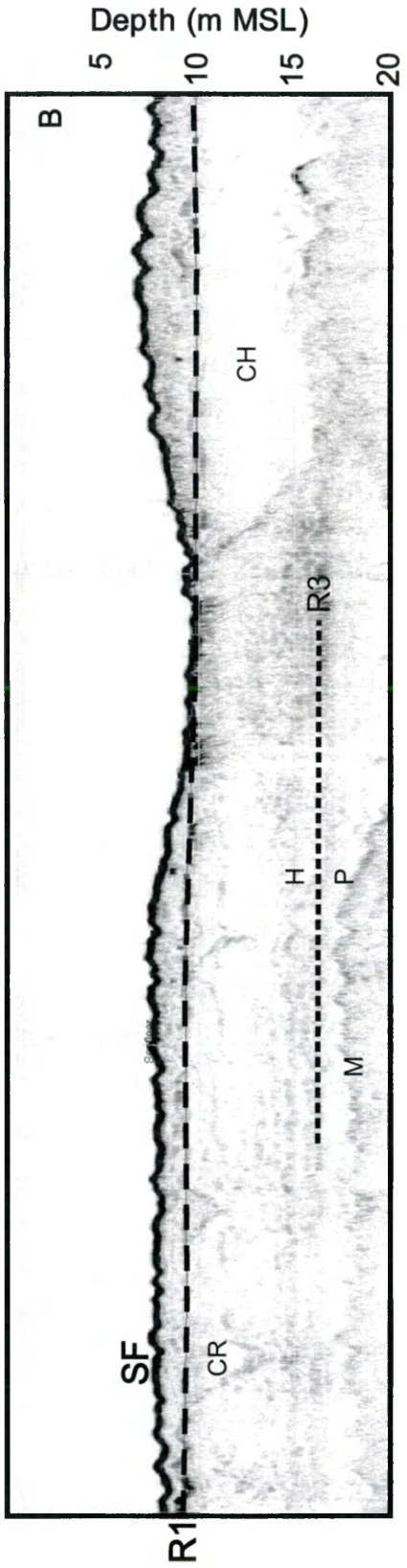
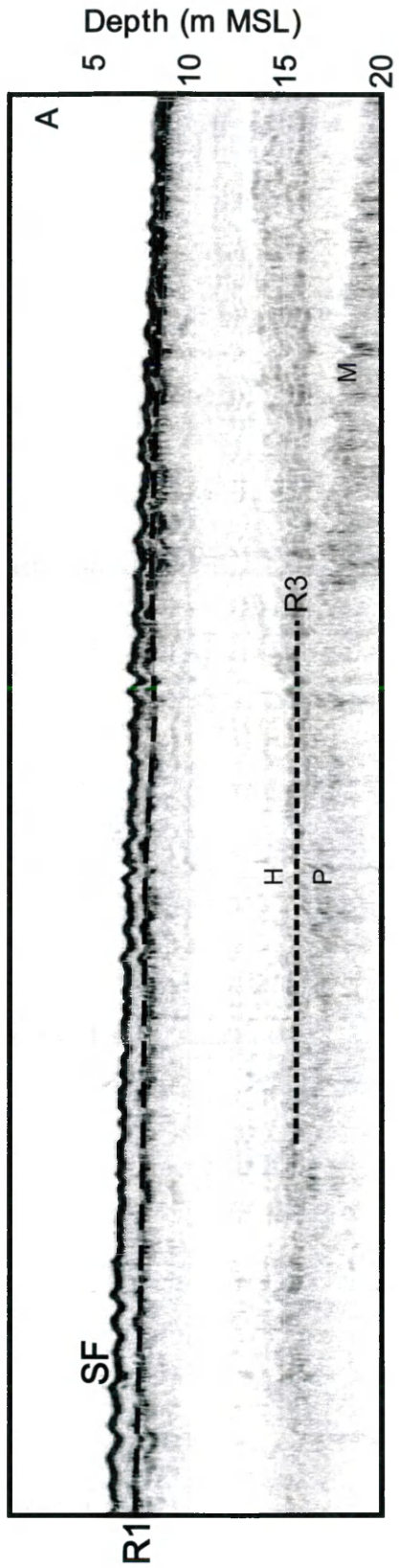






**FIGURE 7**

Example sections of processed chirp seismic data from line C-C'. (a) The upper profile shows the uppermost seismic facies, interpreted as the modern sand sheet, overlying R1, interpreted as the wave ravinement. (b) The lower profile shows a shoreface-attached ridge in cross-section. Note that the R1 surface is exposed in the trough between the shoreface sand sheet and shoreface-attached ridge. Prominent channel-fill structures underlie the ravinement surface.



KEY

- SF (Seafloor)
- R1 (Ravinement)
- CH (Channel)
- CR (Creek)
- Multiple (M)
- Holocene (H)
- Pleistocene (P)

FIGURE 8

Long-term (>75 yrs), decadal (<25 yrs), and inter-annual (<10 yrs) shoreline change (m/yr) and shoreline mobility (m) data for Assateague Island, Virginia. The pronounced north-south regional trend and erosional hotspot occurring immediately north of the active recurved spit are consistent across data sets. A distinct ~1.5-2 km alongshore pattern in decadal, inter-annual, and shoreline mobility data occurs along the northern part of the study area in the vicinity of shoreface-attached sand ridges. Thicker lines indicate statistically significant rates (CI=90%). Gray bars indicate the standard deviation for the rate of change. The insets show shoreline change data for the reach oriented east-west south of Toms Cove and shoreline orientation for southern Assateague Island.

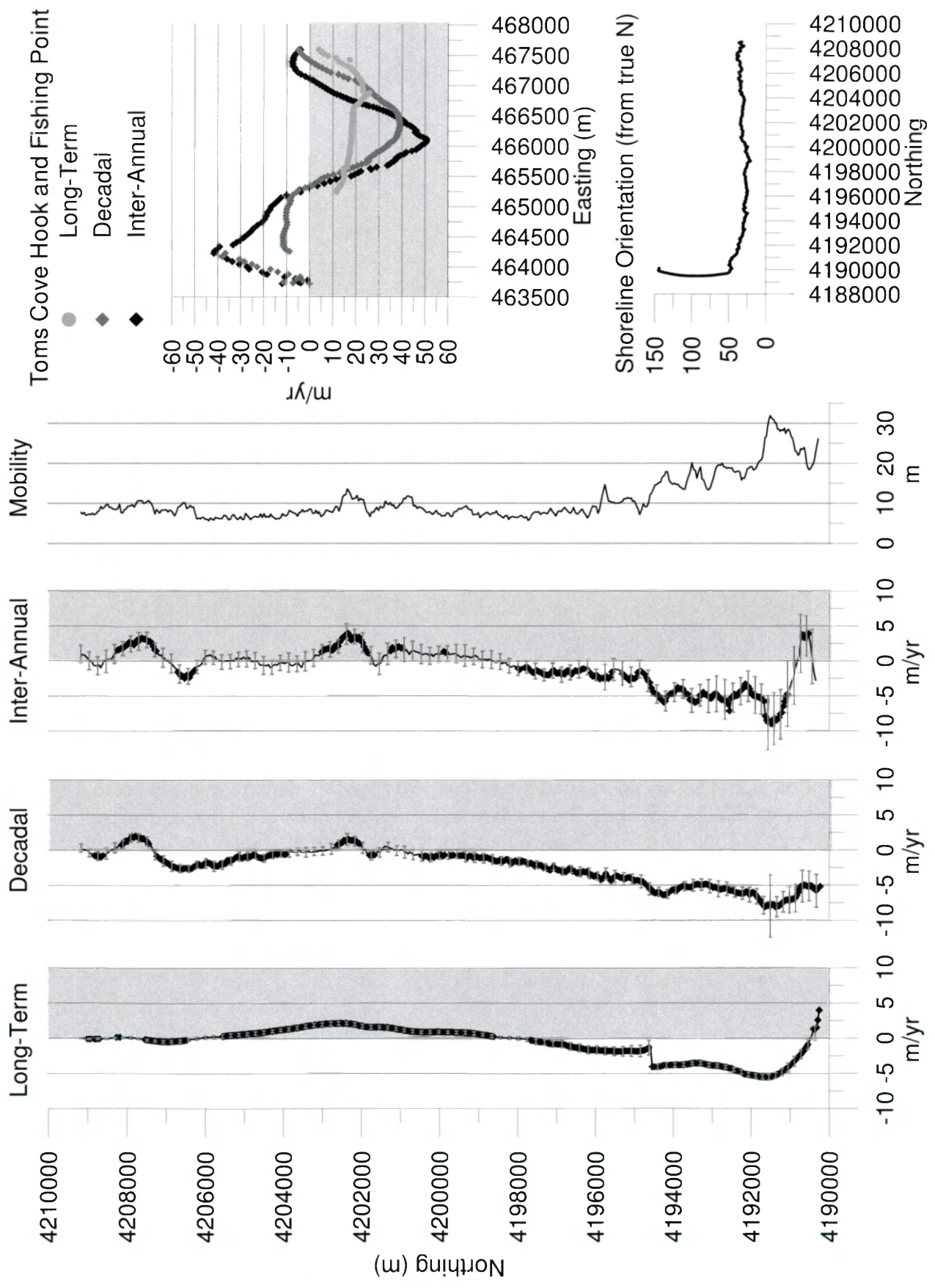
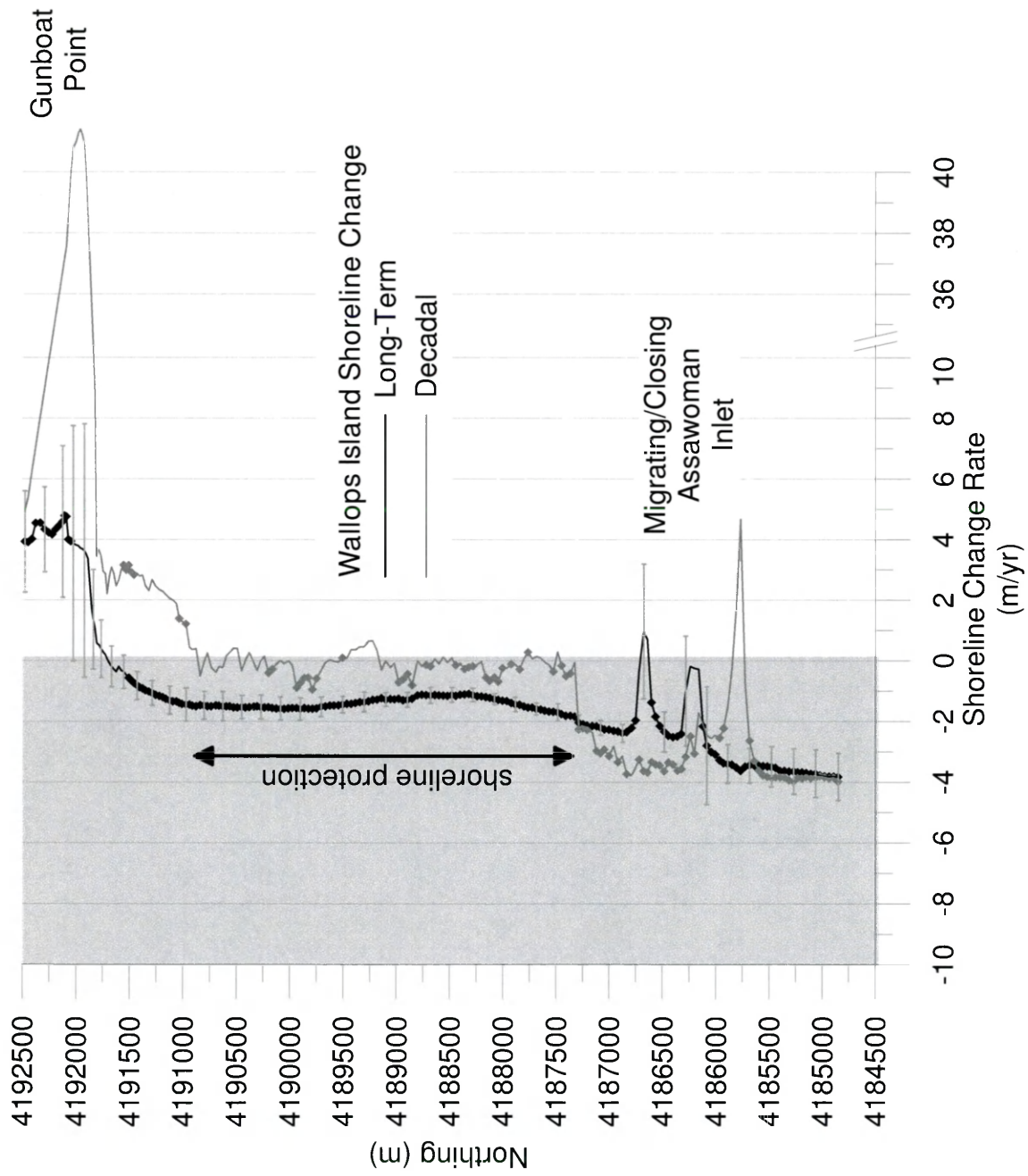


FIGURE 9

Long-term (>75 yrs) and decadal (<25 yrs) shoreline change (m/yr) data for Wallops Island, Virginia. Inter-annual (<10 yrs) and mobility (m) data were not prepared because the short-term shoreline position data were not available. Pronounced accretion, related to inlet processes, has occurred and continues to occur at Gunboat Point, the northern end of the drumstick barrier. The muted erosion along the central 4 km shows the influence of >50 years of shoreline engineering. The southernmost perturbations show the ephemeral opening, closing, and migration of Assawoman Inlet. Thicker lines indicate statistically significant rates (CI=90%). Gray bars indicate the standard deviation for the rate of change. Standard deviation is not shown for decadal change rates since the magnitudes near Gunboat Point are comparatively greater.



**FIGURE 10**

Extensive erosion has continued to occur along the elongated arm fronting Toms Cove since the Ash Wednesday storm of 1962. A 2005 lidar digital elevation model shows the continued landward translation of the low barrier reach via overwash processes. Presently, the southern terminus continues to extend via spit platform, bar welding, and subaerial ridge accretion of the spit.



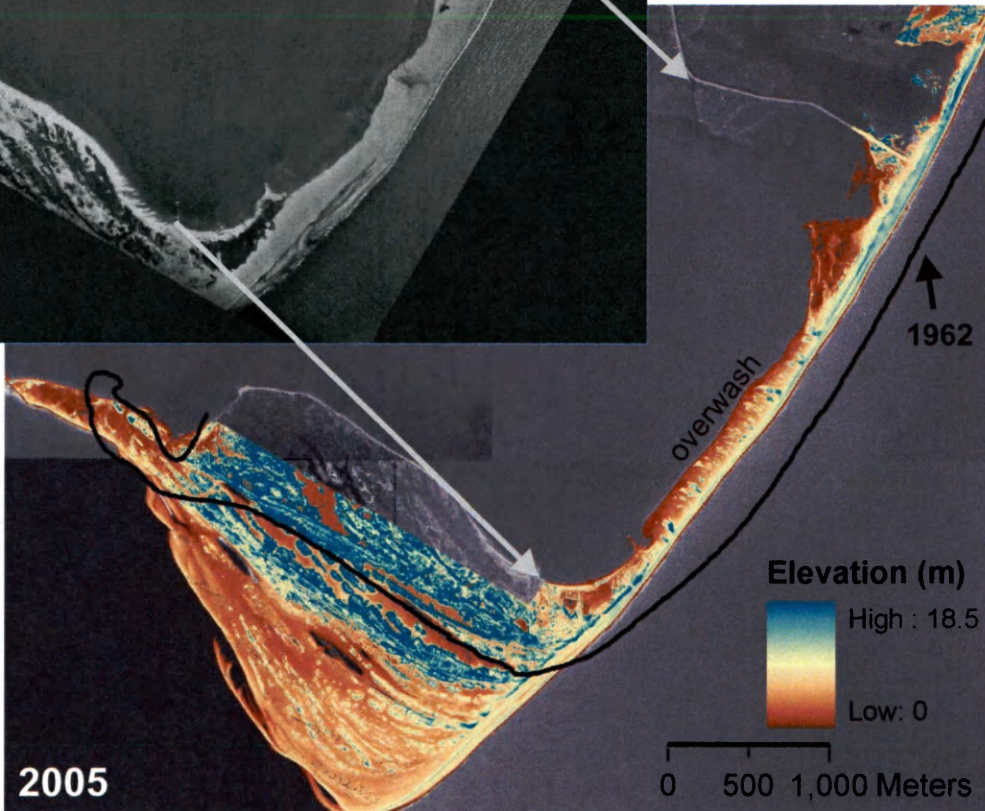
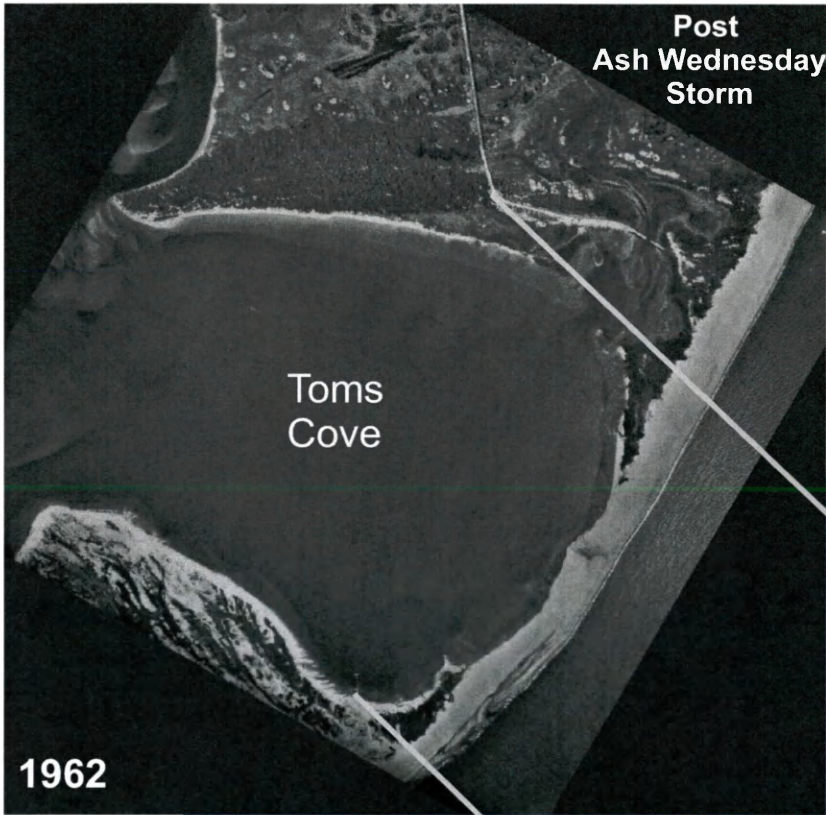




FIGURE 11

Oblique view of nearshore and inner shelf bathymetry. Bathymetric data compiled from 1978/1982 hydrographic surveys available from the National Oceanic and Atmospheric Administration – National Geophysical Data Center. Superimposed grain size data show mean diameter (top) and percent mud (bottom) from grab samples provided by Fenster *et al.* (2008) and the U.S. Army Corps of Engineers – Norfolk District respectively. The medium sand constituting Chincoteague Shoals tends to be relatively coarser than the shoreface along Assateague Island, indicative of different energetic conditions and underlying sediment sources. Grain size distributions notably change south of Chincoteague Shoals, becoming increasingly fine-grained (McBride and Moslow, 1991). A distinct mud-rich lens occurs south of the mouth of Chincoteague Inlet extending several kilometers across the Chincoteague Bight basin.

# 1978/1982 Bathymetric DEM

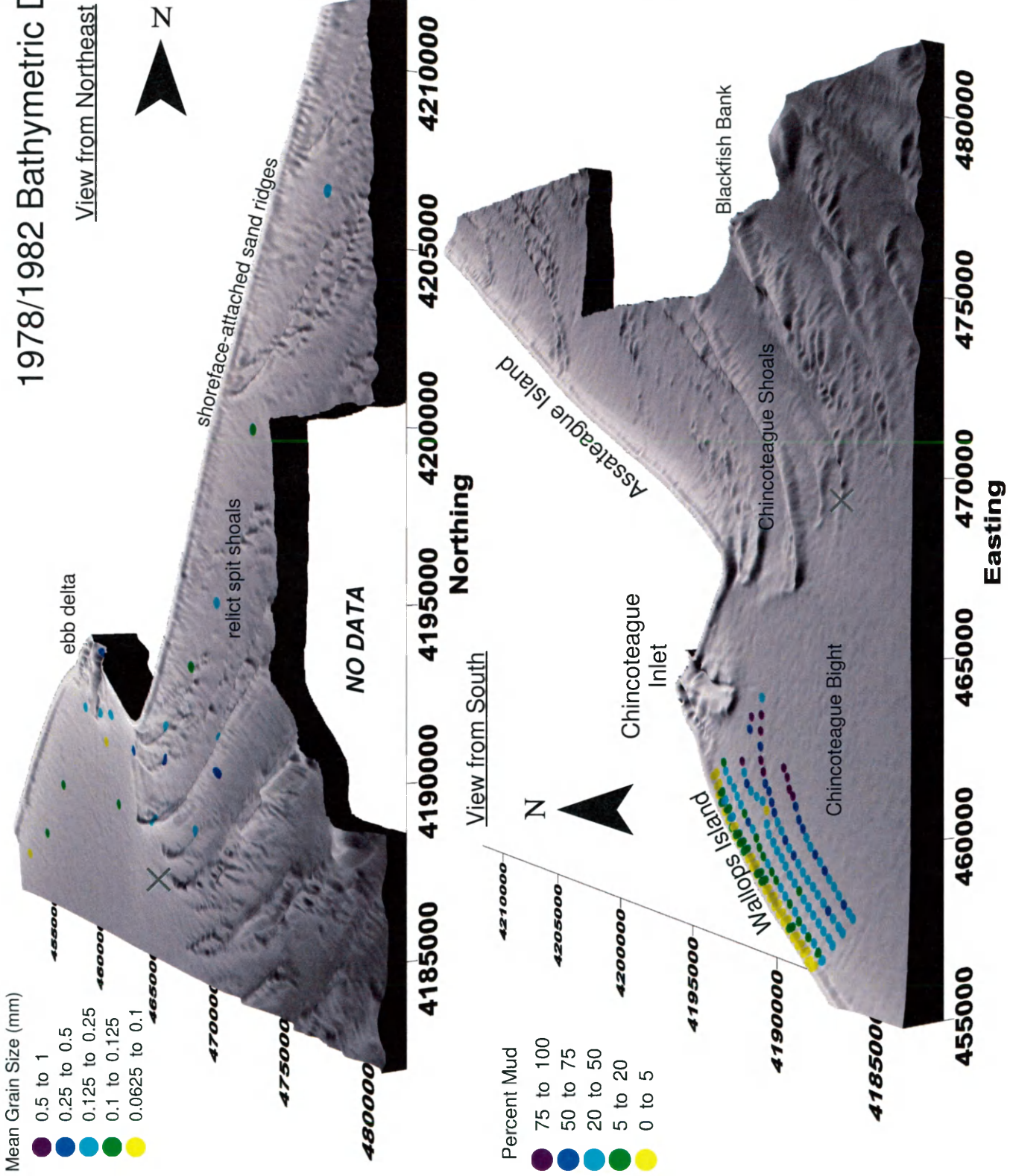


FIGURE 12

(a) Timber groins (1983 photograph courtesy of NASA Goddard Space Flight Center) constructed to curb erosion along a 6.8-km reach of Wallops Island (circa 1961-1972). (b) Limited subaerial beach fronting the rubble seawall constructed during the early 1990s (2006 photograph courtesy of NASA Wallops Flight Facility). (c) 2005 aerial photography contrasting the beach morphology of the seawall-fronted, central reach with the southern end where washover fans extend landward over an extensive marsh platform stretching to the mainland (see Figure 1).

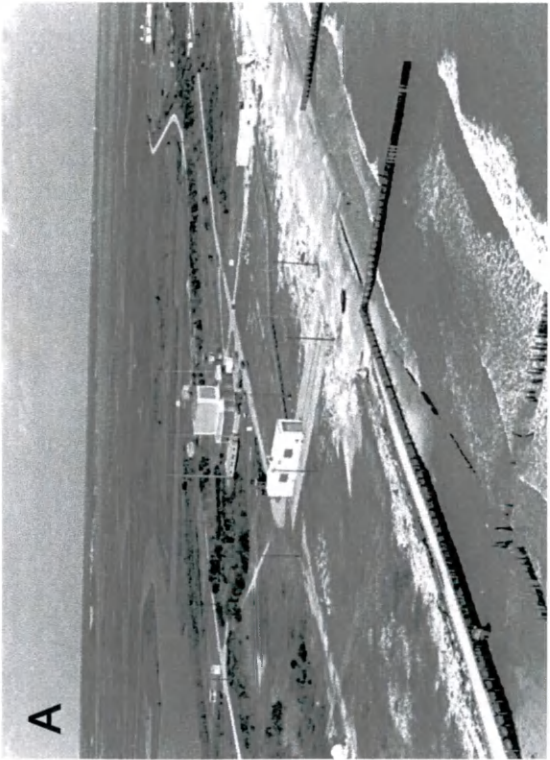


FIGURE 13

(a) Mean profile shapes for Assateague Island and Wallops Island. (b) Example profiles show the variability in profile along Assateague Island, contrasting those characterized by nearshore morphology and those exhibiting a more equilibrium shape. Cross-shore slope is also shown for the characteristic equilibrium profile. (c) Alongshore difference in the normalized weighting on the first eigenfunction for Assateague Island profiles indicating their relatively more reflective (+) or more dissipative (-) state. The profiles presented in (b) are highlighted in (c). (d) Alongshore difference in the normalized weighting on the first eigenfunction for Wallops Islands showing the shoaling tendency and more dissipative state with proximity to the Chincoteague Inlet ebb-tidal delta.



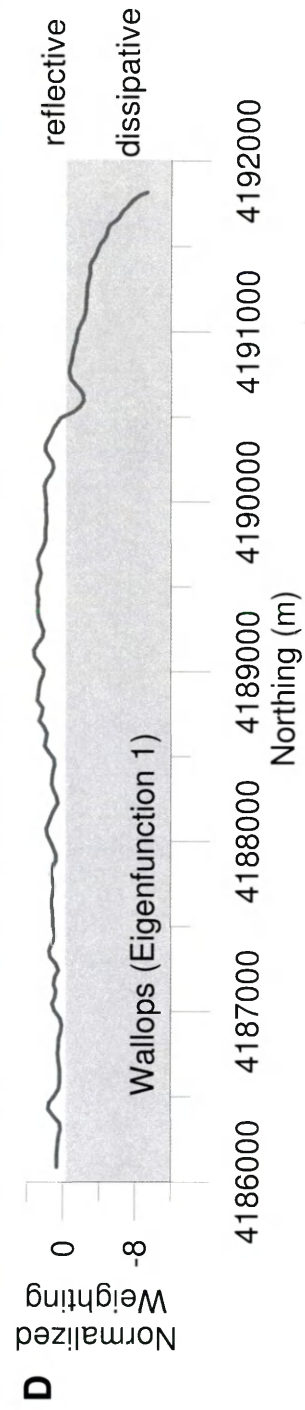
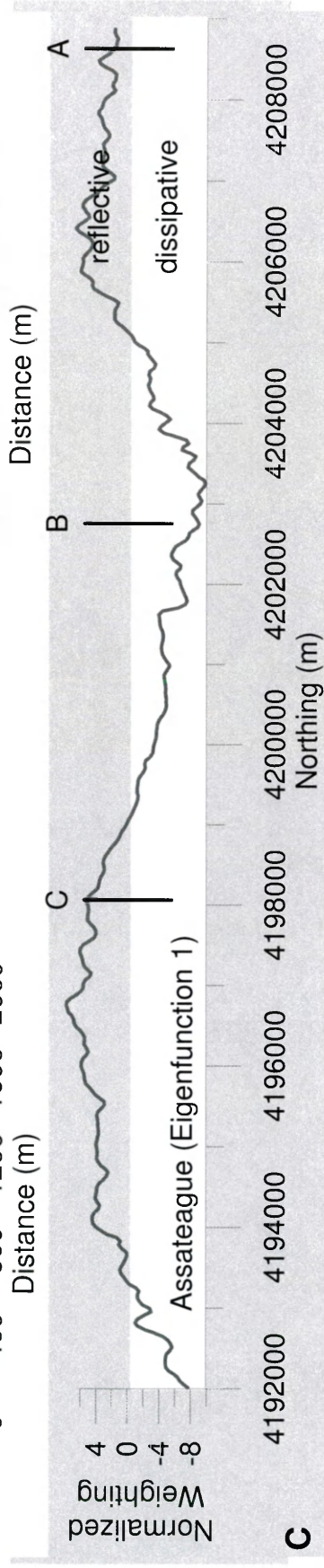
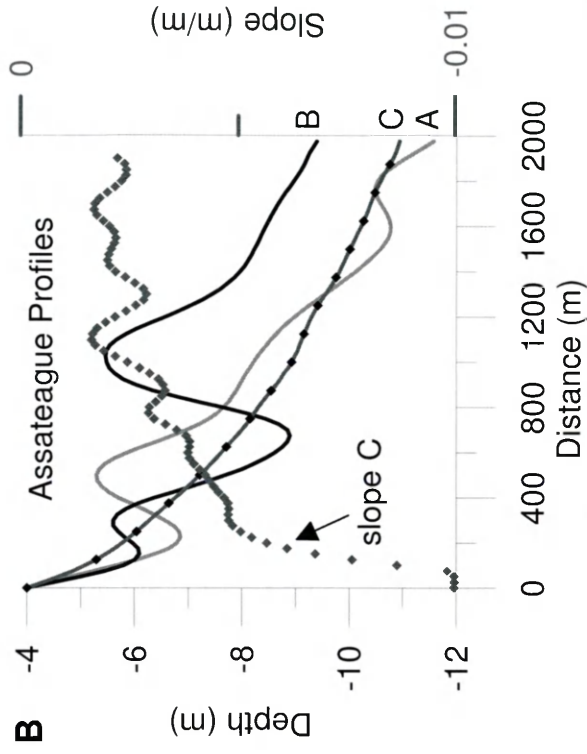
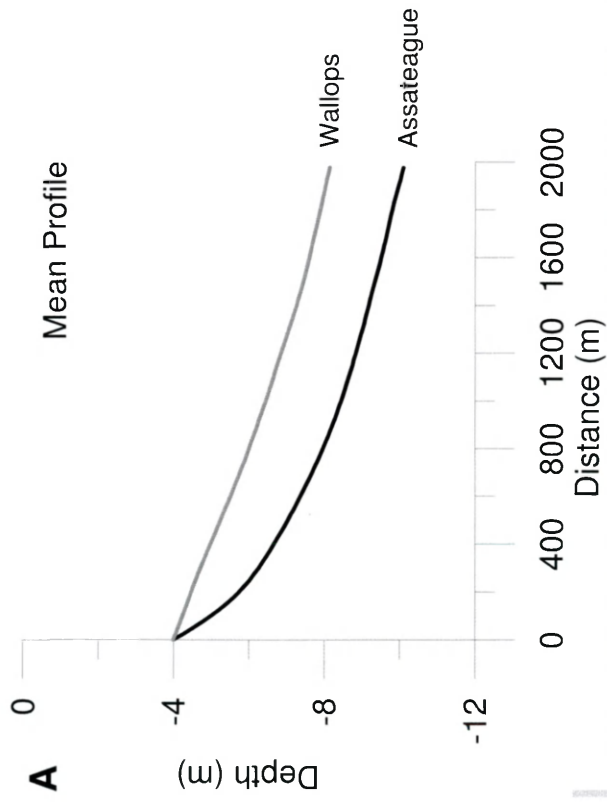


FIGURE 14

Alongshore variability in the normalized weightings on the second through fourth eigenfunctions (cross-shore shapes not shown) for Assateague Island profiles. Eigenfunctions 2 and 3 describe the relative shape of the upper and lower shoreface respectively, highlighting comparatively different alongshore areas, such as that off the relict Morris/Assateague Inlet location between Morris Island and Ragged Point (see Figure 2) and off Toms Cove. In comparison, the fourth eigenfunction delineates where sand ridges (+), smaller shoals (+), and/or associated troughs (-) intersect the shoreface.

### Assateague Island Eigenfunctions 2-4: Alongshore Normalized Weighting

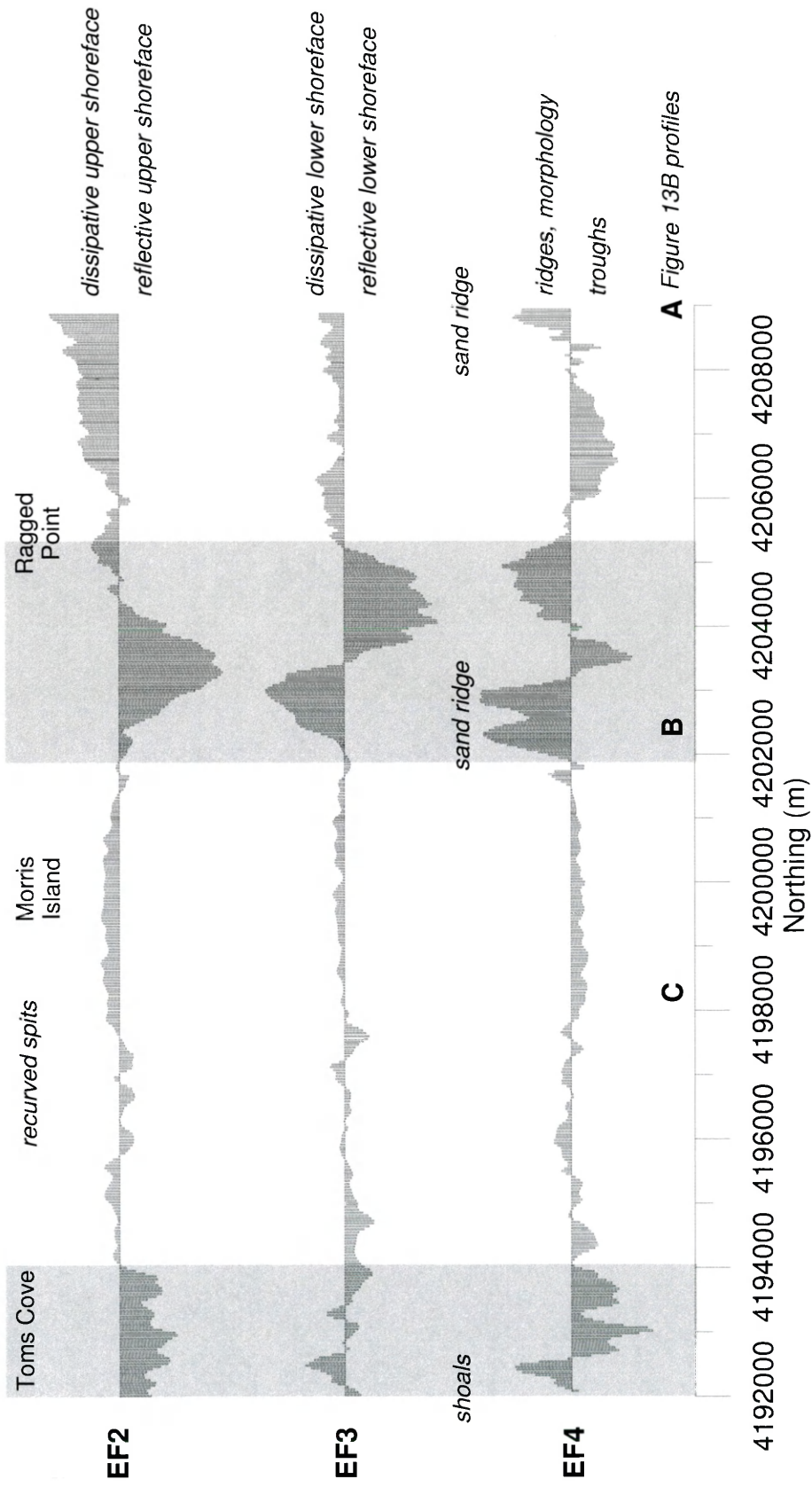




FIGURE 15

Bathymetric change map showing bottom-elevation changes between the 1978/1982 and 1933/1934 hydrographic surveys (corrected for sea level rise). Annualized volumetric-change calculations for zones I-VI (delineated by dashed lines) are reported in Table 6. Isopach shows prominent south-southeast migration of sand ridges (I-III), accretion near the centrally located shoreface-attached sand ridge (I), shoreface erosion along Assateague south of Assateague Light spit (II), southwest migration of Chincoteague Shoals (III), significant deposition south of Assateague Island (III-V), attachment of the Fishing Point spit platform to the Chincoteague Inlet ebb-tidal delta (IV), bypassing of the ebb delta to Gunboat Point (V), erosion of the Wallops Island shoreface (VI), and comparatively little change in the Chincoteague Bight basin (VI).

# Bathymetric Change (1933 to 1982)

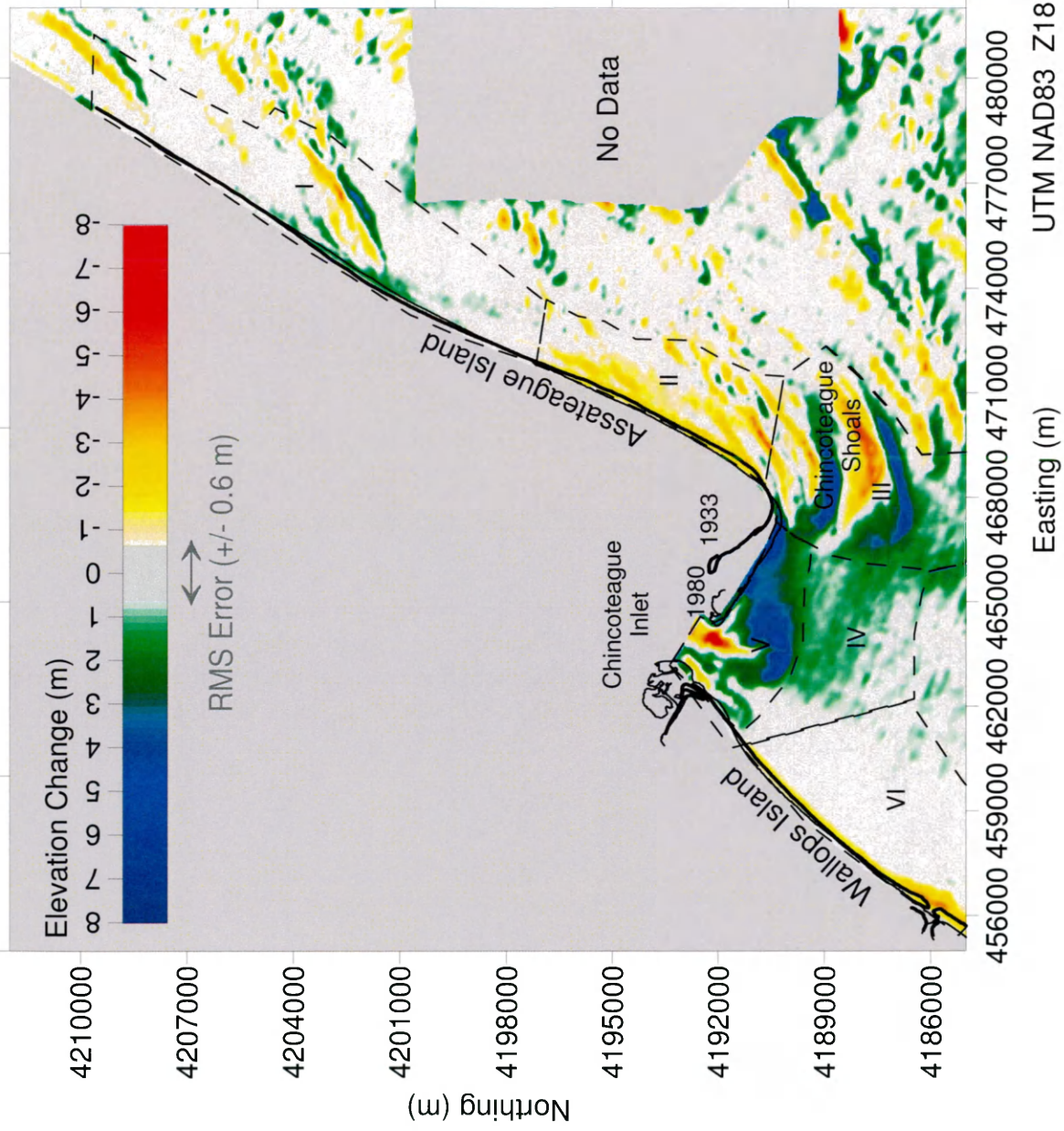
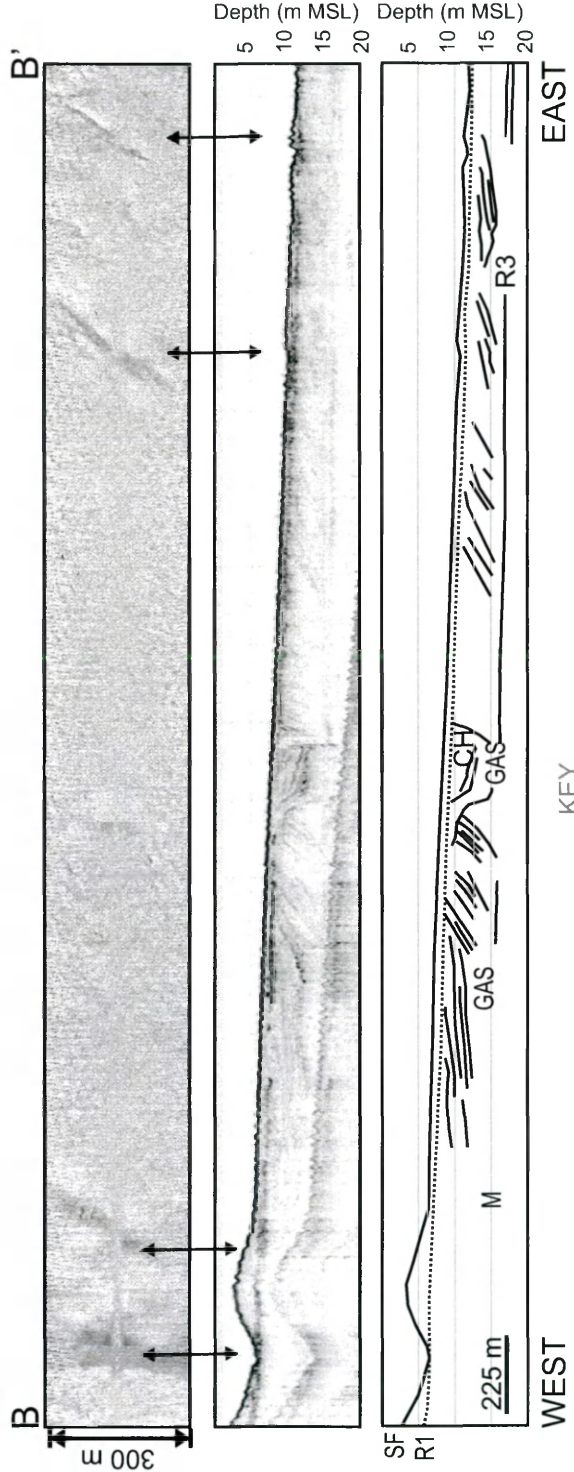
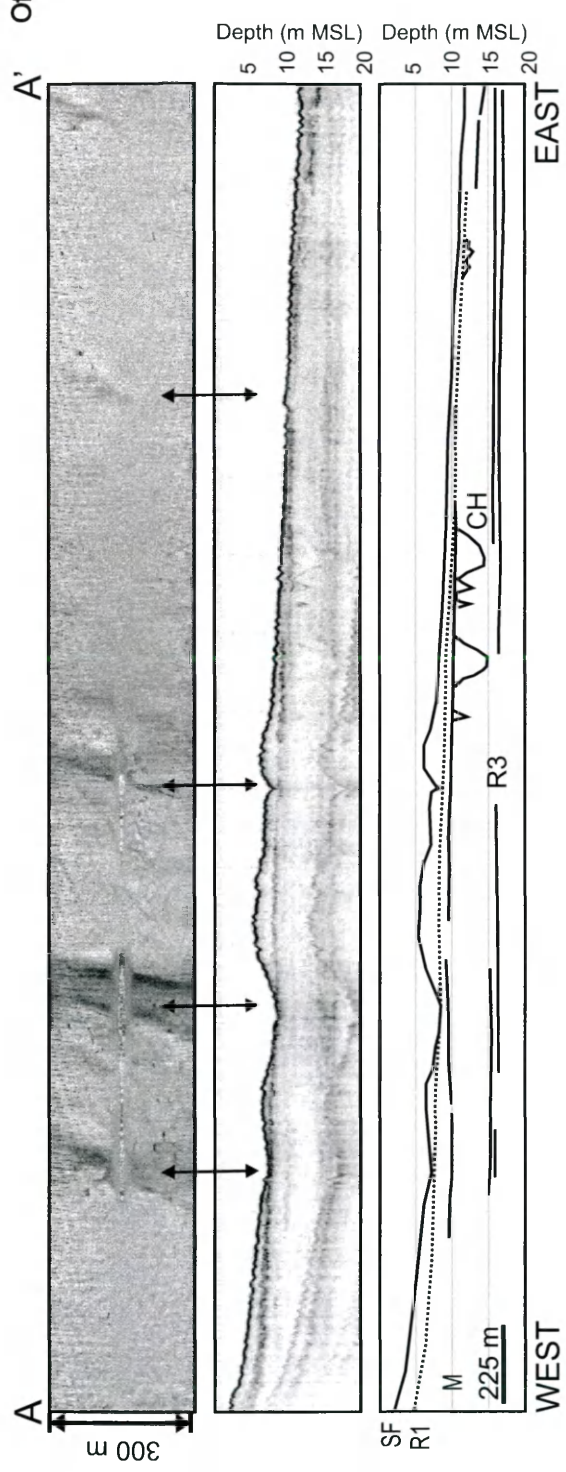


FIGURE 16

Side scan sonar, chirp seismic, and interpreted cross-section for Assateague Island cross-shore lines A and B intersecting shoreface-attached sand ridges. The ravinement is represented by the dotted line, and underlying channel fill and inlet related reflections are demarcated. Depths are referenced to fish depth. Seafloor and seafloor multiples are labeled. See Figure 6 for location.

Assateague Island

Offshore



- KEY
- SF (Seafloor)
  - R1 (Ravinement)
  - CH (Channel)
  - CR (Creek)
  - IF (Inlet Facies)
  - Multiple (M)

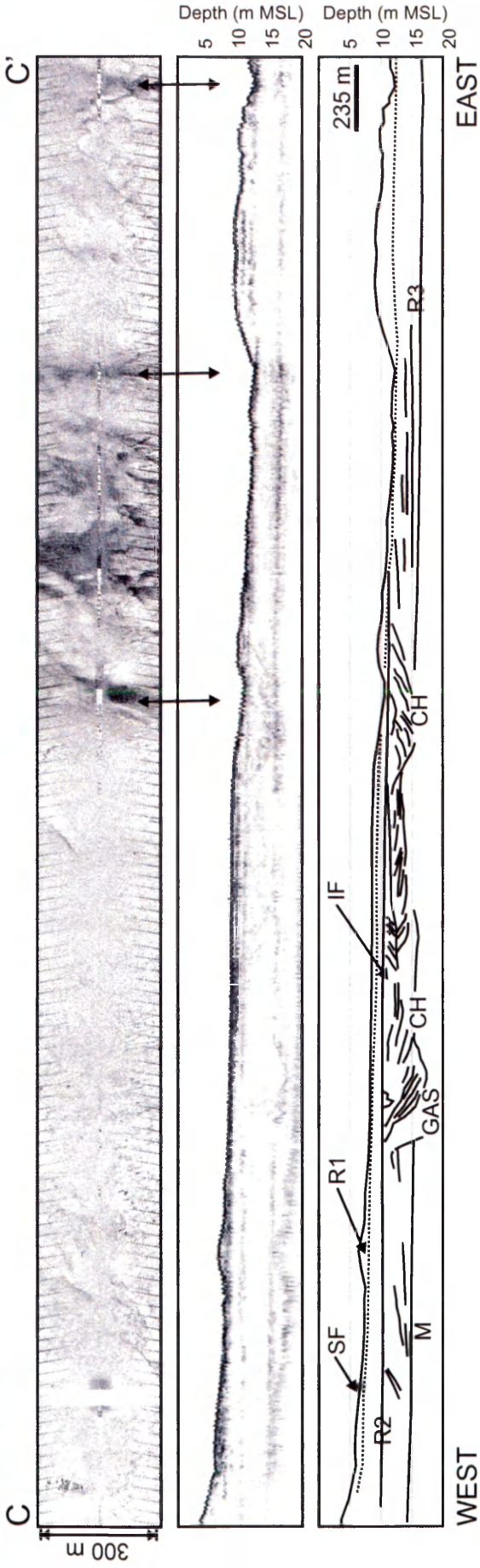
FIGURE 17

Side scan sonar, chirp seismic, and interpreted cross-section for Assateague Island cross-shore lines C and D show contrasting small-scale and large-scale inner shelf topography. The modern sand sheet (A1) overlies the active ravinement (R1), represented by the dotted line. The immediately underlying opaque unit (A2) overtops apparent channel fill and inlet related facies. These two Holocene units are separated by another disconformity (R2), potentially a ravinement surface that formed prior to the development of the shallow marine shoals associated with the southern progradation of the recurved spits. Depths are referenced to fish depth. Seafloor and seafloor multiples are labeled. See Figure 6 for location.



Assateague Island

Offshore



D

D'

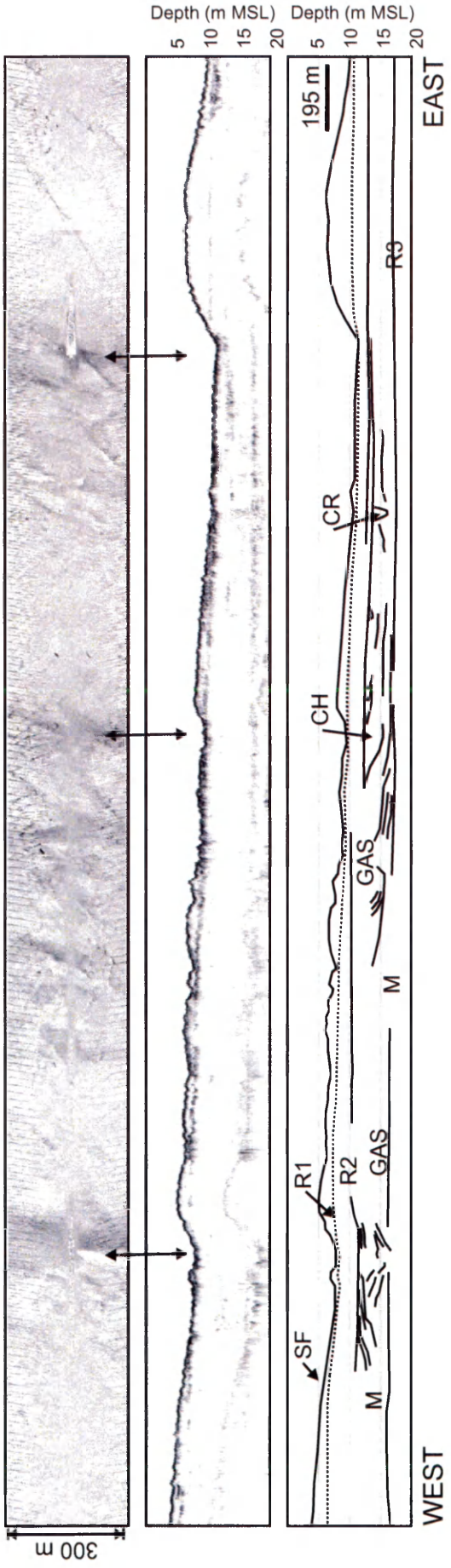
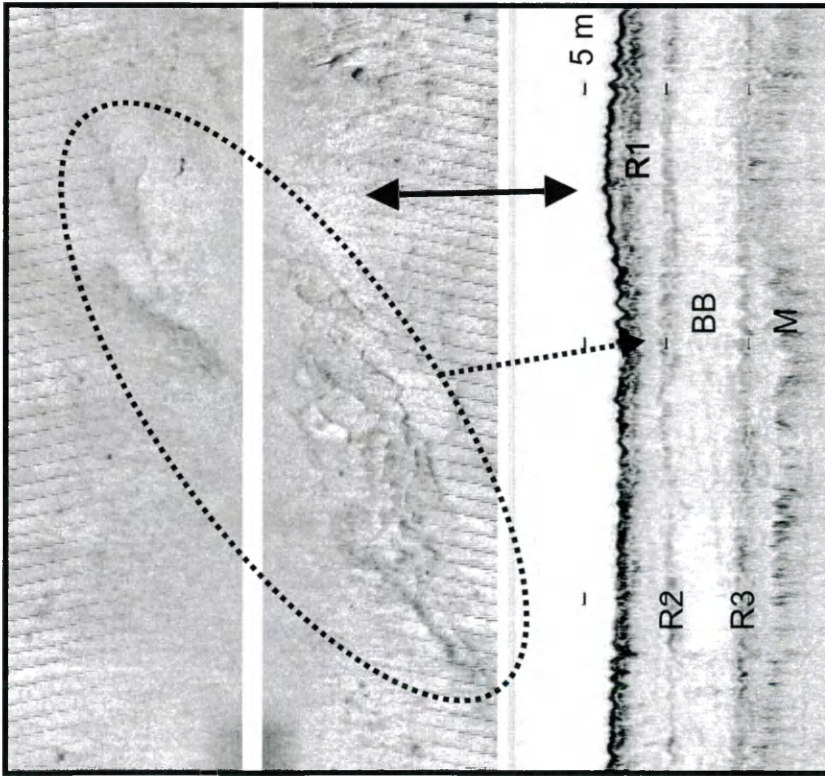
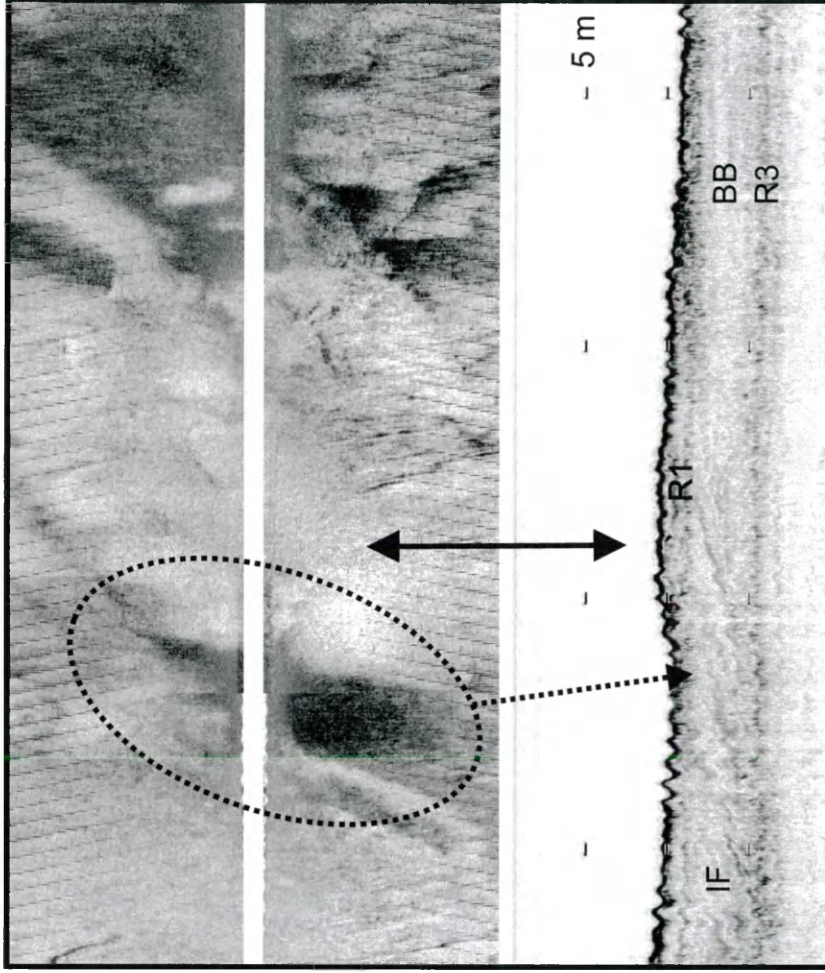


FIGURE 18

Side scan sonar imagery demonstrating the acoustic signature common to the surficial sands and underlying seismic facies offshore of Assateague Island. High backscatter is represented by light tones, whereas low backscatter is represented by dark tones. The distribution of backscatter patterns is closely tied to the seafloor morphology and topography. High backscatter occurs along the modern sand sheet and shoal flanks. Low backscatter occurs where the underlying Holocene backbarrier and lagoonal sediments, and/or the poorly sorted ravinement surface, occur at the seafloor. Intervening backscatter tones commonly occur where the shoal/spit facies (A2) occurs near or at the seafloor.



Line C-C'



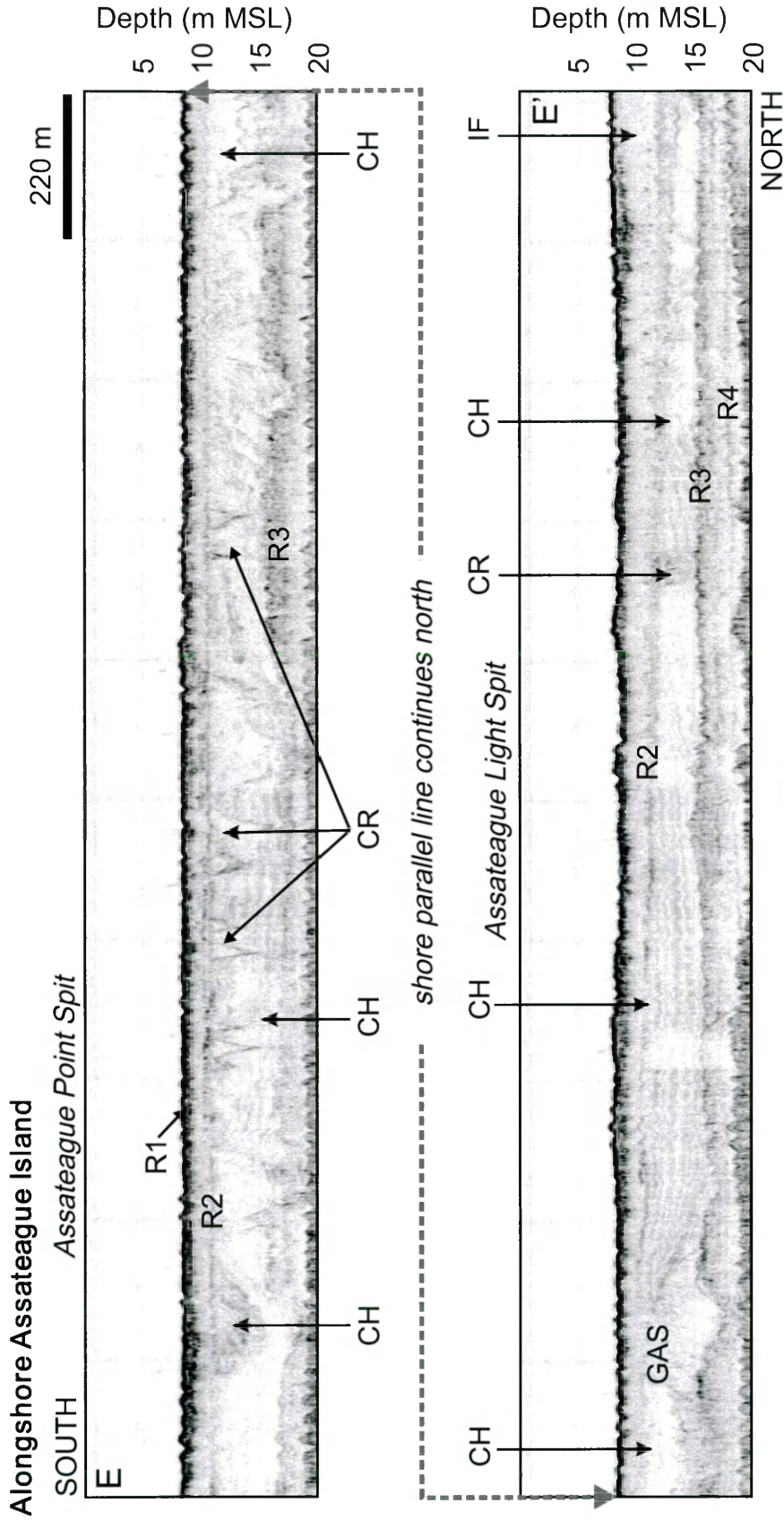
Line C-C'

KEY  
 R1 (Ravinement)    BB (Backbarrier)    IF (Inlet Facies)    Multiple (M)



**FIGURE 19**

Chirp seismic and interpreted cross-section for Assateague Island shore-parallel line E demonstrating the relatively thin sand cover at the lower shoreface. The seismic data show extensive channeling underlying the ravinement at the north end, a potential ebb-tidal delta, and probable marine shoals at the southern end. Depths are referenced to fish depth. Seafloor and seafloor multiples are labeled. See Figure 6 for location.



KEY

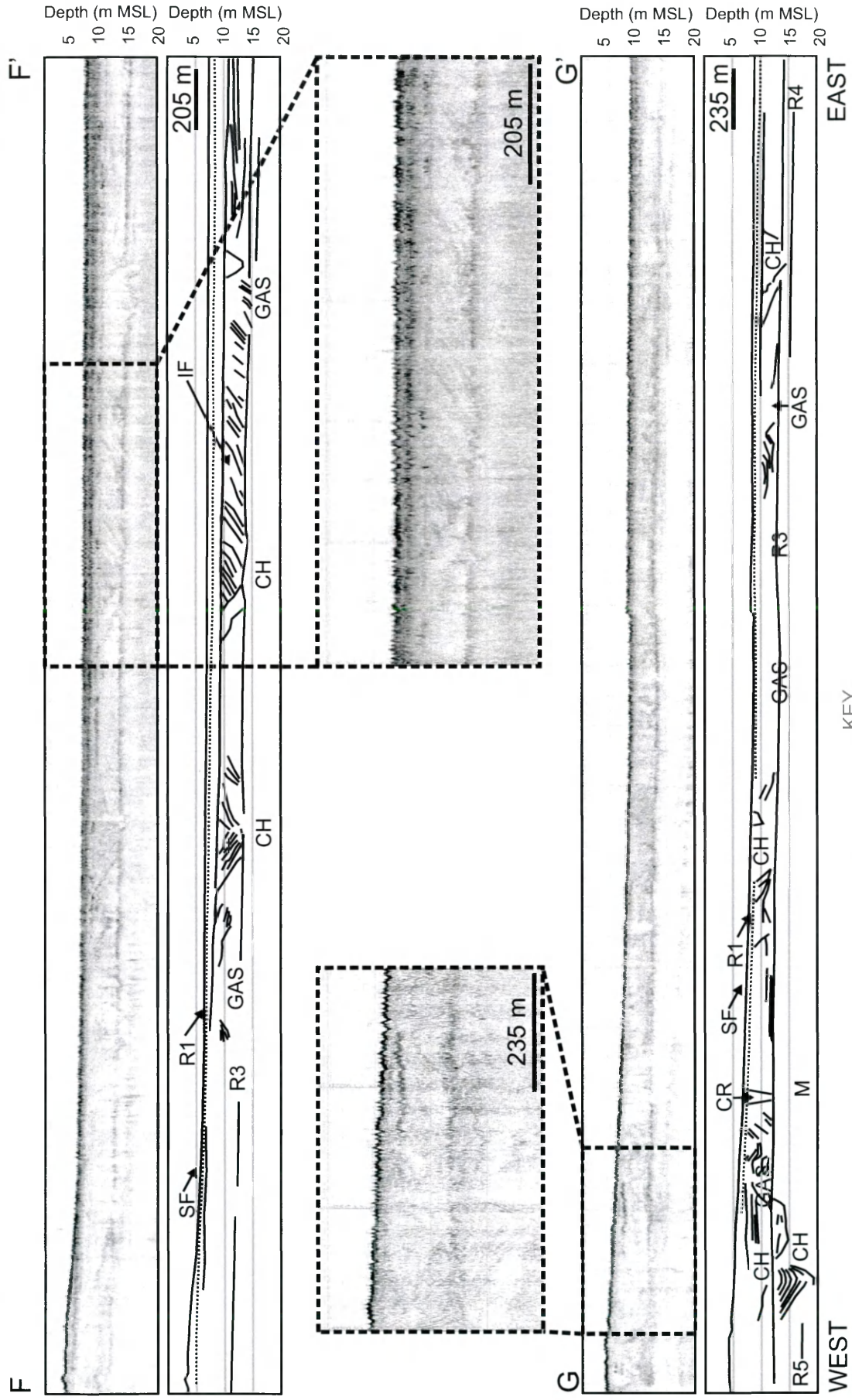
SF (Seafloor)	R1 (Ravinement)	CH (Channel)	CR (Creek)	IF (Inlet Facies)	Multiple (M)
---------------	-----------------	--------------	------------	-------------------	--------------

FIGURE 20

Chirp seismic and interpreted cross-section for cross-shore lines F and G illustrating the extremely thin sand cover, if any, off Wallops Island. The ravinement, represented by the dotted line, truncates channel fill, inlet related, and backbarrier facies. Depths are referenced to fish depth. Seafloor and seafloor multiples are labeled. See Figure 6 for location.

Wallops Island

Offshore



KEY  
 SF (Seafloor) R1 (Ravinement) CH (Channel) CR (Creek) IF (Inlet Facies) Multiple (M)

WEST

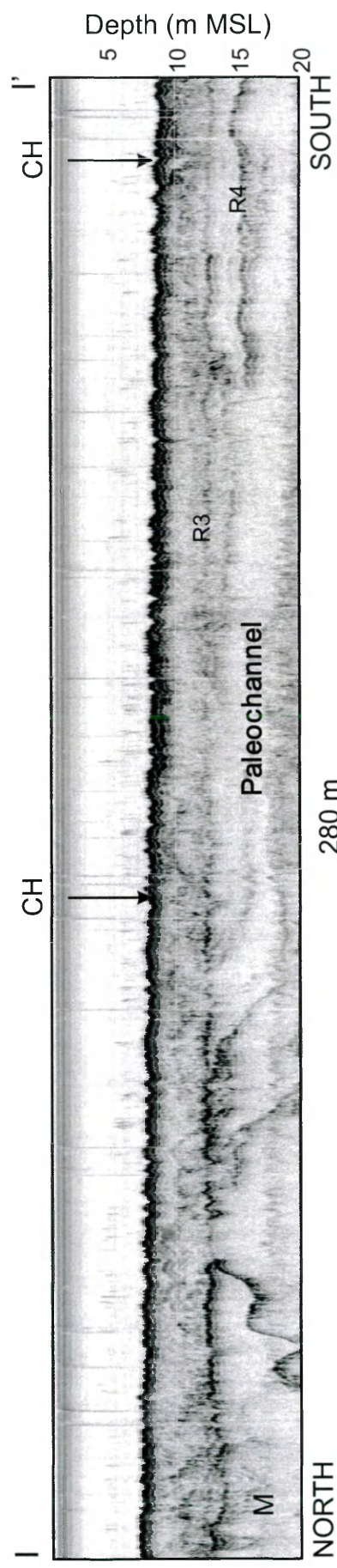
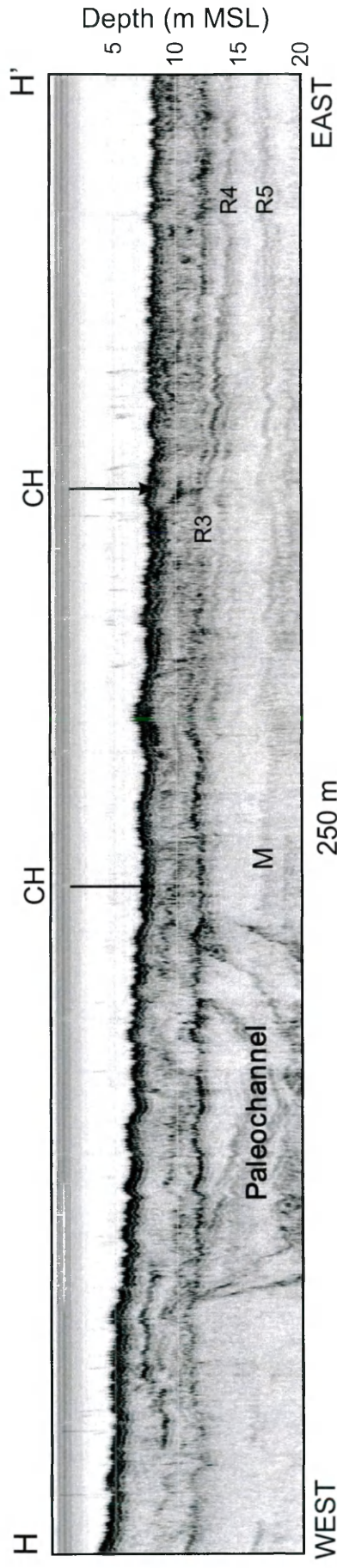
EAST

#### FIGURE 21

Chirp seismic sections for cross-shore line H and shore-parallel line I show the relatively thin to absent sand cover immediately south of Wallops Island and thick underlying Holocene lagoonal / backbarrier facies. The low-gradient Pleistocene unconformity occurs at approximately 12 m below MSL, providing for significant overlying accommodation space. Below this depth, buried, nested paleo-channels (~ 5-7 m deep, < ~750 m wide) filled with transgressive deposits, may be associated with the late Pleistocene capture and drainage of the small mainland watersheds along the Delmarva Peninsula (see Figure 32). Comparable features were not seen in seismic data off southern Assateague Island, indicating subsequent Holocene erosional processes removed the record, and/or the paleo-drainage was organized such that paleo-tributaries did not incise beneath Chincoteague and Assateague Islands. The high amplitude seafloor and shallow reflector returns result from different pulse length setting / gain processing selected to enhance architecture at depth. Depths are referenced to fish depth. See Figure 6 for location.



Off Wallops and Assawoman Islands



KEY  
 SF (Seafloor) R1 (Ravinement) CH (Channel) CR (Creek) IF (Inlet Facies) Multiple (M)

FIGURE 22

Map showing the offshore distribution of interpreted relict paleochannel, tidal channel and creek fill, and inlet-related facies superimposed on the bathymetric model. Known historic inlets are also indicated.

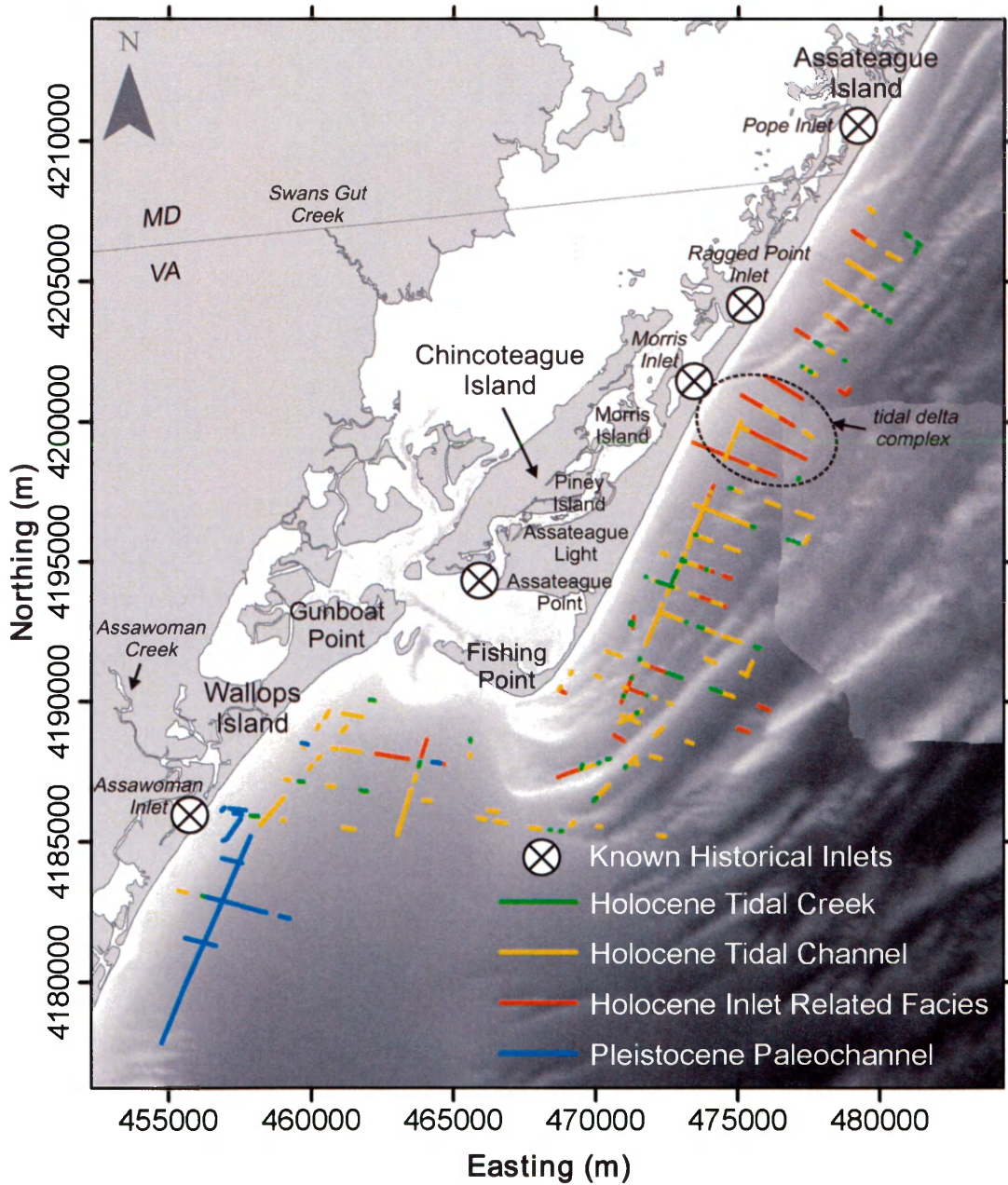
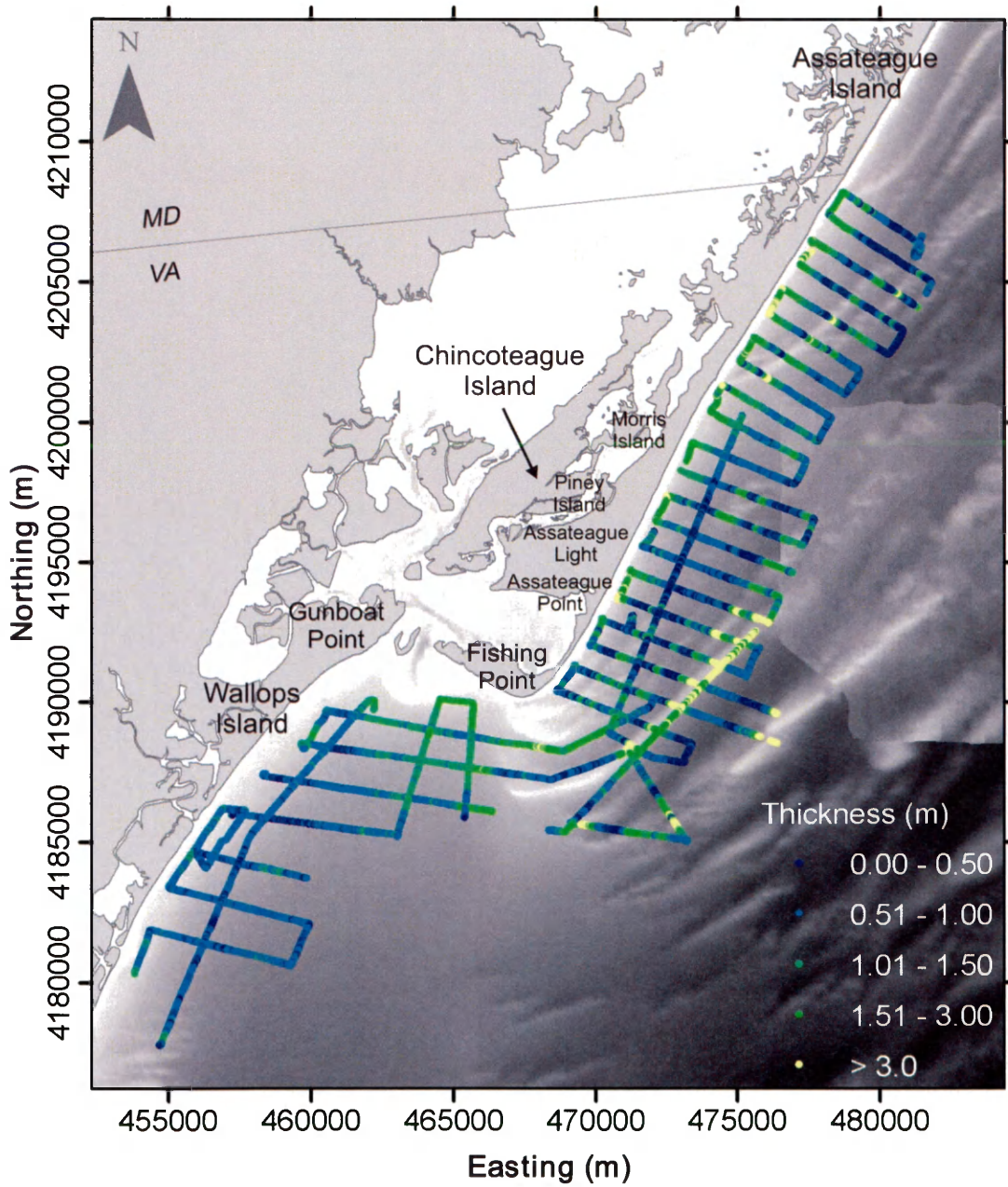




FIGURE 23

Map delineating the thickness of the surficial sand cover as measured from chirp seismic data. The facies being truncated by active ravinement processes south of Morris Island may contribute 'new' sand to the system. Thickness values are presented in meters, assuming a seismic velocity of 1500 m/s.



**FIGURE 24**

Isopach map showing regional sand prism thickness within the extent of the overlap of bathymetry and geophysical data. Much of the shoreface off Assateague Island and Wallops Island is characterized by relatively thin fine to medium sand with a locally muddy cover. Black symbols represent the location of legacy and recent vibracores, whereas the white arrows distinguish the location of vibracores shown in Figure 25.

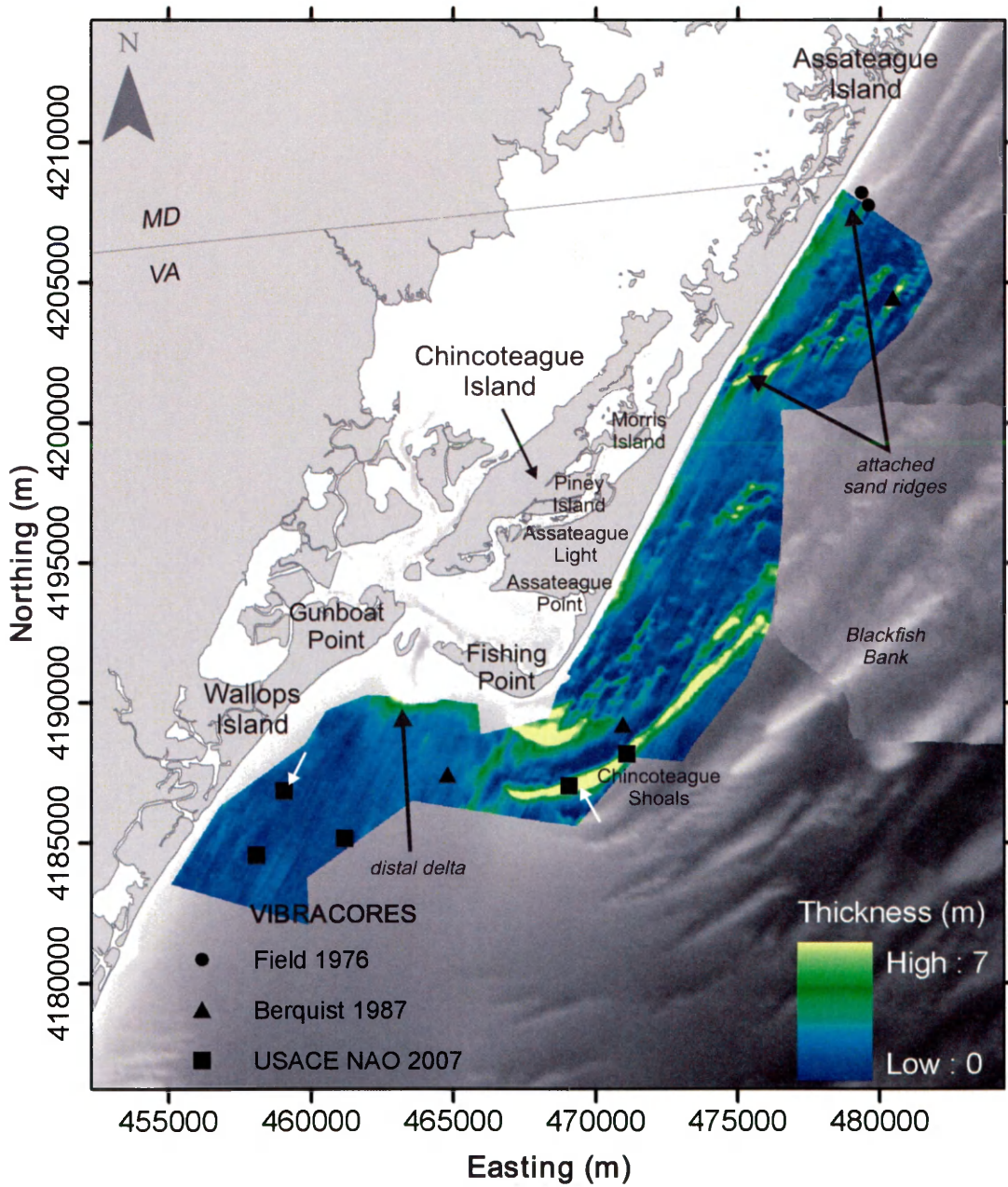
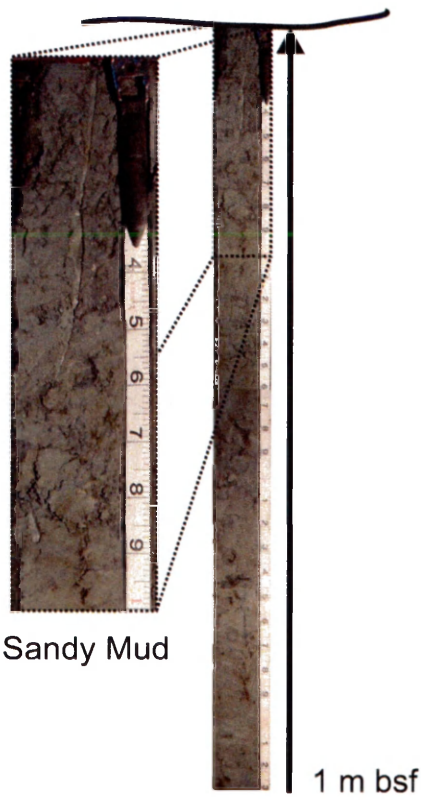


FIGURE 25

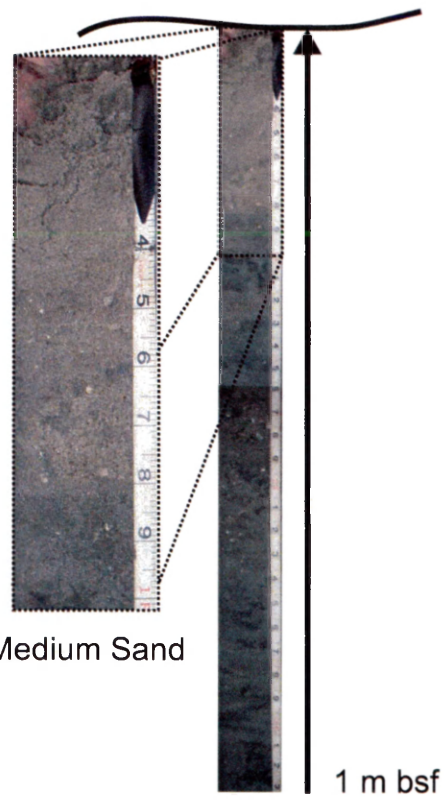
Digital photographs of 20-ft vibrocores collected in 2007 in ~7-8-m water depth off central Wallops Island and southern Assateague Island on Chincoteague Shoals (courtesy of Gregg Williams, U.S. Army Corps of Engineers - Norfolk District). Off Wallops Island, a cohesive, sandy mud continues down-core, confirming the relatively thin or entirely absent sand cover seen in the chirp seismic data. On Chincoteague Shoals, a medium sand persists the entire length of the core, confirming the chirp seismic data which showed a local maximum sand thickness of ~7 m. Core locations are indicated in Figure 24.

Wallops Island Shoreface



Sandy Mud

Chincoteague Shoal



Medium Sand



## FIGURE 26

(a) Plan view example of the inner shelf directional-slope model used to delineate the presence of morphology on the shoreface. The central shoreface-attached ridge intersects the shoreface at the location of a former inlet. The 4-m and 8-m contours are displayed. Relatively steep gradient of upper shoreface in black, nearshore morphology in white, and increasingly planar lower shoreface and inner shelf in gray. (b) Nearshore sand cover for the shoreline reach from the Maryland/Virginia state line south to the southern limit of Toms Cove. Sand thickness is clipped between the 4-m and 8-m isobaths, the landward limit of the seismic data and the *approximate* depth of closure. Sediment thickness generally decreases from north to south. The eroding Toms Cove beach segment is characterized by the thinnest cover. Sediment thickness increases at the location of relict spits Assateague Light and Assateague Point, shaded in dark gray (Morton *et al.*, 2007). Some of the isopach variability on the updrift and downdrift sides of shoreface-attached ridges is an artifact related to the time lapse between bathymetric and geophysical surveys; nonetheless, on a regional scale the comparative differences are adequately represented.

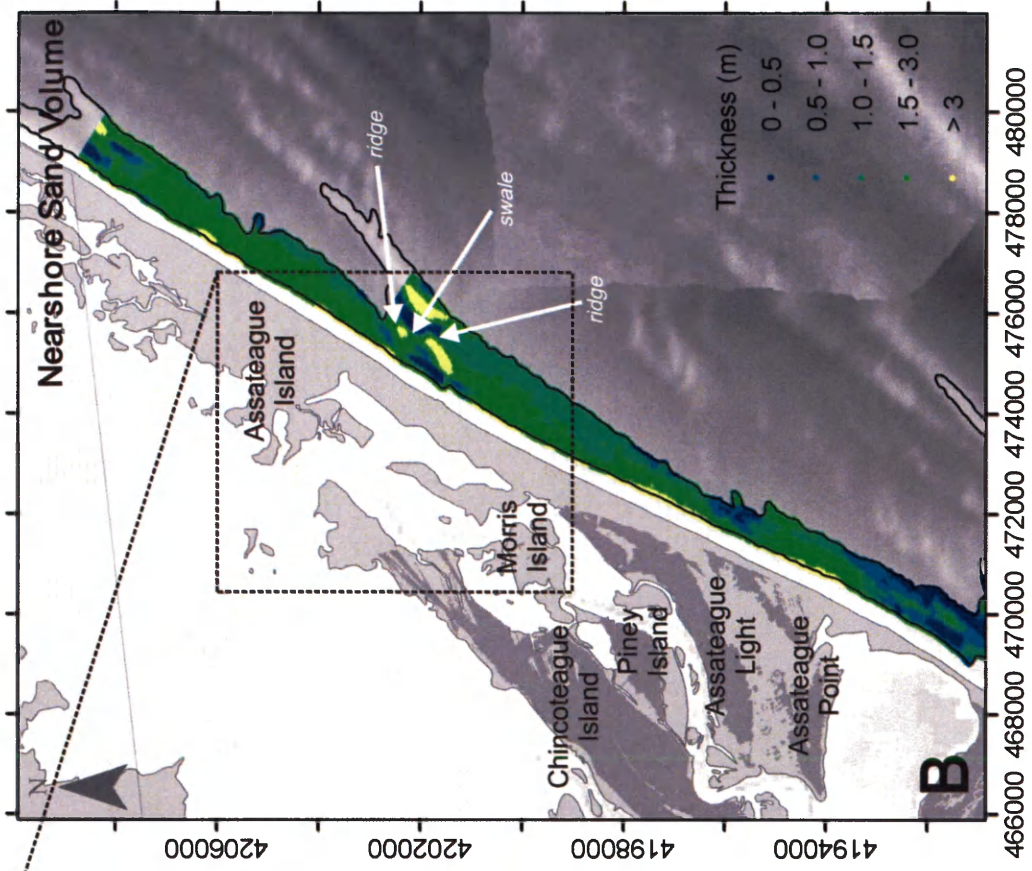
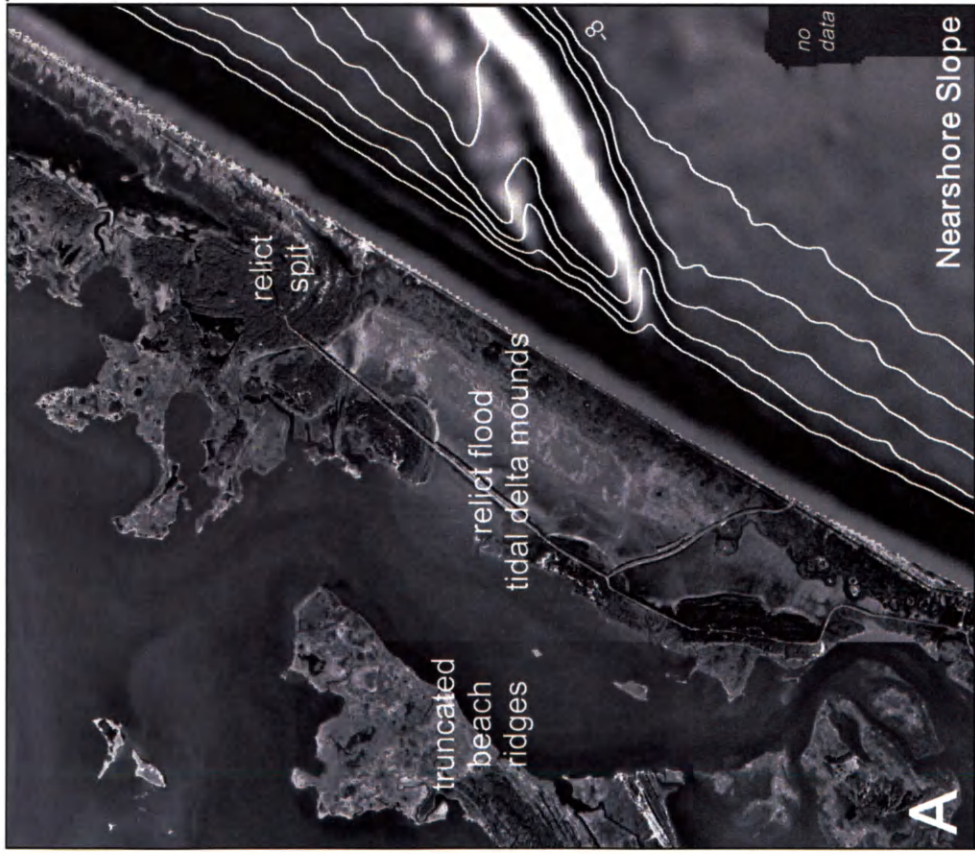
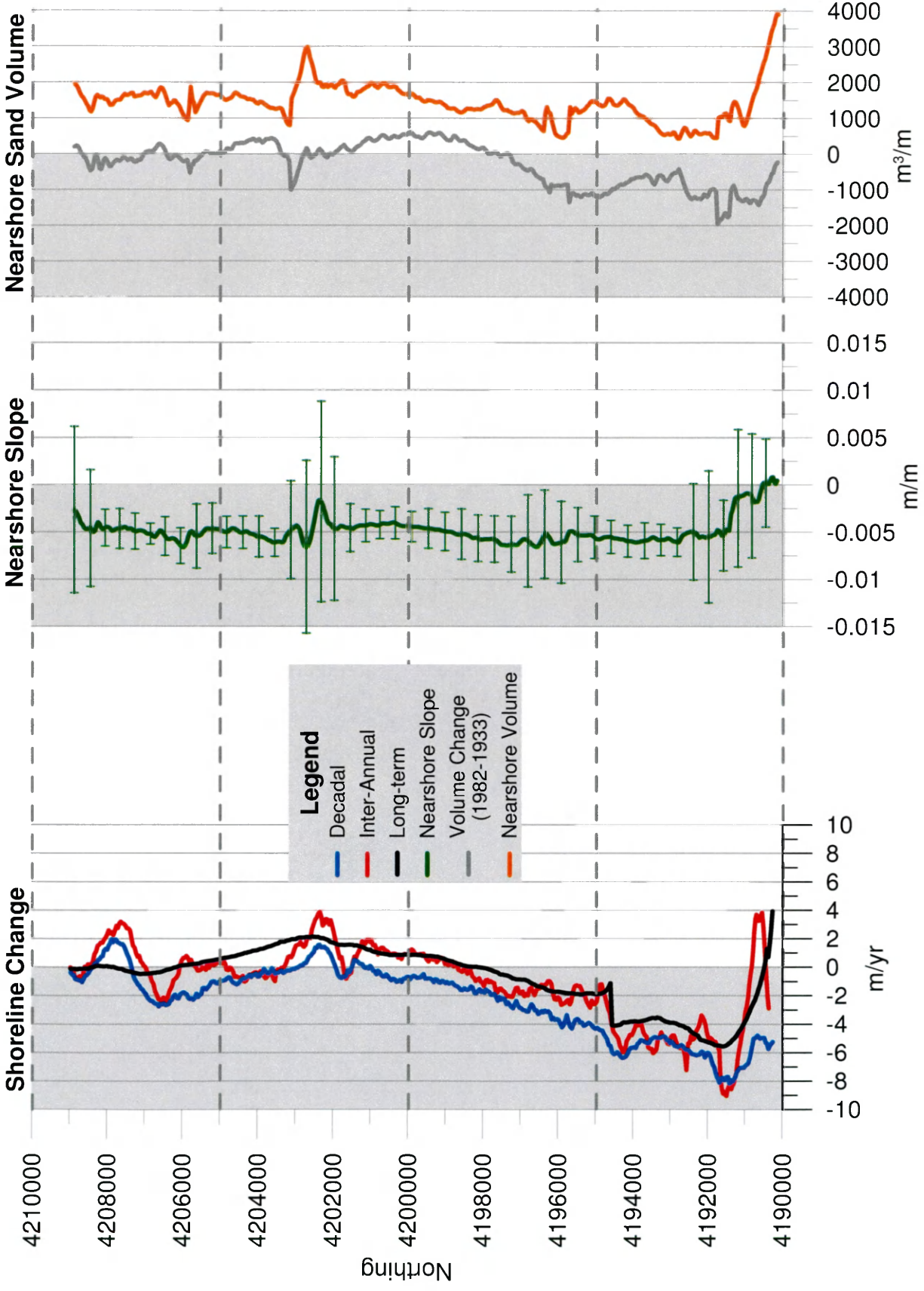




FIGURE 27

Inter-annual, decadal, and long-term shoreline change rates (m/yr) compared to cross-shore slope (m/m) and nearshore sand volume ( $\text{m}^3/\text{m}$ ) in cross-correlation analysis. Horizontal bars on the slope metric represent the standard deviation. The alongshore trend in volume change ( $\text{m}^3/\text{m}$ ) between 1933 and 1982 corroborates the trend in nearshore sand volume.



**FIGURE 28**

(a) Nearshore slope (smaller slopes indicate morphologic features, in particular shoreface-attached sand ridges) and inter-annual shoreline change rate (negative values indicate erosion) for southern Assateague Island. (b) Correlogram showing cross-correlation (CCF) of slope and inter-annual shoreline change rate. The critical value for the 90% confidence interval is indicated in red.

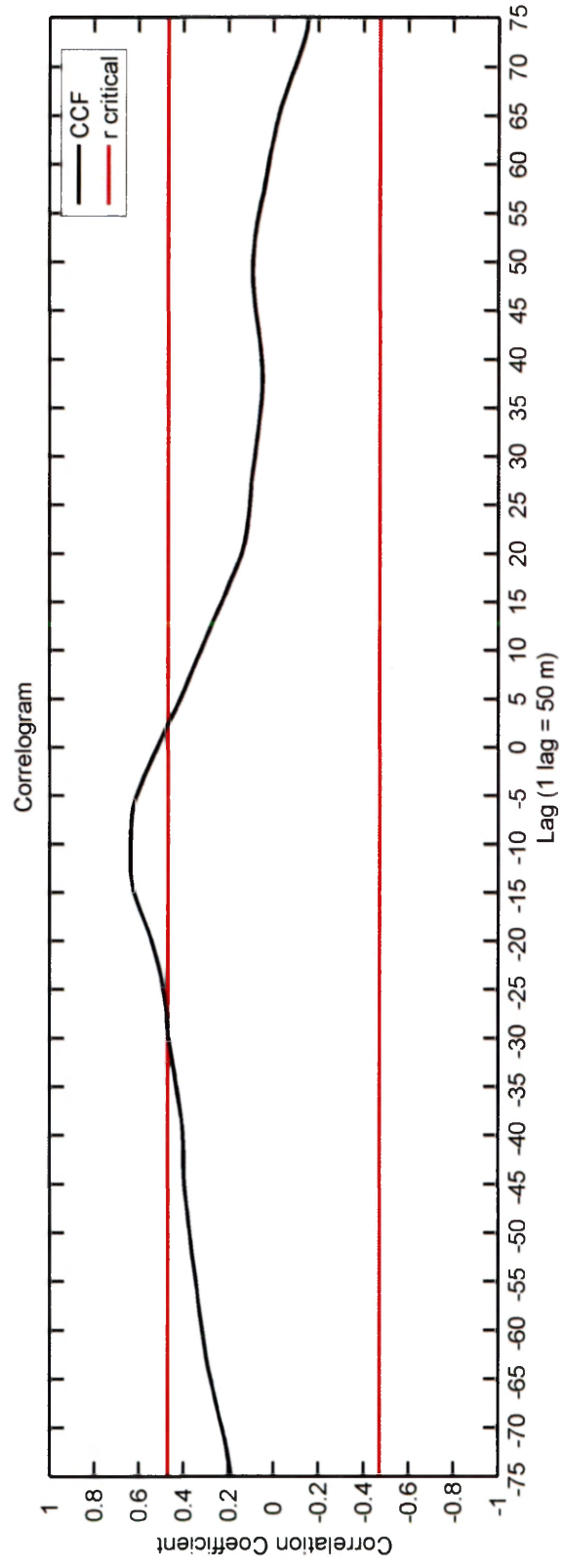
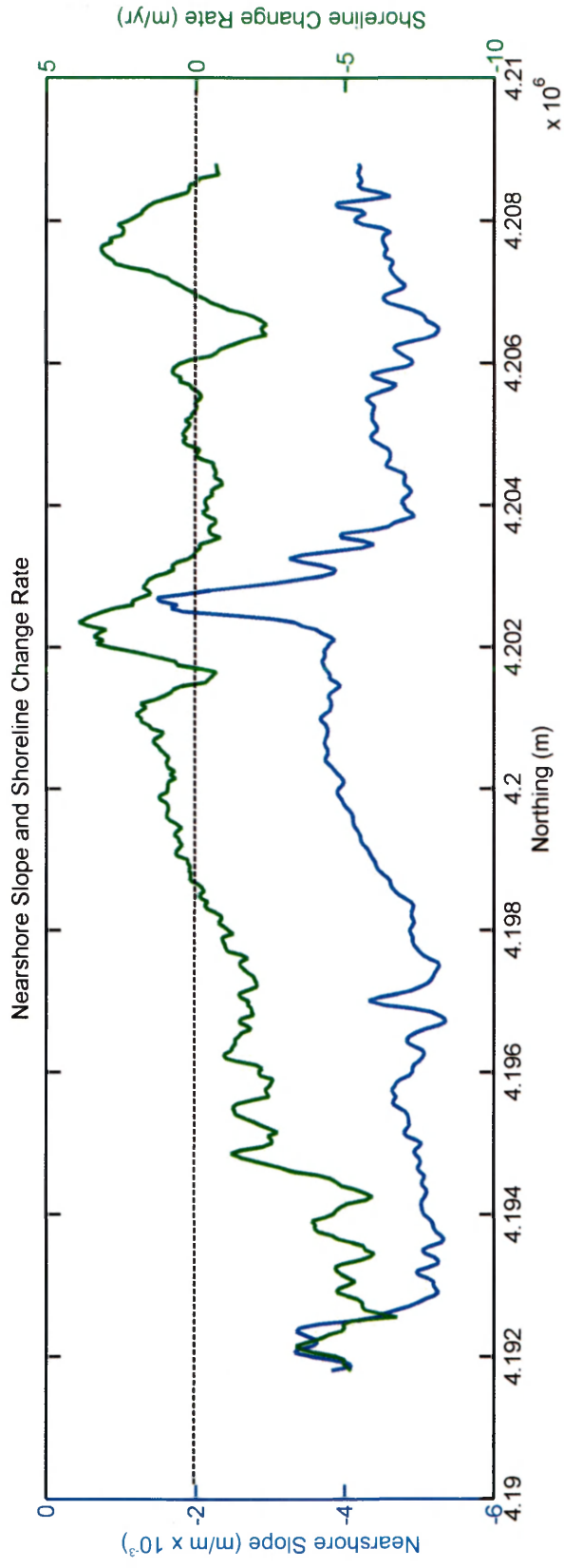
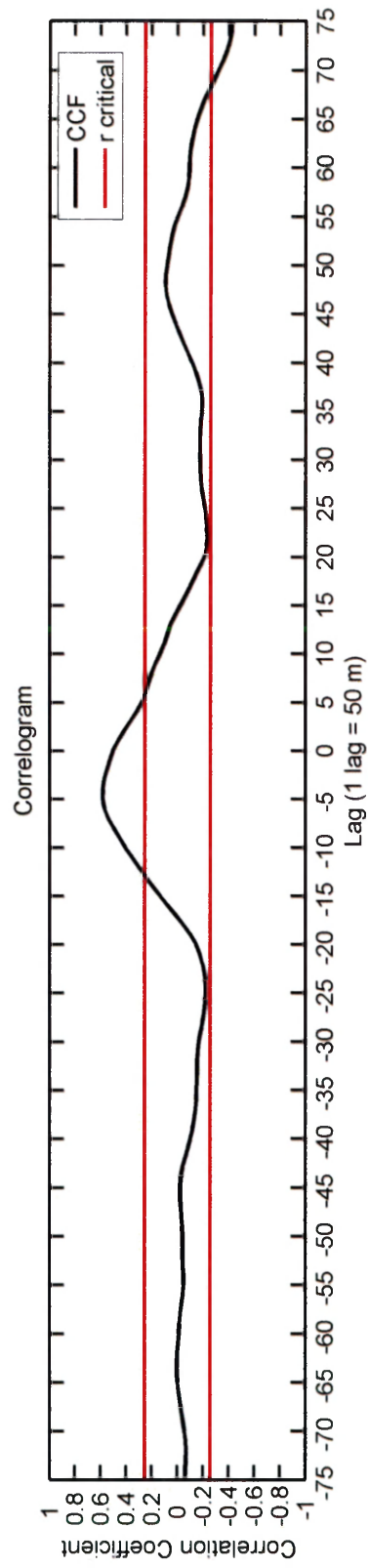
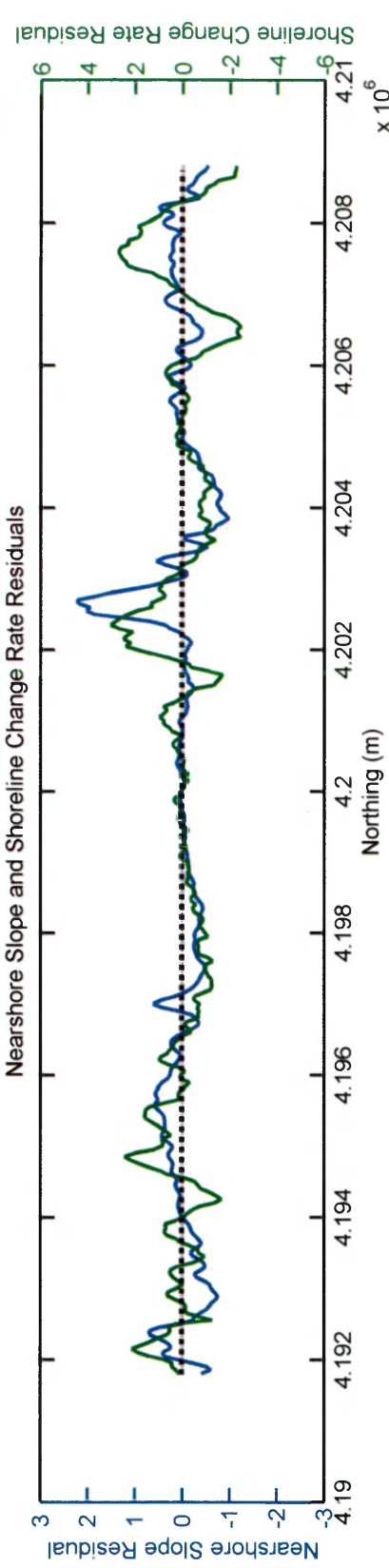
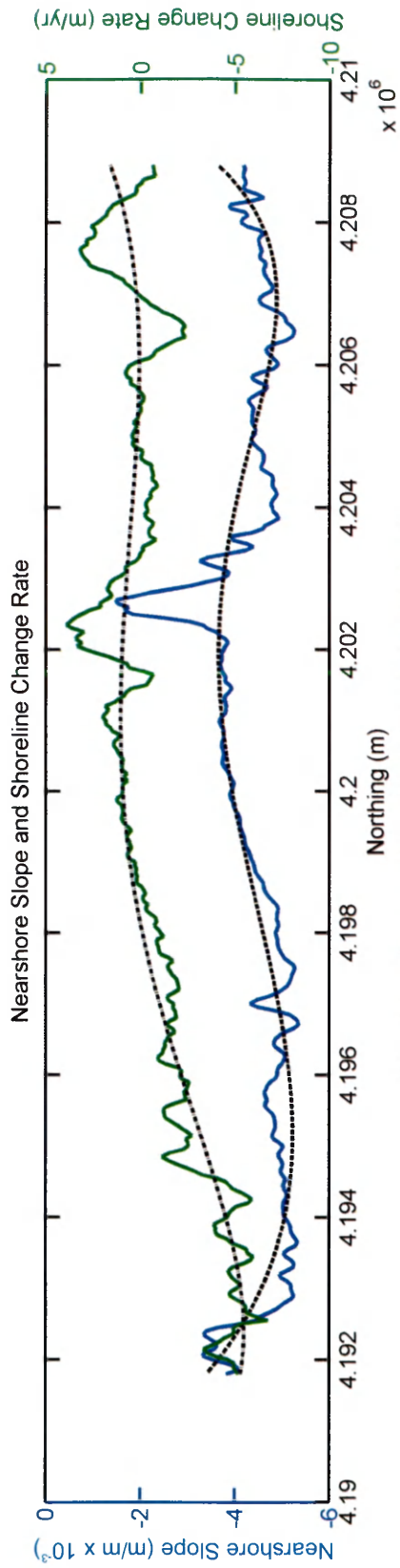


FIGURE 29

(a) Polynomial fitting of nearshore slope and inter-annual shoreline change rate. (b) Residuals from polynomial fitting, characterized by negative autocorrelation, show distinct alongshore periodicities on the order of 0.5-2 km. Deviations in shoreline-change residual lag the nearshore-morphology residual to the south, showing a strong positive relationship (*i.e.*, increasing or decreasing together). (c) Correlogram showing cross-correlation (CCF) of residuals. Any correlation coefficient occurring above the critical value is statistically significant at the 90% confidence interval.



**FIGURE 30**

(a) Nearshore sand volume (gradients in volume indicate morphology) and inter-annual shoreline change rate (negative values indicate erosion). A north-south trend persists in nearshore sand volume and shoreline change, and shoreline change tends towards erosion with decreasing nearshore volume. (b) Correlogram showing cross-correlation (CCF) of nearshore volume and inter-annual shoreline change rate. The critical value for the 90% confidence interval is indicated in red.

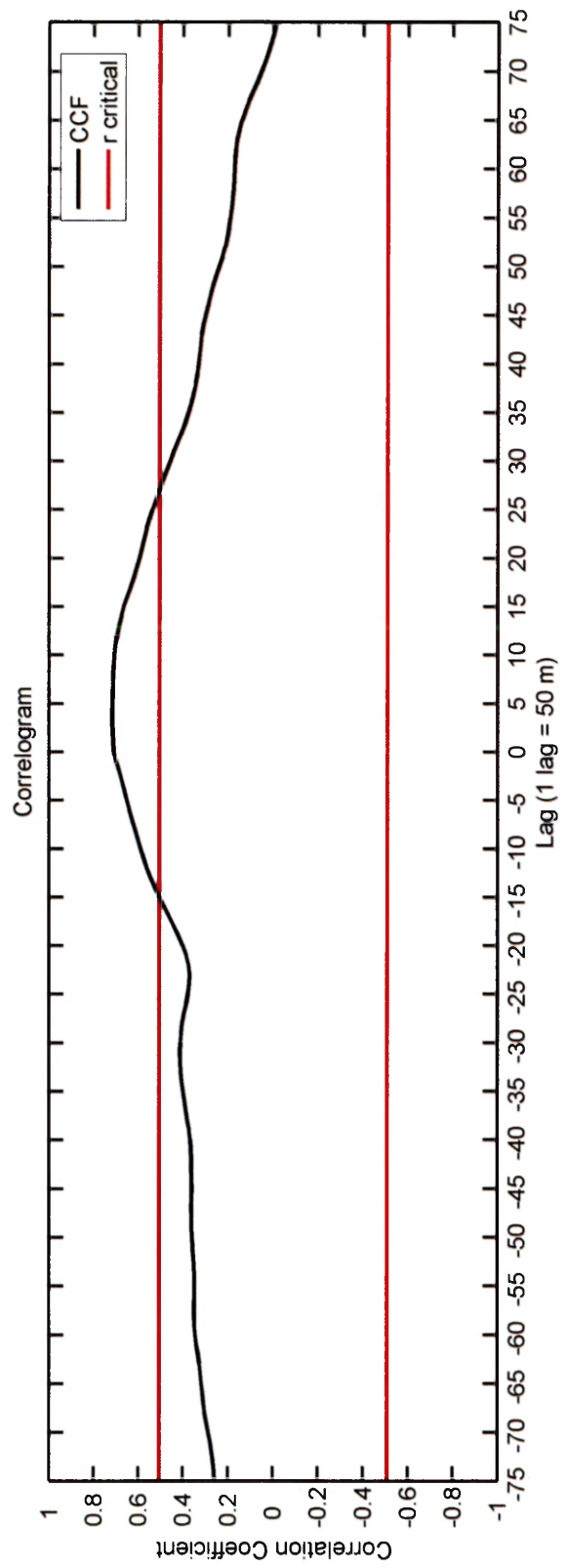
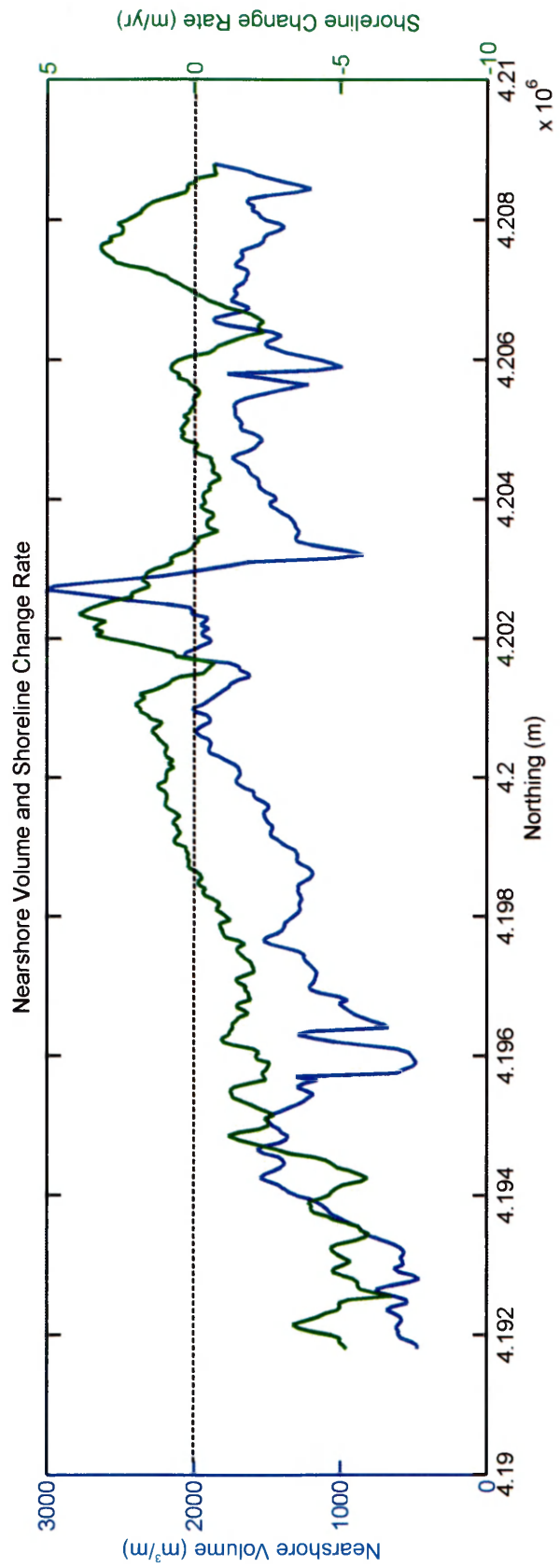
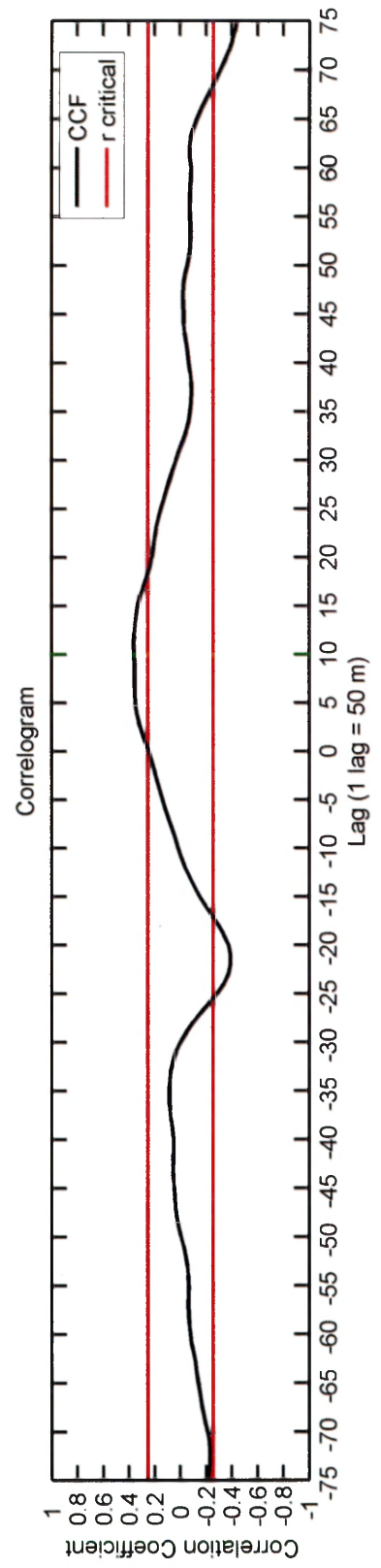
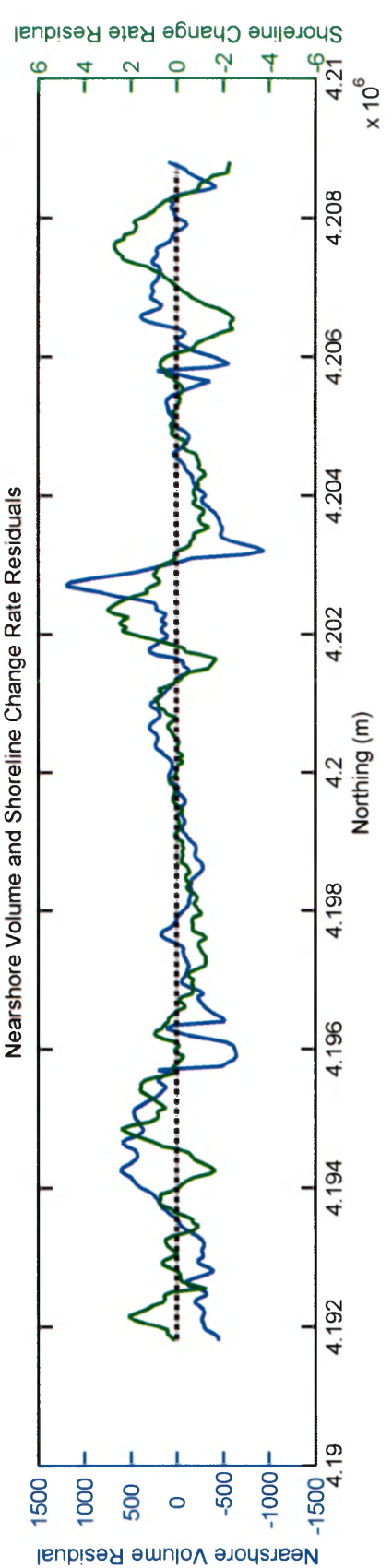
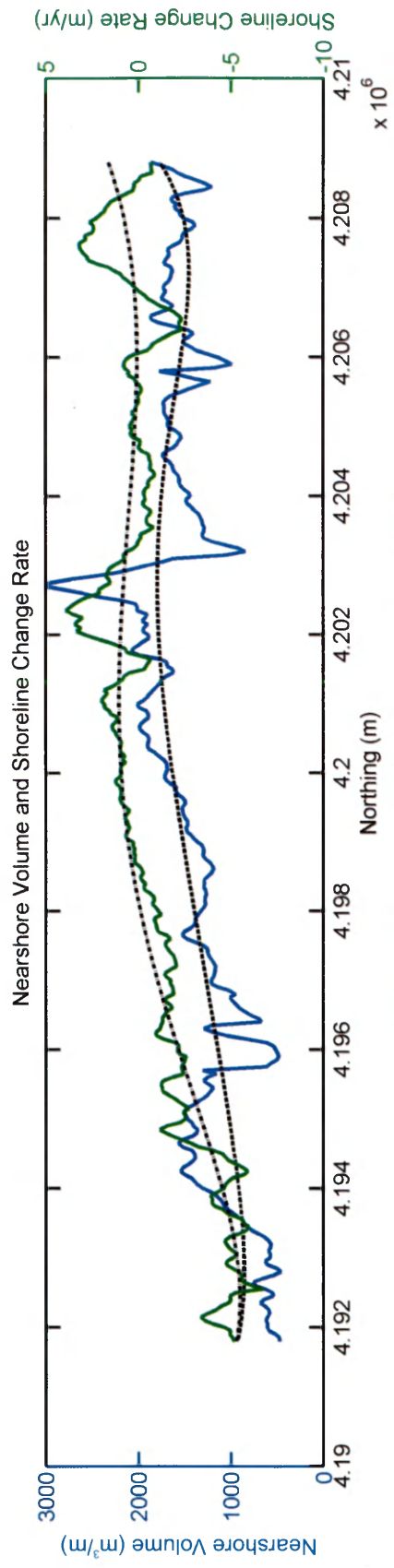




FIGURE 31

(a) Polynomial fitting of nearshore sand volume and inter-annual shoreline change rate. (b) Residuals from polynomial fitting, characterized by negative autocorrelation, show distinct alongshore periodicities on the order of 0.5-2 km. Deviations in shoreline-change residual show a complex spatial and directional association with the nearshore-volume residual. (c) Correlogram showing cross-correlation (CCF) of residuals. Any correlation coefficient occurring above the critical value is statistically significant at the 90% confidence interval.



#### FIGURE 32

Map showing the modern barrier island configuration, adjacent Chincoteague Bay watershed, and a proposed, south-southeast oriented flooded Chincoteague paleo-valley (Oertel *et al.*, 2007). The projected paleo-drainage may elucidate the following observations. The Pleistocene age (Stage 5e) mainland scarp (dashed line) behind Wallops Island trends north along the west side of Chincoteague Bay towards Sinepuxent Neck. The presumed southern extension of the Pleistocene age Sinepuxent Neck (Stage 5?) into Virginia is absent. The primary seismic paleo-channel offshore southern Wallops Island exhibits a strong north-south orientation and intimating alignment with the deeply incised Chincoteague Channel (Chincoteague Inlet). The proposed north-south paleo-drainage system likely captured the seaward-flowing Assawoman Creek (VA) and (potentially) Swan Gut Creek (VA/MD state line). In contrast, the ancestral St. Martin River in Maryland drained to the southeast (beneath Fenwick Island), perhaps capturing the northernmost paleo-tributaries immediately south of Sinepuxent Neck (Toscano *et al.*, 1989). The embayed emplacement of late Holocene barriers (dotted line) from Wallops Island north to Pope Island (believed to have fronted the ocean at ~2-3ka) may have been influenced by intersection with the flooded paleo-valley. The offset Chincoteague Bight basin may also owe (in part) its featureless character to this template and its effect on hydrodynamic processes. Shoal complexes, Chincoteague Shoals south to Parramore Banks, skirt the seaward edge of the Chincoteague Bight, further signifying the basin's differences from the regional trend.

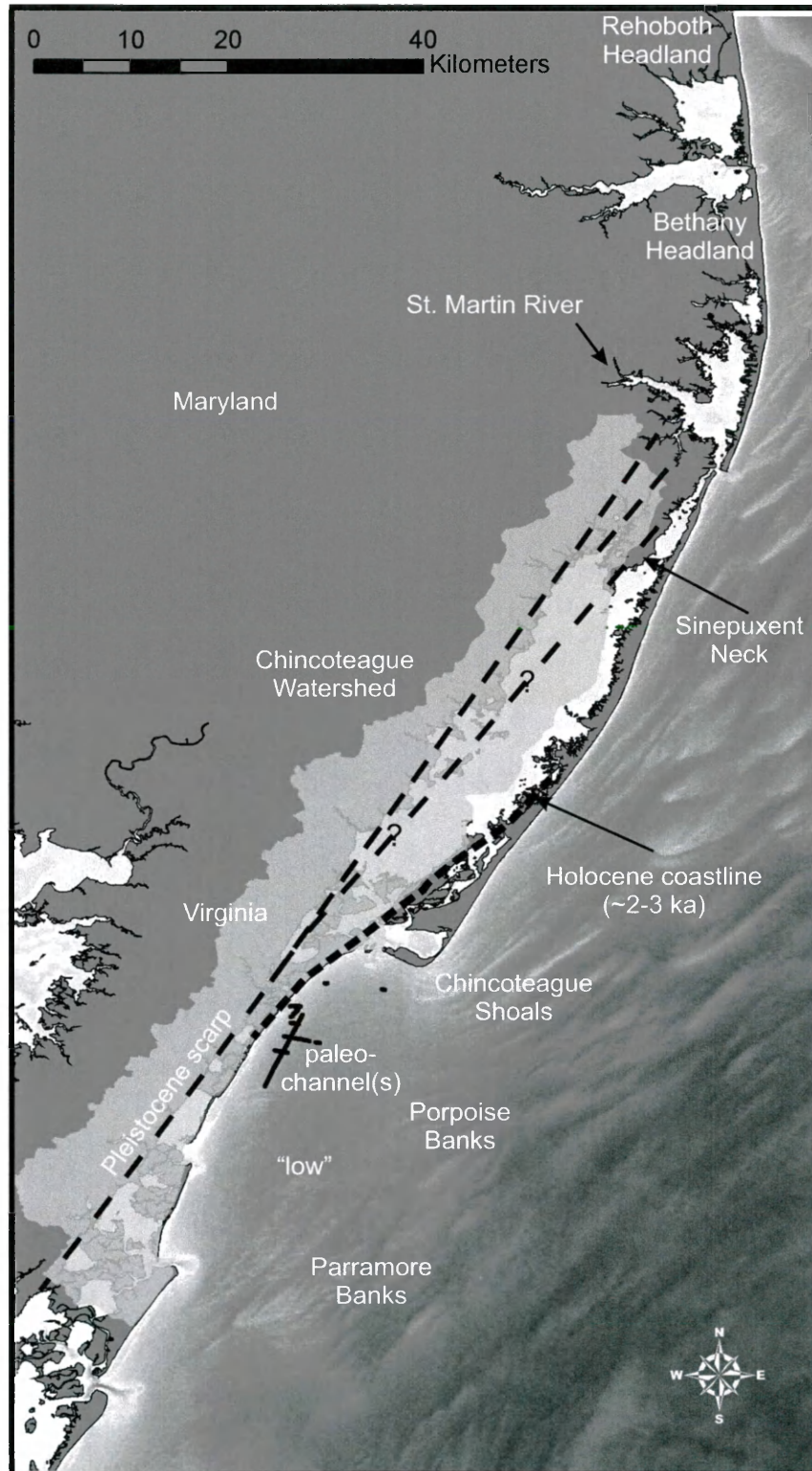


FIGURE 33

Alongshore patterns in shoreline change (presented as plan view area) for 1850-2005 and 1980-2005 time intervals correspond to alongshore variability in predominant geomorphologic environments of Assateague Island (VA) (Morton *et al.*, 2007) and corresponding alongshore gradients in the thickness (white = thick) of the nearshore sand prism. Long-term and decadal shoreline erosion occur at the same alongshore length scales as the recurved spits, a shoreline reach also characterized by increasing shoreline angle. The central zone of decadal stability and historical accretion (including prograding dune and shoreface) is spatially coincident with the migrating relict Assateague Inlet, shoreface-attachment of a sand ridge, and a beach segment characterized by historic overwashing and more recent dune progradation (Figure 2).



### Legend

-  Overwash
-  Delta Accretion Mound
-  Beach/Spit Ridge
-  Barrier Core
- Shoreline Change
  -  Accretion
  -  Erosion

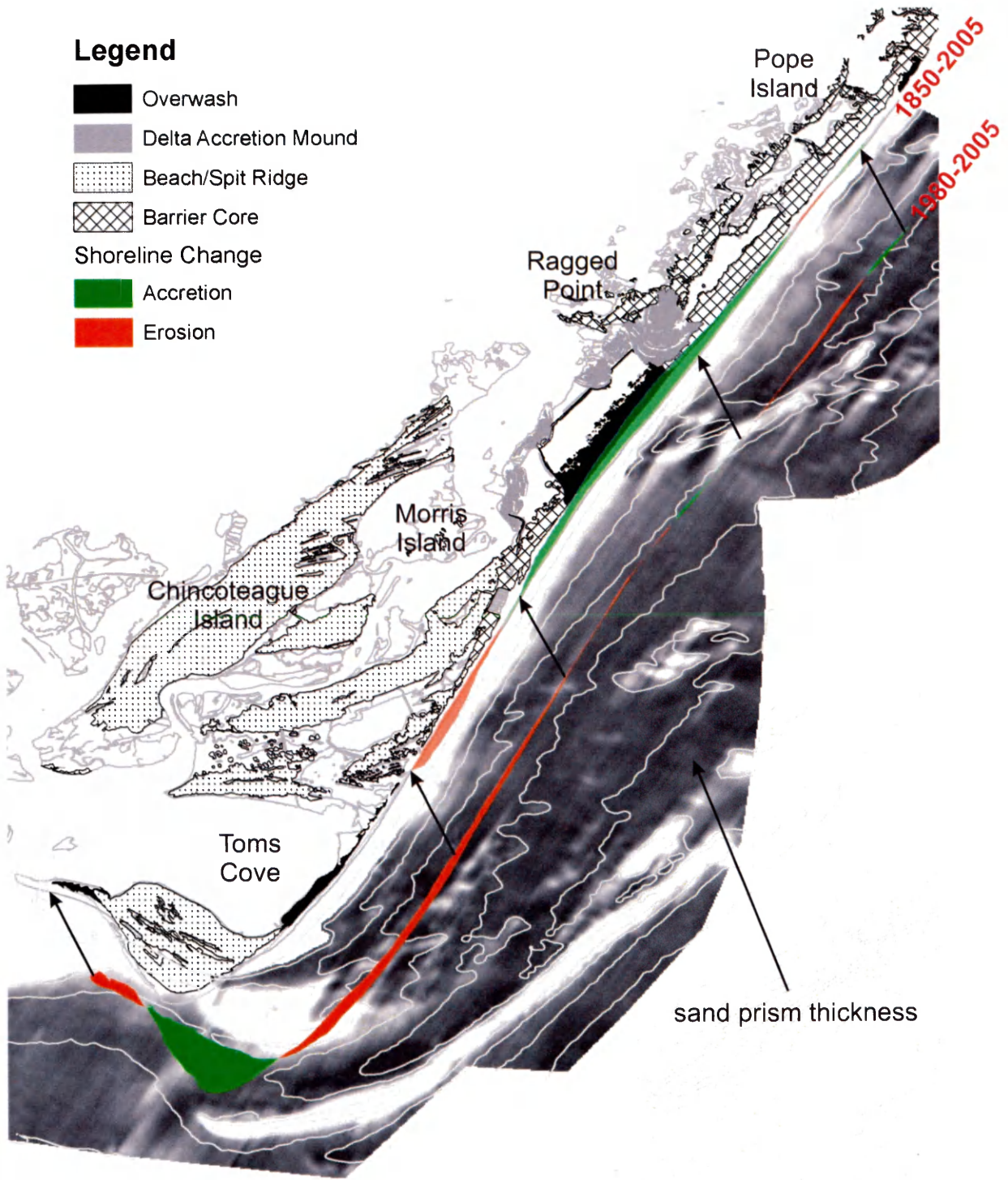


FIGURE 34

Conceptual illustration showing possible length scales that could be used to define a cross-shore zone of 'shoreline' influence. This study presumed that the 8-m isobath adequately represented mean, long-term closure and that the variable cross-shore distance between the 4-m and 8-m isobaths effectively captures relative differences in the nearshore sand prism. One possible alternative is the entire cross-shore section from storm run-up limit seaward to a location on the inner shelf that represents extreme event closure. As the sample sand-prism thickness and comparative bathymetric profiles show, other definitions are possible. The thickness isopach shows a seaward-thinning prism out to at least 4 km. The elevation change between 1978/1982 and 1933/1934 at this sample location suggest a different long-term depth of closure (~ -10 m). Although measurable seafloor lowering occurs further offshore on the inner shelf (below 10 m), these changes may not be as relevant to shoreline change, unless there is notable onshore flux from these locations.

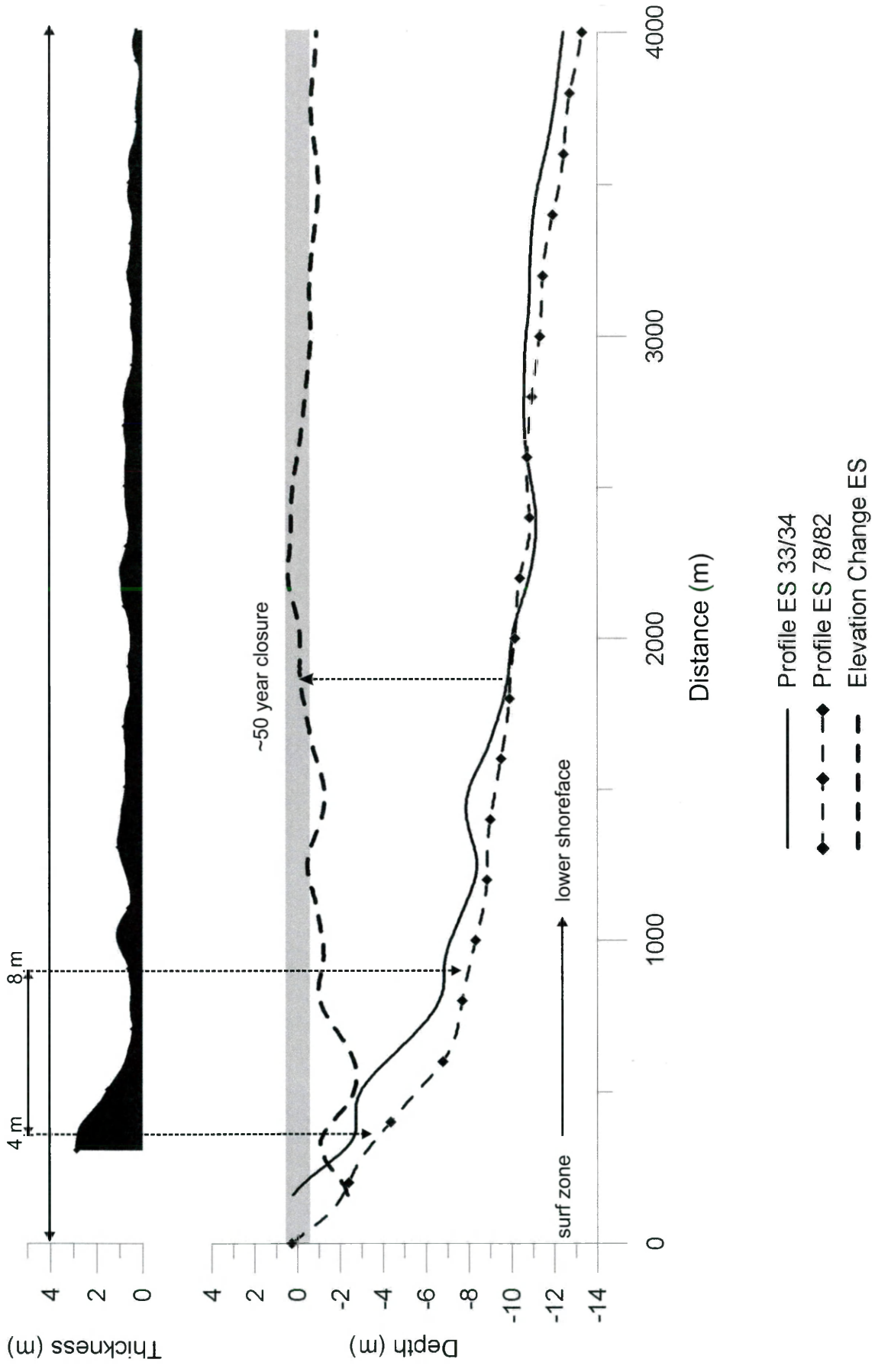




FIGURE 35

(a) Nearshore sand volume defined above the wave ravinement/proto-ravinement surface. The cell size is  $25 \text{ m}^2$ . (b) Volume flux defined by the 1933/1334 – 1978/1982 rate of seafloor lowering. The cell size is  $25 \text{ m}^2$ . (c) Years required to remove the calculated nearshore sand volume provided the calculated volume flux and assuming a fixed ravinement surface (only solved in areas where flux was positive, *i.e.*, seafloor lowering).

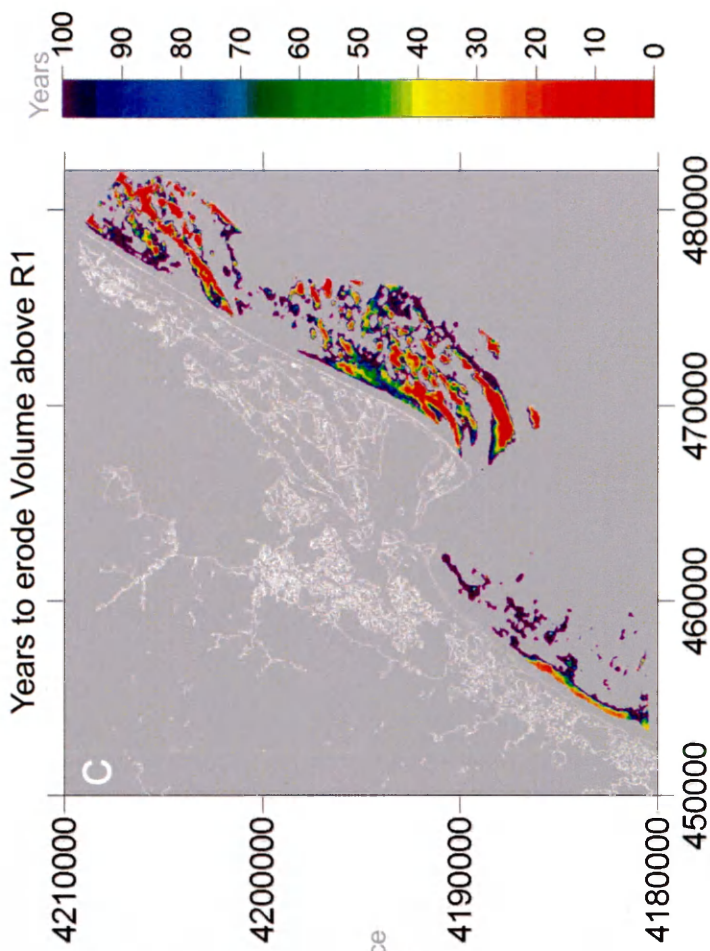
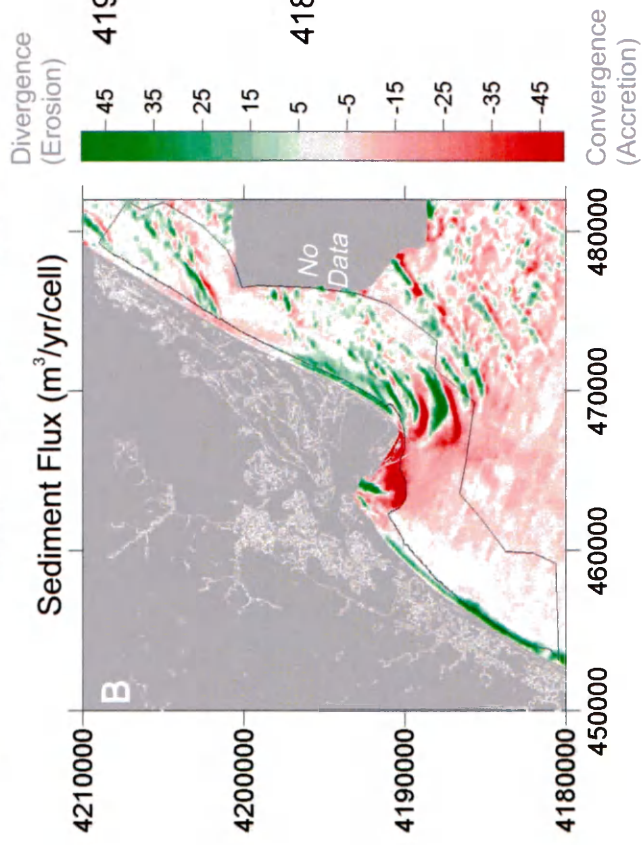
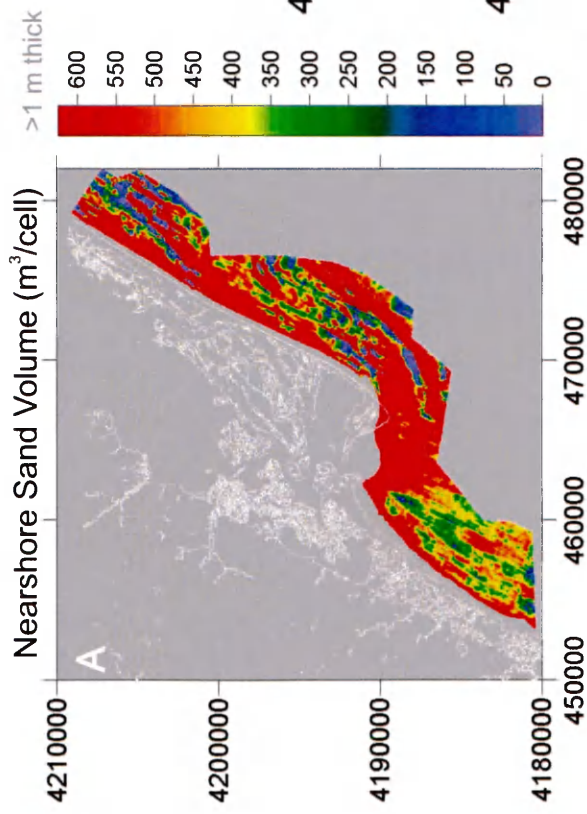


FIGURE A-1

Short-term (<10 yrs) shoreline mobility and shoreline change data for southern Assateague Island. Data series show a divergent N-S trend, with increasingly variable signals approaching Fishing Point (Figure 1).

### Assateague Island (VA) Shoreline Mobility and Change

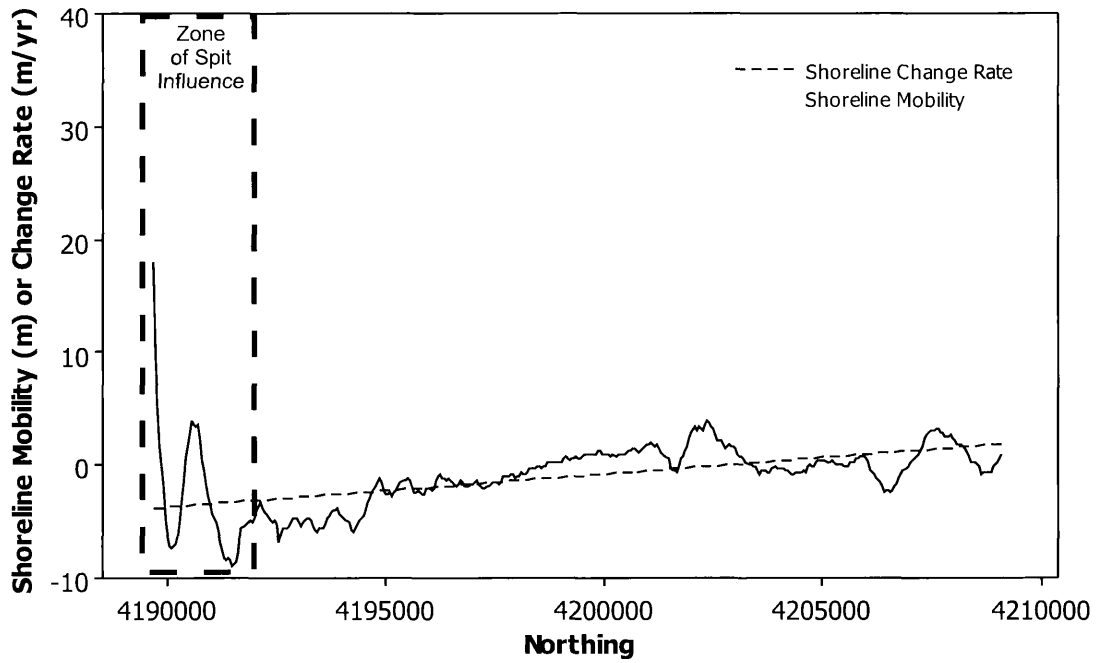
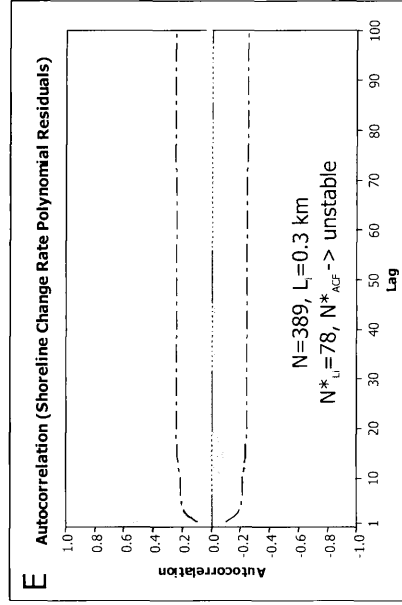
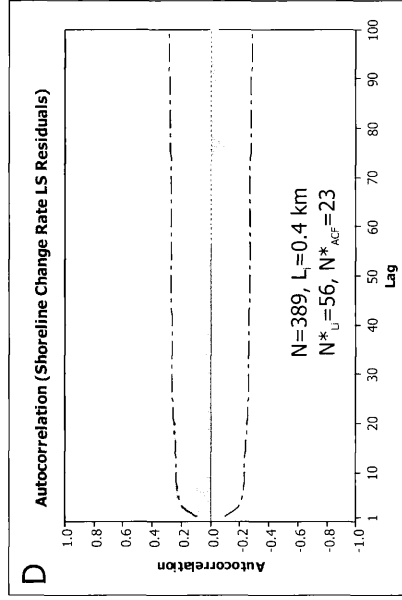
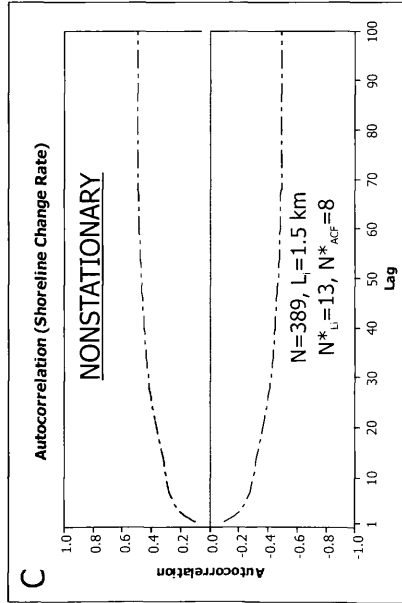
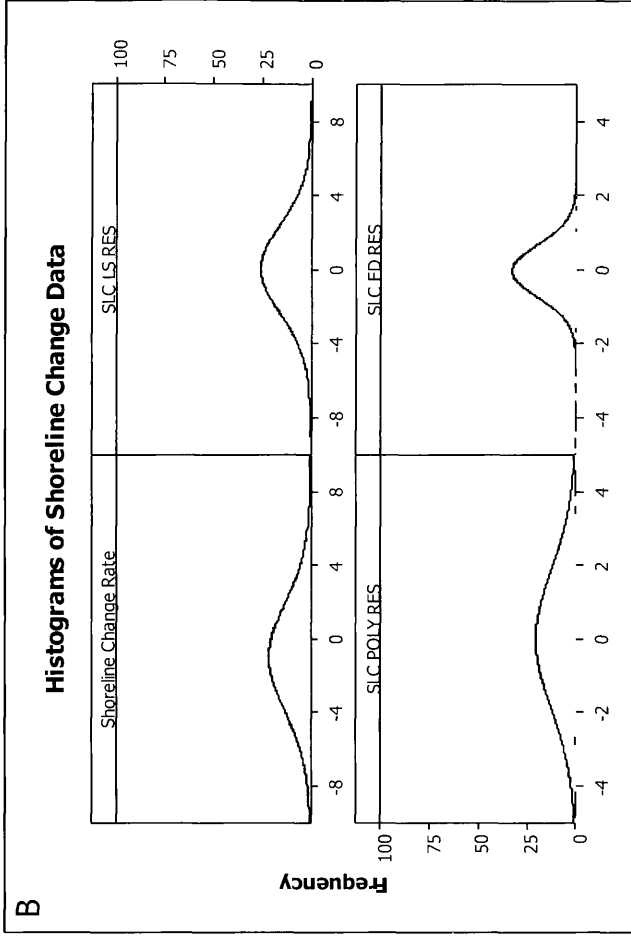
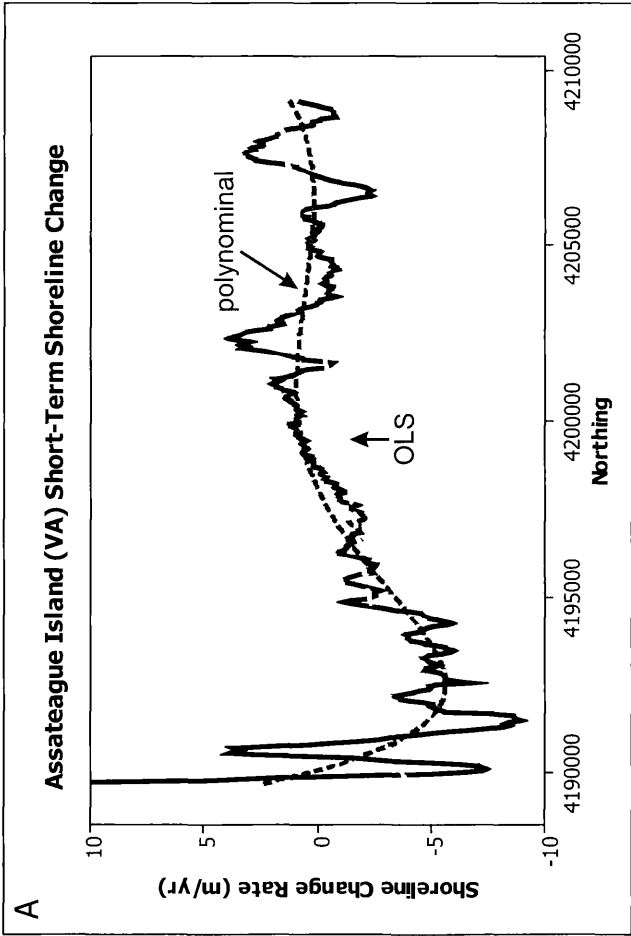


FIGURE A-2

(a) Least squares and polynomial fits to inter-annual shoreline change data. (b) Histograms showing the distribution of untreated and treated shoreline change data. (c) Correlogram showing the autocorrelation function for untreated shoreline change data. (d) Correlogram showing the autocorrelation function for the residuals of the least squares fit to shoreline change data. (e) Correlogram showing the autocorrelation function for the residuals of the polynomial fit to shoreline change data. Negative autocorrelation introduced by treatment method. In panels C-E, correlation coefficients larger than the delineated critical value are significantly different from zero. Calculated effective sample size are labeled on each correlogram, where  $N^*_{Li}$  and  $N^*_{ACF}$  reflect different methods of calculation.



**FIGURE A-3**

(a) Cross-correlation of shoreline mobility and shoreline change using untreated data. (b) Cross-correlation of residuals from least squares fitting. (c) Cross-correlation of residuals from polynomial fitting.

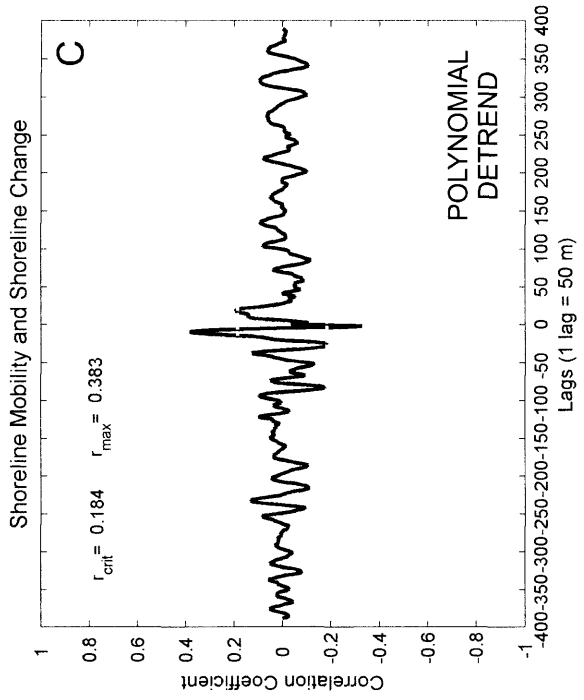
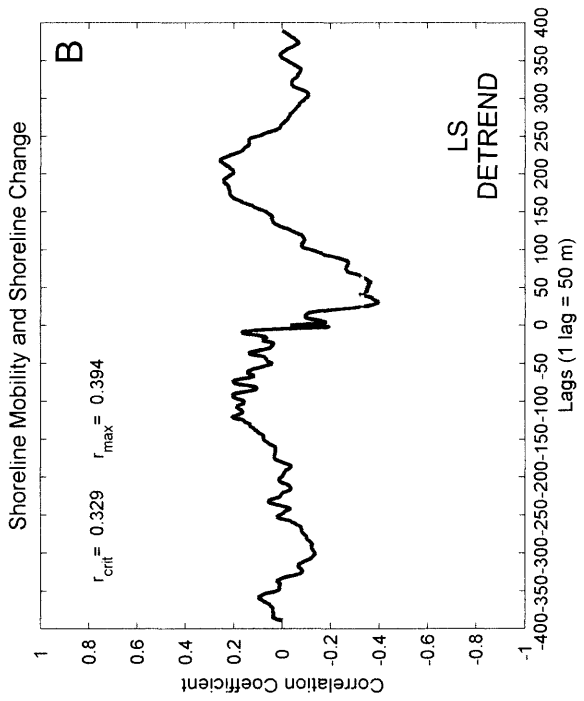
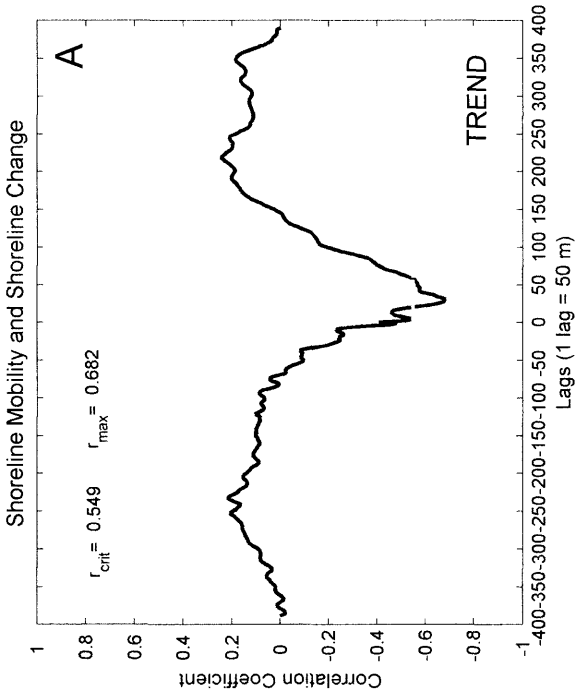
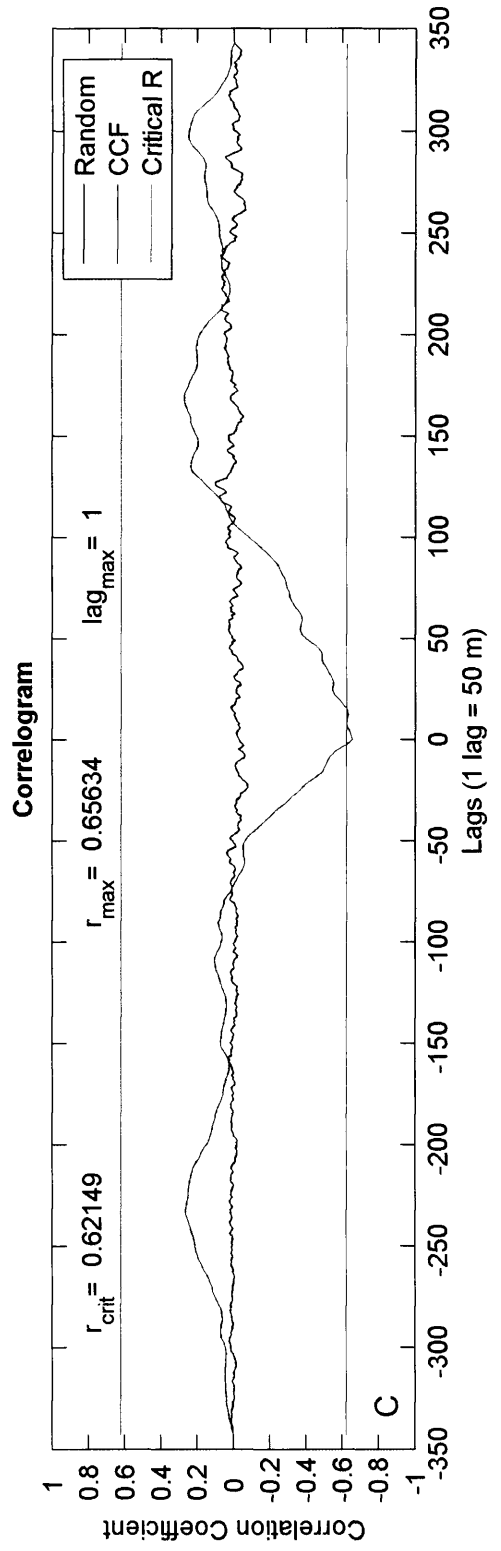
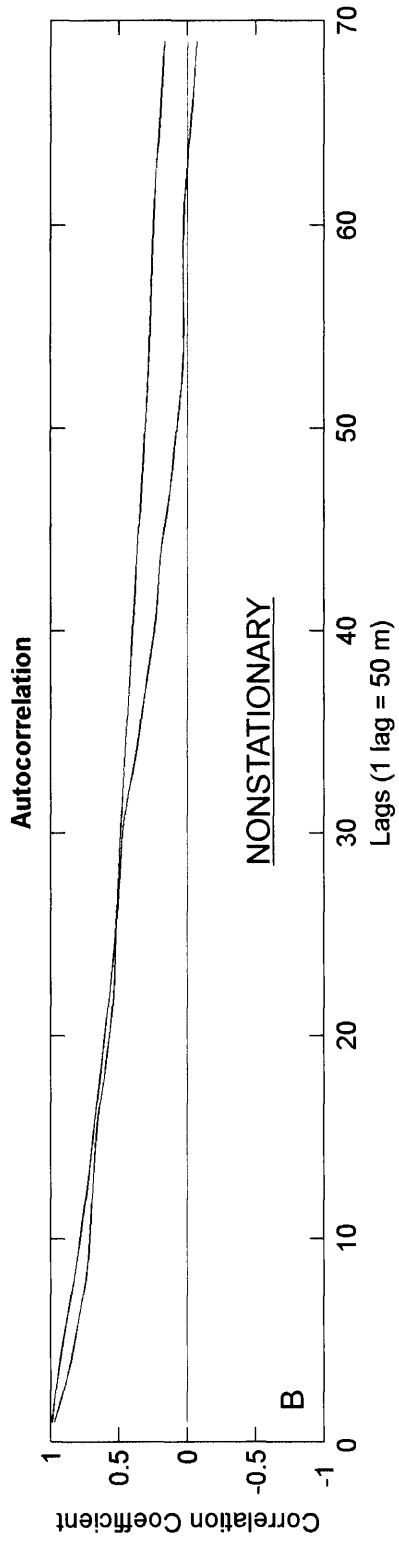
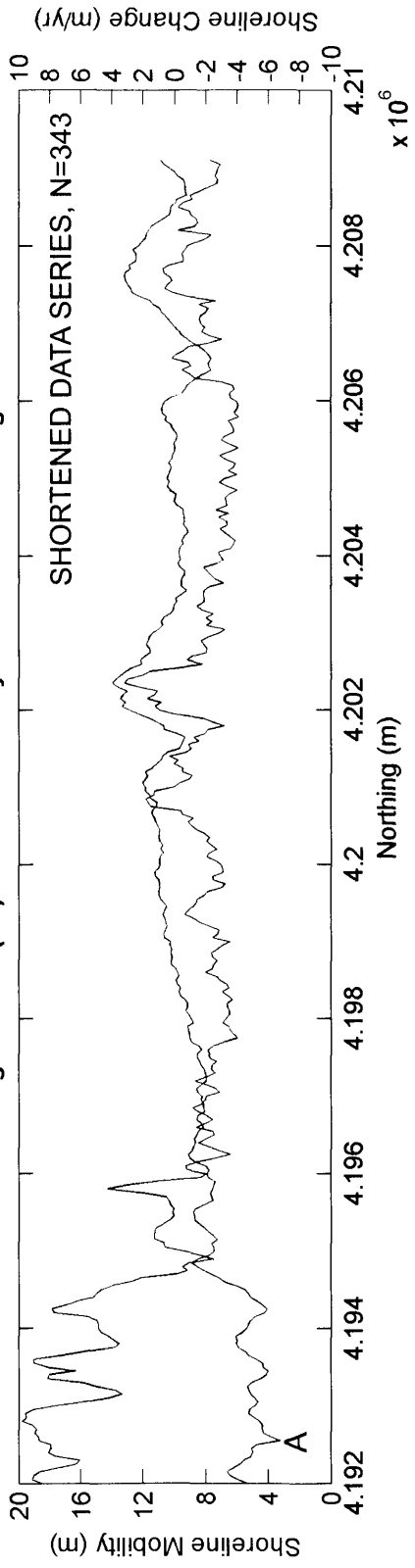




FIGURE A-4

Autocorrelation function (b) and cross-correlation (CCF) (c) of shoreline mobility and shoreline change using untreated shoreline change data (a) with the distinct signal of Fishing Point removed (Figure A-2). Comparing (c) with Figure A-3A, a significant difference is seen in the spatial lag corresponding to the peak correlation coefficient. This difference reflects the extreme sensitivity of cross-correlation to variance in the data series.

# Assateague Island (VA) Shoreline Mobility and Shoreline Change



**FIGURE A-5**

Autocorrelation function (c) and cross-correlation (CCF) (d) of shoreline mobility and shoreline change using the residuals (b) from a polynomial fit (a) of the shoreline change data, again removing the distinct signal of Fishing Point.

# Assateague Island (VA) Shoreline Mobility and Shoreline Change

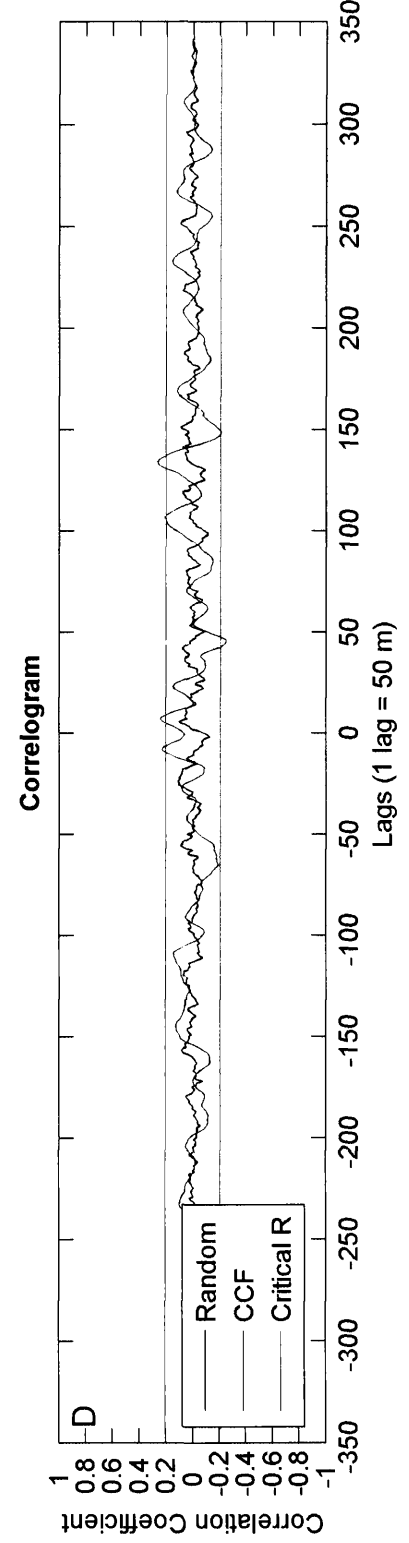
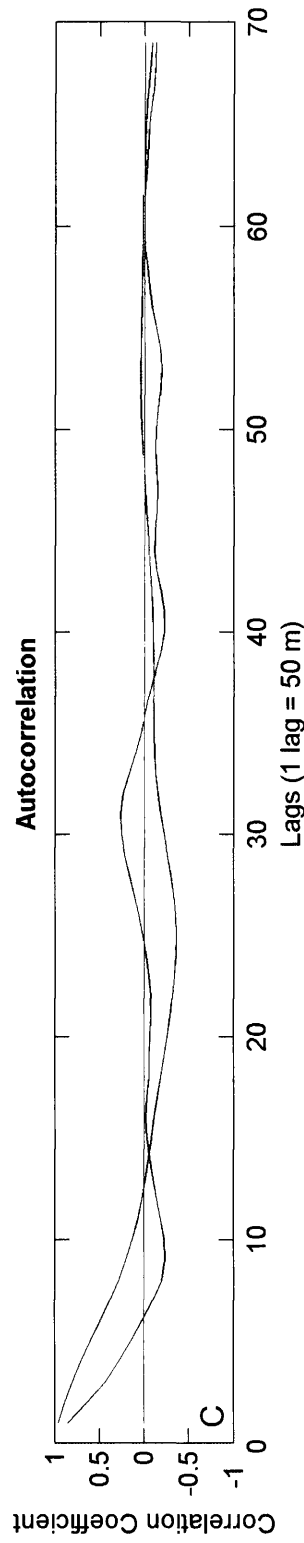
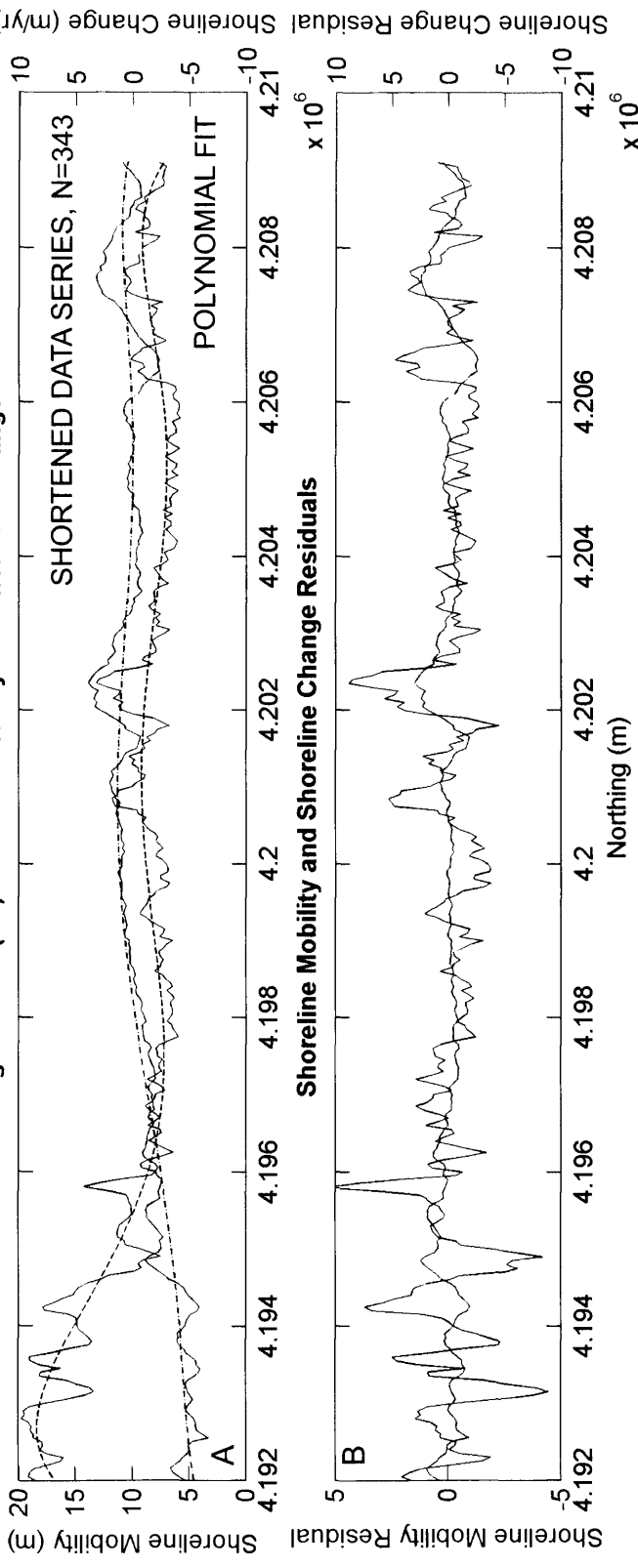
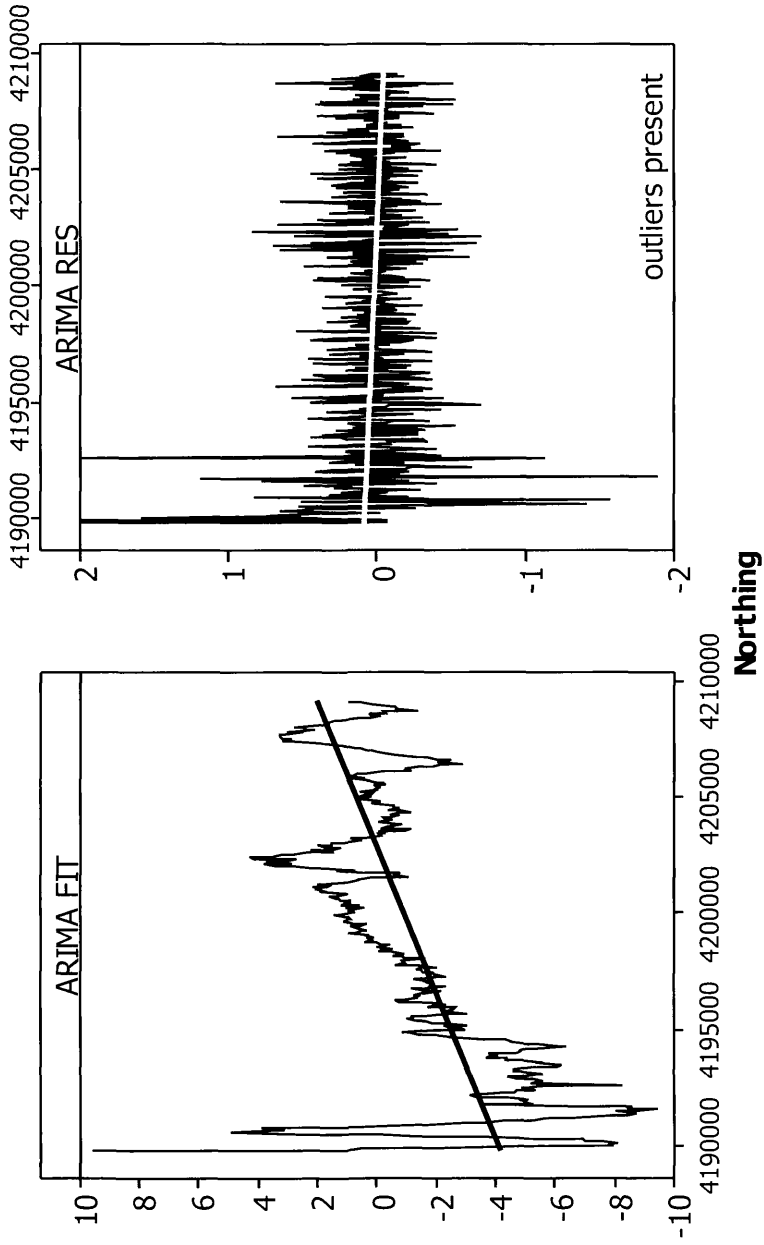


FIGURE A-6

(a) ARIMA(1,1,0) model and model residuals for the shoreline change data. (b) Correlogram showing the autocorrelation function of the residuals. (c) Correlogram showing the partial autocorrelation function of the residuals. The ARIMA model removes all wavelength patterns of interest.

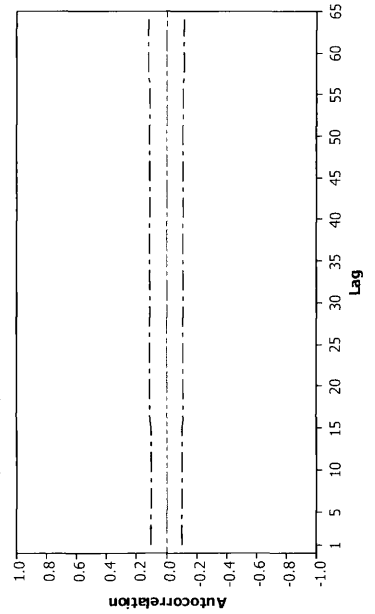
# Shoreline Change ARIMA (1,1,0) Model

A



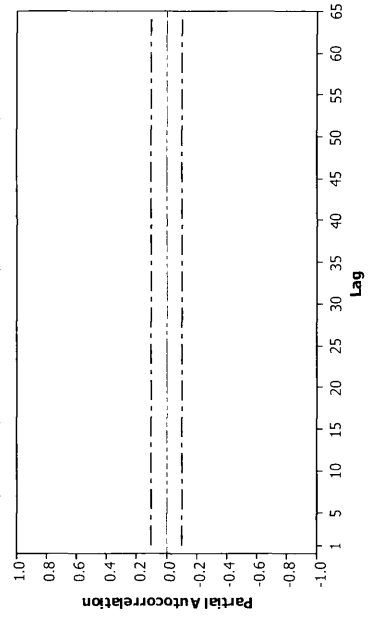
B

**ACF of ARIMA (1,1,0) Residuals**  
(with 5% significance limits for the autocorrelations)



C

**PACF of ARIMA (1,1,0) Residuals**  
(with 5% significance limits for the partial autocorrelations)



Geoffrey Laird Wikel was born in Wilmington, Delaware on October 13, 1976. Graduated from St. Mark's High School in Wilmington, DE in June 1994. Earned a B.S. in Natural Science and Mathematics and B.A. in English from Washington and Lee University in Lexington, Virginia in June 1998. Worked as a geologist in the Coastal and Estuarine Geology Program with the Maryland Geological Survey from 1998 to 2002. Worked as a coastal scientist with the Ohio Office of Coastal Management in 2004. Presently employed as a physical scientist with the Marine Minerals Program within the Minerals Management Service. Entered the Joint Degree Graduate Program in the School of Marine Science and Thomas Jefferson Program in Public Policy at The College of William and Mary in August 2004 and August 2005 respectively.